RF Phase Modulation of Optical Signals and Optical/Electrical Signal Processing

by

Nikolaos I. Andrikogiannopoulos

Dipl., National Technical University of Athens
(2004)

Submitted to the Department of Electrical Engineering and Computer Science
in partial fulfillment of the requirements for the degree of

Master of Science in Electrical Engineering and Computer Science

at the

MASSACHUSETTS INSTITUTE OF TECHNOLOGY

June 2006

Author ……..
Department of Electrical Engineering and Computer Science
May 25, 2006

Certified by ……....
Vincent W. S. Chan
Joan and Irwin M. Jacobs Professor
Electrical Engineering & Computer Science and
Aeronautics & Astronautics
Director, Laboratory for Information & Decision Systems
Thesis Supervisor

Accepted by ……...
Arthur C. Smith
Chairman, Department Committee on Graduate Students

RF Phase Modulation of Optical Signals and Optical/Electrical Signal Processing

by

Nikolaos I. Andrikogiannopoulos

Submitted to the Department of Electrical Engineering and Computer Science
on May 25, 2006 in partial fulfillment of the
requirements for the degree of
Master of Science in Electrical Engineering and Computer Science

Abstract

Analog RF phase modulation of optical signals has been a topic of interest for many years, mainly focusing on Intensity Modulation Direct Detection (IMDD). The virtues of coherent detection combined with the advantages of Frequency Modulation, however, have not been explored thoroughly. By employing Frequency Modulation Coherent Detection (FMCD), the wide optical transmission bandwidth of optical fiber can be traded for higher signal-to-noise performance. In this thesis, we derive the FM gain over AM modulation – the maximum achievable signal-to-noise ratio (by spreading the signal's spectrum) for specific carrier-to-noise ratio. We then employ FMCD for a scheme of remote antennas for which we use optical components and subsystem to perform signal processing such as nulling of interfering signals. The performance of optical processing on different modulation schemes are compared, and some important conclusions are reported relating to the use of conventional FMCD, FMCD with optical discriminator (FMCD O-D), and IMDD. Specifically, the superiority of conventional FMCD is shown; and, on the other hand, the inferiority of FMCD O-D is shown (same performance as IMDD) because of the use of an O-D. Finally, the remote antenna scheme is generalized for N antennas and N users.

Thesis Supervisor: Vincent W. S. Chan
Title: Joan and Irwin Jacobs Professor of Electrical Engineering & Computer Science, and Aeronautics & Astronautics
Director, Laboratory for Information and Decision Systems

Acknowledgments

I would like to thank, first and foremost, my advisor, Professor Vincent Chan for his patience, support and guidance. It has been inspiring working close to such an experienced and talented research advisor, listening to his insightful suggestions and being taught how to evaluate the significance among different research directions.

I would also like to express my gratitude to Dr. Terrence McGarty for his helpful insights during our lengthy discussions and his support throughout my thesis.

Also, I would like to thank Guy Weichenberg, Yonggang Wen, Jihwan Patrick Choi and Lillian Dai for all their help.

I am also grateful to MIT, the Paris Kanellakis Fellowship, and DARPA for their financial support.

Last, my deepest thanks to my parents for all their love, support and sacrifices throughout the years without which this thesis would never have come into existence.

Contents

List of Figures

List of Tables

Chapter 1

1 Introduction

1.1 Introduction and Motivation

Optical fiber has been established as the medium of choice in high-capacity digital transmission systems. However, applications that involve point-to-point routing of analog signals have also benefited from the excellent propagation characteristics of optical fiber. Analog transmission of microwave signals over optics has been demonstrated for video-signal distribution, micro-cellular radio, and remote microwave-antenna schemes [4].

The use of analog modulation for microwave signals within fibers, known as Radio Frequency (RF) Optical can benefit much from the fact that the whole received signal spectrum can be modulated optically. This replaces the need for demodulating the received signal and converting it from analog to digital format. The equipment used for this latter function – analog-to-digital (A/D) converters – for broadband signals is very expensive, and in some cases cannot meet the specifications for very broadband signals.

There are many kinds of Analog Optical Modulation and detection schemes. The two basic approaches, which we will discuss in Chapter 2, are:

1) Intensity Modulation Direct Detection (IMDD)
2) Coherent Detection (CD), using Analog Modulation (AM), Frequency Modulation (FM), or Phase Modulation (PM)

In this thesis, we will focus on CD using FM. The advantages of using Frequency Modulation Coherent Detection (FMCD) are manifold. Compared to IMDD, FMCD can achieve a higher signal-to-noise ratio (SNR) by expanding the bandwidth of the signal into an extremely wideband FM optical bandwidth. An extensive analytical discussion on the benefits of this is provided in Section 2.4. The technique of noise suppression in conventional FM receivers has been known as weak noise suppression and is responsible for the superior performance of FM radios. However, this trade-off between bandwidth and SNR presents a certain threshold above which the noise induced into the spectrum degrades the performance of the signal significantly. This so-called FM threshold is one of the topics that will be discussed in detail in this work.

Having derived the necessary analytical tools for FMCD, we next look into important applications where the use of coherent detection could provide an advantage over IMDD. One of the most widely studied applications for IMDD has been for antenna remoting [4], [24], which is processing signals received by several remote antennas. IMDD has been preferred because of its simplicity. Our goal is to employ FMCD for this application and to justify the added complexity by proving the superior performance of our proposed modulation scheme. In this context, the second part of the present study focuses on the case of remote antennas connected to a central station through a fiber-optic network. In this scheme, we propose that most of the signal processing be conducted in a centralized way, allowing for further processing – combining constructively versions of the signal, nulling interfering signals - and use less processing equipment near the antennas as in Figure 1-1.

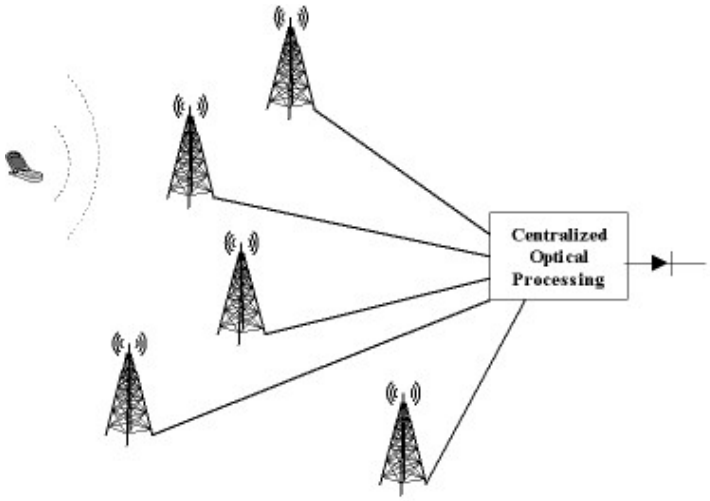

Figure 1-1: Remote Antenna Scheme

Centralized processing provides benefits over typical decentralized processing techniques. In our deployment, different versions of the received signal (from every antenna) reach the central station and they can be combined to achieve better SNR than with just one of the antennas. What is more, interference between users can be suppressed, or even cancelled, due to the diversity that can be achieved through the many versions of the received signal.

Central processing techniques also benefits from analog optical transmission. The toolbox of optical processing consists of delay fibers, shifters, optical switches, combiners, and splitters. All of these equipment are cheap, insensitive to modulation bandwidth, and can be used before digitizing the signal and performing the usual signal processing that is presently done digitally. Moreover, the optical processing can be effective at frequencies much higher than the limits of electrical equipment and can therefore be used for handling wideband signals.

To summarize, the use of optical signal for the transmission of microwave signals in conjunction with optical-electrical central processing has the potential of significantly lowering the cost of a remote antenna application such as a mobile network or the cost of construction of a phased array antenna and providing broadband, inexpensive, and extremely efficient signal processing compared to electrical processing. The use of FM in this technique is novel, and provides significant RF gain over IMDD, and hence superior SNR performance.

Our contributions include:

1. Derivation of an analytical expression for the SNR of FMCD over all the range of CNR indicating the threshold phenomenon. This study was made possible by combining elements from the literature [7], [9], [11].
2. Performance comparison among FMCD with conventional FM receiver, IMDD and FMCD O-D. The performance of the conventional FMCD is based on our own results for the maximum performance of FMCD which is when it operates exactly on the derived threshold and also FMCD O-D is entirely based on the analysis that is carried in this thesis.
3. Proposal of a simple remote antenna structure employing FMCD with two antennas and two users where optical processing consists of adjusting two delay lines so as to null an interfering signal.
4. Comparison among the modulation schemes in the context of the simple antenna scheme
5. Proposal of a new simple antenna scheme employing FMCD with separate heterodyne detection for every signal. This scheme is shown able to scale for N antennas and N users. Discussion on the use of the existing least-mean-square algorithm (LMS) and the modifications required for it to work under FMCD.

1.2 Prior Work

Analog optical links have been the subject of considerable attention for a variety of applications, including remoting antenna and cable television distribution systems. Work on analog links has concentrated almost exclusively on direct-detection (DD) systems using intensity modulation (IMDD) mainly because of its simplicity [3]-[6].

To date, analog links based on coherent detection have received relatively little attention [3]-[6] compared to IMDD due to the increased complexity of coherent detection (CD). CD systems have several potential advantages over DD systems. Coherent systems can approach shot-noise-limited performance with sufficient LO laser power. In addition, coherent systems can detect the phase of the optical carrier. Thus, while DD systems are best suited for amplitude or intensity modulation (AM or IM), CD systems can use AM, PM, or FM. In our work, we investigate the performance of FMCD motivated by the success of angle modulation techniques in microwave transmission systems.

Prior work on optical FM has concentrated on deriving the SNR of FMCD links [1], [7] and on the variation of this SNR along the transmission distance [2]. In this thesis, we do not investigate the distance limits of the FM SNR. Instead, by taking into account the optical noise sources and combining it with the analysis used for typical radio FM systems [9], we derive the SNR of FMCD very close to what has been done in [7] for optical FM. We proceed to find the FM threshold as a function of the modulation bandwidth. Most of the previous work, even on typical radio frequency FM [8] has not been interested in finding an analytic expression for the threshold phenomenon of FM due to the stochastic nature of the phase induced noise. The FM threshold has been studied very little and only in the field of estimation theory by Van Trees [11], [12]. Our approach is based on the analytical expression for the probability of anomaly derived by Rice for conventional electrical FM systems [9]. Our results on the FM threshold are consistent with the results of [12]. Moreover in [12], the Rician analysis has been shown to be close to experimental results. Our work presents a complete formula for the SNR over all the range of carrier-to-noise ratio CNR by incorporating properly the probability of anomaly of Rice. The FMCD mentioned so far can also be called conventional FM discrimination because it mainly consists of a square law detector followed by an electrical discriminator. It is called conventional because it uses a microwave FM discriminator operating under the same principles that electrical systems do.

Before using our results on the FM threshold for conventional FM receivers in a remote antenna scheme, we characterize the performance of a FM O-D system. To characterize the performance of the O-D, we follow closely the analysis of [16] on Mach Zehnder optical discrimination and extend these results to derive some useful formulas for the SNR of FMCD with an O-D.

Using the maximum achievable SNR - at the point of the threshold that we studied - for conventional FM when given a certain CNR, we then proceed to employ FMCD in a remote antenna scheme. Remote antennas or phased array antennas using optical fiber have used mostly IMDD or no modulation at all in literature [4], [24]. The novel part of our approach is that we employ FMCD operating near the threshold, thus providing the maximum SNR that FM can achieve.

We first consider a two-antenna and two-user remote antenna setup (as shown in Fig. 4-2) and find the necessary condition such that an interferer can be nulled. We extend this observation to a more generalized scheme involving N antennas and N users (Figure 4-19).

As we increase the number of users and antennas, we observe the similarities our research bears with that of adaptive antenna systems [18]-[20]. These systems have demonstrated several advantages, among which is increased sensitivity of the received signal to interfering sources. The adaptation process in such systems is based on the minimization of the mean-square error by the least-mean-square (LMS) algorithm [20]. The difference in our system is that we have frequency modulated signals. The weights required by the LMS algorithm, which typically are applied either directly to the signals or to the amplitude modulated signals, cannot be applied in FM in the same manner. A different approach has to be followed. We show this to be the change of the FM modulation index, which is basically the dynamic FM action of changing the signal's amplitude in AM.

1.3 Thesis Outline

In this thesis, we study the use of FMCD in a remote antenna scheme combined with optical/electrical processing. The thesis is organized as follows:

In Chapter 2 we discuss the differences between IMDD and CD Systems. In addition, we derive the SNR of IMDD.

Chapter 3 is devoted entirely to FMCD, starting by initially deriving the CNR of FMCD, taking into account optical noise sources. This is followed by the weak noise analysis of conventional FM systems. The very well known formula for FM systems is re-derived using the previously calculated CNR. This formula is valid only when there is no anomaly in the phase of the signal, which is true when the CNR is high. In order to find the SNR for the whole range of CNR values, we follow the Rician analysis; and by considering the probability of anomaly [9], we derive a complete formula. The next part of this chapter is our analysis on FMCD with a Mach Zehnder interferometer performing as an optical discriminator. An analytical derivation of the corresponding SNR is provided and the case of a sinusoidal signal is investigated. The chapter continues with a novel comparison of all of the modulation schemes that were discussed so far and ends with a discussion section.

Chapter 4 introduces a remote antenna scheme employing FMCD with two users and two antennas. We derive the necessary condition for nulling one of the two users and restrict our analysis in this

thesis to nulling. At this point we also present a heterodyne separate detection version of the above scheme which has better performance. Next, we proceed with the investigation of nulling and we show that the necessary condition for nulling applies also for IMDD for which we derive the resulting SNR. The SNR of FMCD O-D in the remote antenna scheme is also derived in this section. The chapter continues with a comparison among the modulation schemes - analogous to that of chapter 3 - for the case of the remote antenna setup. We then generalize the two antenna scheme for N antennas and N users. We propose configurations that can use adaptive beamforming for remote antenna setups that operate under FMCD.

Finally, chapter 5 is devoted to a complete examination of all the results in all of the preceding chapters, and offers directions for future research.

Chapter 2

2 Modulation of Microwave Signals onto Optical Carriers

2.1 Introduction

This chapter introduces the different kinds of analog modulation, namely IMDD and CD. In the rest of the thesis, we are interested only in CD, and specifically in conjunction with FM. The current chapter begins with an introduction to the two modulations followed by a study of the IMDD performance. The performance of CD will be discussed in greater detail subsequently in the thesis. Finally, with the help of the existing literature, we discuss the advantages and disadvantages of coherent and direct detection systems.

2.2 IMDD and CD

RF optical transmission is defined as the technique by which an RF signal is imposed on an optical carrier, with optical fiber being the transmission medium. The original RF signal is recovered at the receiver by performing detection on the optical signal. Two basic approaches to optical-signal modulation and recovery are possible.

The first and simpler alternative is intensity-modulation direct-detection (IMDD) as shown in Figure 2-1. In this case, the optical-source *intensity* is either directly modulated by the input microwave signal, or passes through an external intensity modulator. The resulting intensity-modulated signal passes through the optical fiber to the photodiode, where the modulating signal is returned in the electrical domain.

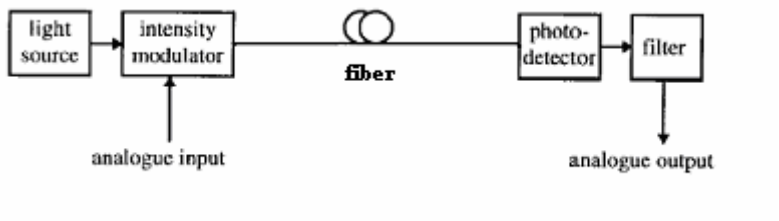

Figure 2-1: IMDD transmission system, [7].

In a coherent system Figure 2-2, the optical source can be modulated in *intensity*, *frequency,* or *phas*e by the input microwave signal, either directly or by passage through an external modulator. The modulating signal passes through the optical fiber to the receiver, where it is combined with the input from a local-oscillator (LO) laser. The combined signal illuminates the photodiode to produce an electrical signal centered on an intermediate frequency (IF) between the unmodulated optical source and the LO laser. This signal is further processed to recover the analog input signal.

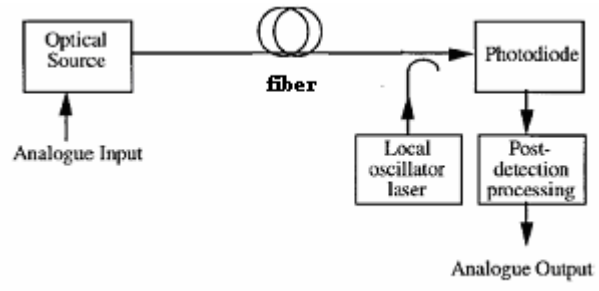

Figure 2-2: Optical Coherent System, [7].

2.3 Noise Mechanisms in Optical Links

Shot noise and thermal noise are the two fundamental noise mechanisms responsible for current fluctuations in all-optical receivers even when the input optical power is constant. Of course, additional noise is generated if the input power itself is fluctuating because of intensity noise associated with the transmitter.

The main categories of noise [15] are:

Thermal noise: At a finite temperature, electrons move randomly in any conductor. Random thermal motion of electrons in a resistor is manifested as a fluctuating current even in the absence of an applied voltage. The load resistor in the front end of an optical receiver adds such fluctuations to the current generated by the photodiode. This additional component is referred to as thermal noise. Mathematically, thermal noise is modeled as a stationary Gaussian process with a spectral density, I_{th}^2, that is frequency-independent up to 1THz (nearly white noise) and is given by

$$\overline{I_{th}^2} = \frac{4kT}{R_L} B \tag{2.1}$$

where k is Boltzmann constant, T is the absolute temperature, R_L is the load resistor, and B is the signal's bandwidth.

Shot noise: This kind of noise is a manifestation of the fact that the electric current consists of a stream of electrons that are generated at random times. Mathematically, it can be modeled as a stationary random process with Poisson statistics, which in practice can be approximated by Gaussian statistics

$$\overline{I_{sh}^2} = 2q\left(\bar{I}_d + I_{dk}\right)B \tag{2.2}$$

where $\bar{I}_d$ is the mean optically generated current and I_{dk} is the photodiode dark current.

Optical source relative intensity noise: This is the excess intensity noise due to noncoherent behavior of the transmitter, and is given by

$$\overline{I_{nRIN}^2} = \overline{I_d^2} \cdot RIN \cdot B \tag{2.3}$$

where *RIN* is the source relative intensity noise value.

2.4 Intensity Modulation Direct Detection (IMDD)

In this section, we focus on the most popular analog modulation scheme – intensity modulation [1]-[6] – and we re-derive the SNR of this scheme [1].

In an IMDD system, as depicted in Figure 2-1, the analog signal to be transmitted can be represented by *m(t)*. The optical power at the detector is proportional to the power of amplitude of the signal properly weighted by the modulation index γ

$$P_o = P_u\left[1 + \gamma \cdot m(t)\right] \tag{2.4}$$

where P_u is the mean received optical power and γ is the modulation index $\left(\gamma \cdot m(t) > -1\right)$.
The mean square signal current at the detector output is the signal part of the mean received power (2.1). That is,

$$\overline{I_s^2} = \left(RP_u\gamma\right)^2 \cdot \overline{m^2(t)} \tag{2.5}$$

where

$R = \frac{\eta q}{hv}$ is the responsitivity of the p-i-n photodiode,

η: quantum efficiency of the photodiode

q: electrical charge

h: Planck's constant

v: the frequency of light

Noise arises from the transmitter and the photodetector. Fundamentally the noise is limited by the quantum nature of photon-detection. We represent the one-sided cumulative spectral density of noise as N_0, consisting of the sum of the variances of the noise terms that were mentioned in the previous section - shot, thermal, relative intensity noise - when no amplifiers are present.

Taking into account that the signal power is given by (2.2) and that the noise power is N_0B, we have the following expression for SNR:

$$SNR_{IMDD} = \frac{(RP_u\gamma)^2 \cdot \overline{m^2(t)}}{N_0 \cdot B} \tag{2.6}$$

where

$N_0 = \frac{4kT}{R_L} + 2e(I_0 + I_{dk})$,

B the message's *m(t)* bandwidth,

I_{dk} the diode's dark current, usually negligible.

The table on the following page presents the shot noise limit, in which case the shot noise is assumed to dominate and we derive the corresponding SNR accordingly.

For optical powers below the RIN limit, shot-noise limited reception can be achieved if the thermal contribution is small, giving

$$SNR_{DD} = \frac{RP_u \cdot \gamma^2 \cdot \overline{m^2(t)}}{2qB} = \frac{\gamma^2 \overline{m^2(t)}}{2}\left(\frac{\eta P_u}{hvB}\right) = \frac{\gamma^2 \overline{m^2(t)}}{2} CNR \qquad (2.7)$$

when $N_0=2q(RP_u)$

Table 2-1: IMDD-SNR Limit of practical interest

2.5 Comparison between Coherent and Direct-Detection Dystems

Coherent-transmission systems offer three main advantages over systems using direct detection [1]:

1. Shot-noise limited reception can be achieved, even at low received-signal powers, simply by increasing the LO power.
2. Intensity, frequency, or phase modulation modes can be used, whereas DD systems are limited to intensity modulation.
3. The excellent frequency selectivity that can be achieved using electrical post-photo-detector filters is translated into the optical domain by the coherent-detection technique. This enables the realization of dense wavelength-division-multiplexing schemes for multi-channel transmission, or channel-selection schemes.

We now review these advantages in turn. The first is of reduced importance for systems operating at a wavelength of 1550 nm, now that effective optical amplifiers are available. However, if we consider passive optical networks, this remains a valuable characteristic of coherent systems. It is also of importance to systems operating at the 1300 nm wavelength, in order to take advantage of the silica-fiber dispersion minimum, and the low noise and high output power of semiconductor-laser-pumped Nd-YAG lasers. This is also of interest in systems operating at a 850 nm wavelength, for compatibility with GaAs microwave monolithic-integrated-circuit (MMIC) technology. Effective optical-fiber amplifiers are not available for either of these wavelengths [1].

The alternative strategy for shot-noise-limited IMDD systems of increasing the source power is limited by the onset of stimulated-Brillouin scattering (SBS) and other nonlinear effects in optical fiber. Thus, coherent transmission remains of interest for long-distance systems, where high SNR is required.

The second advantage enables SBS to be reduced by broadening the optical-signal bandwidth beyond the SBS linewidth (~20 MHz at the 1550 nm wavelength), using frequency or phase modulation. Use of frequency or phase modulation also enables a tradeoff to be made between optical-signal bandwidth and received SNR; this is the topic of Chapter 3 and constitutes the motivation for finding the FM threshold.

The importance of the third advantage depends upon whether the ability to switch among many sources carried on the same fiber is required.

There are three main disadvantages of coherent-transmission systems, relative to those using direct detection:

1. The frequencies of the LO laser and signal must be controlled to differ by the required IF, whereas in the DD system, it is only necessary that the source laser frequency be suitable for the photodiode used.
2. The linewidths of source and LO lasers must be suitable for the modulation mode used, whereas in DD systems, the required source linewidth is mainly determined by the optical fiber dispersion penalty.
3. The polarization state of the LO and signal must be matched at the photodiode.

However, none of the above three issues are fundamental and can be circumvented with today's technology.

Polarization matching can be achieved by active-polarization control of the LO signal for maximum detected-signal output [27], or using polarization-diversity reception [25].

While the disadvantages of coherent-transmission systems can all be overcome, the penalty is an increase in system complexity relative to DD systems. Whether the coherent-system approach should be used in a particular application therefore depends upon whether the performance advantages are sufficient to justify the increase in complexity.

Chapter 3

3 Frequency Modulation Coherent Detection (FMCD)

3.1 Introduction

A crucial part of this thesis is to investigate further the FM type of CD. In the foregoing chapter we presented the advantages of CD and we concluded that the increased complexity of CD with respect to DD systems has to be justified by superior performance. In this part of the thesis, we will investigate the performance of FM. We study both the conventional form, which uses an electrical discriminator, and the all-optical form, which employs an optical discriminator (O-D).

The chapter starts in Section 3.2 by introducing the reader to the fundamental characteristics of FMCD, deriving the known formula for the FM signal field, the resulting photocurrent, and the CNR of FMCD. After this section, the chapter is divided into two parts. Section 3.3 focuses on the conventional FM discriminator, which has been studied to some extent in the literature [7] and Section 3.4 focuses on FMCD with O-D in which a Mach Zehnder interferometer is used, which is a significant extension of the initial approach of [16].

Within Section 3.3, we follow closely the previously studied FMCD analysis in [7], re-deriving the simplified formula for the SNR of FM assuming that the CNR is high enough for some approximation to be made (weak noise assumption). This formula is actually the same for radio frequency FM receivers [9]. Next, by considering the Rician approach that is mentioned in [9] and combining it with the simplified formula of [7] we are able to produce a full formula for the SNR of FM and determine the FM threshold. This is a significant result (in Section 3.3.5) and provides the maximum SNR for a given optical bandwidth, or inversely, the maximum SNR for fixed CNR. In Section 3.3.6 we comment on the results obtained for a signal of specific second order characteristics, and show that the threshold does not depend strongly on the second order

characteristics of the signal. Then, in Section 3.3.7, we discuss the literature [9], [11], [12] on FM feedback systems and highlight that the threshold extension phenomenon, which is common practice in FM receivers, can also be used for FMCD yielding a lower threshold and therefore allowing us to use more bandwidth expansion under the same CNR. We end the conventional FM section in 3.3.8 by calculating how much accuracy we sacrifice in the rest of the thesis when we use the known simplistic SNR formula of FM, instead of the full one that we derived, to describe the operation of FM near its peak performance.

In the second half of this chapter, Section 3.4, we answer the question of where the electrical-optical interface in FMCD should be. By attempting to use an O-D instead of an electrical discriminator, we extend the analysis of [16] on O-Ds to derive that the performance of the FMCD O-D and show that it is actually the same as IMDD and much worse than that of conventional FMCD. This is expected since we lose all the benefits of weak noise suppression because we demodulate our signal before detecting and thus the noise is not suppressed as in the conventional case.

A comparison among the different modulation schemes is offered in Section 3.5 where conventional FMCD is compared with IMDD and FMCD O-D and a brief numerical example is given.

The chapter concludes with Section 3.6 on a discussion of the results.

3.2 Fundamentals of FMCD

An optical FMCD system is a direct emulation of RF FM broadcast and communications systems in the optical domain and uses the same basic concepts. In an optical link, the laser output provides a carrier of very high frequency (200-400 THz). As with RF carriers, there are two independent characteristics - amplitude and phase or frequency - which can be modulated by the signal to be transmitted. In optical FM (OFM), the carrier frequency deviates from its central frequency proportionally to the amplitude of the signal to be transmitted. Both random and impulse noise can be reduced by using a wide passband receiver containing an amplitude limiter, which constitutes a conventional receiver which we will investigate thoroughly in Section 3.3. Therefore, regarding conventional FM and received CNR, much greater than unity, FM systems can provide improved SNR relative to amplitude modulated systems [2], [7], [10], [13], [14].

The OFM system has three main features which distinguish it from its RF equivalent. First, the optical carrier frequency is very high relative to the bandwidth of the signal to be transmitted. As a result, a large frequency deviation relative to the signal bandwidth can easily be achieved with good linearity. On the other hand, a small relative carrier frequency drift will be significant compared with the signal bandwidth. Second, because no photodetector has a bandwidth matching the optical carrier frequency, either demodulation in the optical domain or down-conversion of the received signal from the optical frequency to a much lower intermediate frequency is needed. Third, due to the high optical carrier frequency, the laser generates far more phase/frequency noise than an RF oscillator and we consider that this phase noise equal to noise since it can be cancelled as reported in [31].

In an FMCD link, as shown in Fig. 2-2, the signal electric field at the photodiode is

$$E_s = |E| \exp\left\{ j\left[\omega_s t + 2\pi \cdot \Delta f \int_0^t m(\tau) d\tau + \phi_s(t) \right] \right\} \tag{3.1}$$

where Δf is the maximum frequency deviation, and in our case, corresponds to the optical modulation bandwidth; $\varphi_s(t)$ is a random initial phase and $m(t)$ is the normalized signal varying from -1 to 1.

The local oscillator electric field is

$$E_{LO} = |E_{LO}| \exp\{j[\omega_{LO} t + \phi_{LO}(t)]\} \tag{3.2}$$

with ω_{LO} being the local oscillator frequency, and $\phi_{LO}(t)$ the local oscillator phase.

Defining the intermediate frequency (IF), $\omega_{IF} = \omega_s - \omega_{LO}$, the signal incident on the photodiode is

$$V_{in} = \left[|E| \exp\left\{ j\left(2\pi \cdot \Delta f \int_0^t m(\tau) d\tau + \phi_s(t) \right) \right\} + |E_{LO}| \exp\{ j(-\omega_{IF} t + \phi_{LO}(t)) \} \right] \exp\{ j\omega_s t \}. \tag{3.3}$$

For $\omega_{IF} << \omega_s$ so that the receiver can handle the incident optical bandwidth, the output current from the photodiode is proportional to $V_{in} V_{in}^*$, so that, taking into account that $|E|^2 = P_u$ and $|E_{LO}|^2 = P_{LO}$, the current is given by

$$\boxed{I(t) = I_0 + I_s \cos\left[\omega_{IF} t + 2\pi \cdot \Delta f \int_0^t m(\tau) d\tau + \phi_s(t) - \varphi_{LO}(t) \right]} \tag{3.4}$$

where $I_0 = R(P_{LO} + P_u)$, $I_s = 2R\sqrt{P_{LO} P_u}$, and the responsitivity of the diode $R = \dfrac{\eta q}{h\nu}$.

The above equation can be rewritten in terms of signal and LO power as:

$$I(t) = R(P_{LO} + P_u) + 2R\sqrt{P_{LO} P_u} \cos\left[\omega_{IF} t + 2\pi \cdot \Delta f \int_0^t m(\tau) d\tau + \phi_s(t) - \varphi_{LO}(t) \right]. \tag{3.5}$$

The first term represents direct detection of the signal and LO, respectively. The second term is of more interest for two reasons. Its amplitude is proportional to the square root of the local-oscillator power. Thus, the detected signal can be made larger simply by increasing the local

oscillator power. Secondly, because the detected signal is proportional to the square root of the source-output power, it is obvious that AM and PM can also be deployed, but this is beyond the scope of this chapter.

We now define a quantity which will be widely used in the rest of the thesis: the FM modulation index

$$\beta = \frac{\Delta f}{B}$$

where Δf is the optical bandwidth, and B is the signal's bandwidth (i.e. the bandwidth of $m(t)$).

In Fig. 3-1, we present the bandwidth expansion that occurs in the FM case. In this figure, we observe that FM has the ability of being able to expand the signal's bandwidth, and, as we will see in the following subsections, the performance gain by doing so can be significant. We also note that the bandwidth can conversely be suppressed and therefore it is possible to have β<1. The modulation index cannot, on the other hand, increase infinitely. This last point is related to the FM threshold phenomenon, which we will discuss in great detail in later sections.

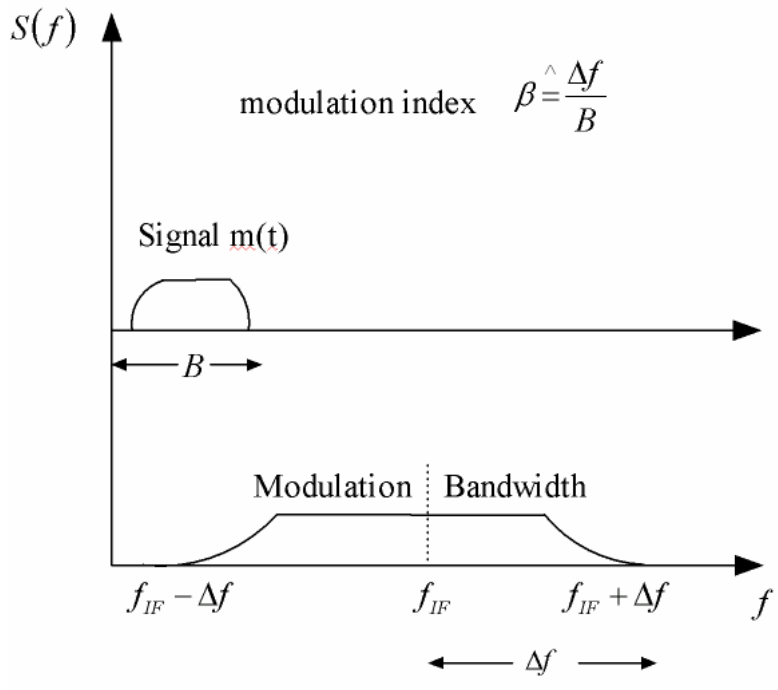

Figure 3-1: FM Bandwidth Expansion

We proceed now to define the second most important quantity related to FM, which is the carrier-to-noise–ratio (CNR). The CNR is defined as the power of the carrier divided by the power of the

noise induced in the bandwidth of the signal [1], [9]. The sources of noise in a coherent system are similar to those in a direct-detection system, which are mentioned in Section 2.3

Recalling (3.4), the CNR after photo-detection is

$$CNR = \frac{I_s^2 / 2}{N_0 B} \tag{3.6}$$

where I_s is the amplitude of the modulated carrier in the IF, N_0 is the one sided noise spectral density, and B is the signal *m(t)*'s bandwidth, as shown in Fig. 3-1. The noise spectral density N_0 is the sum of the thermal, shot, and intensity noise components, as discussed in Section 2.3

$$N_0 = \frac{4kT}{R_L} + 2q\left(I_0 + I_{dk}\right) \tag{3.7}$$

Where $I_0 = R\left(P_{LO} + P_u\right)$, I_{dk} is the negligible dark current. As a result, by increasing the LO power, shot noise limited reception is obtained, giving

$$CNR = \frac{I_s^2 / 2}{N_0 B} = \lim_{P_{LO}\to\infty}\left[\frac{2R^2 P_{LO} P_u}{2qR\left(P_{LO} + P_u\right)B}\right] = \lim_{P_{LO}\to\infty}\left[\frac{RP_{LO} P_u}{q\left(P_{LO} + P_u\right)B}\right] = \frac{RP_u}{qB} = \frac{\frac{\eta q}{h\nu} P_u}{qB}$$

$$\boxed{CNR = \frac{\eta P_u}{h\nu B} = \frac{\eta |E|^2}{h\nu B}} \tag{3.8}$$

The CNR derived in (3.8) shows that the LO power cancels out for high LO power and the resulting CNR depends only on the initial signal power P_u and the induced shot noise. This derived CNR will be widely used in the rest of this thesis. Some typical CNR values are presented in Table 3-1.

CNR (dB)	$\mathbf{P_u}$ (dBW)
0 -- {-111.472} 5 -- {-106.472} 10 -- {-101.472} 15 -- {-96.4723} 20 -- {-91.4723} 25 -- {-86.4723} 30 -- {-81.4723} 35 -- {-76.4723} 40 -- {-71.4723} 45 -- {-66.4723} 50 -- {-61.4723} 55 -- {-56.4723} 60 -- {-51.4723} 65 -- {-46.4723} 70 -- {-41.4723} 75 -- {-36.4723} 80 -- {-31.4723}	

Table 3-1: Shot noise limited CNR for η=0.9, B=50MHz according to (3.8)

3.3 Conventional FM Receiver

3.3.1 Setup

The conventional FM receiver has been extensively studied for radio frequencies [8]. A good reference for conventional FM receivers can be found in [9]. In this section, we use the structure of the conventional FM receiver studied in [9] adapted to the optical domain. The following analysis follows closely that of [9] and verifies the results of [7].

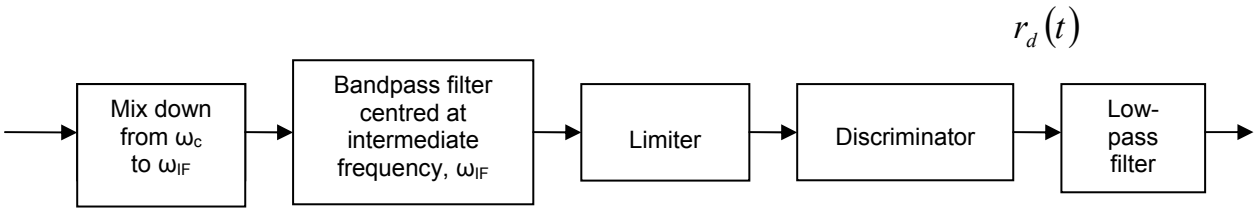

Figure 3-2: Conventional FM receiver

A conventional FM discriminator is shown in Fig. 3-2. We first mix the received signal down to intermediate frequency ω_{IF} . A bandpass filter with a bandwidth large enough to pass the modulated signal nearly undistorted is the next component. A limiter removes any amplitude variations. The discriminator has an output proportional to the difference between the instantaneous frequency and the intermediate frequency. Finally, a low-pass filter removes as much of the remaining noise as possible.

3.3.2 Weak Noise Analysis

For the conventional FM receiver described above, we now re-derive the classical FM weak noise analysis [7], [9]. At the FM discriminator output – that is, after discriminating the argument of (3.4) - the mean squared signal current assuming no detector gain is:

$$\overline{i_s^2} = 4\pi^2 \Delta f^2 \overline{m^2(t)} \quad (3.9)$$

The noise process at the input to the discriminator is bandlimited because of the restricted bandwidth that the discriminator. Thus, we can decompose the noise into two low-pass processes $(n_c(t), n_s(t))$ multiplying quadrature carriers and using the representation

$$\begin{aligned} I(t) &= I_S \cos[\omega_{IF} t + x(t)] + n(t) \\ I(t) &= [I_S + n_c(t)\sqrt{2}]\cos[\omega_{IF} t + x(t)] + n_s(t)\sqrt{2}\sin[\omega_{IF} t + x(t)] \\ I(t) &= \left[\sqrt{(I_S/\sqrt{2} + n_c(t))^2 + n_s^2(t)}\right]\sqrt{2}\cos\left[\omega_{IF} t + x(t) + \tan^{-1}\left(\frac{n_s(t)}{I_s/\sqrt{2} + n_c(t)}\right)\right] \end{aligned} \tag{3.10}$$

where $x(t) = 2\pi \cdot \Delta f \int_0^t m(\tau) d\tau$ and having assume that $\phi_s(t) = 0, \varphi_{LO}(t) = 0$ due to the phase cancellation reported in [31].

The one sided spectral density of the quadrature components $n_s(t)$, $n_c(t)$ is

$$S_{n_c}(\omega) = S_{n_s}(\omega) = \begin{cases} N_0 & ,\omega < B \\ 0 & ,\omega > B \end{cases}. \tag{3.11}$$

Next, the limiter removes the envelope variations. The discriminator output is the instantaneous frequency deviation of the sinusoid from ω_{IF}. Differentiating the argument and dropping the ω_{IF} term, we obtain the argument of (3.10) differentiated and under the weak noise assumption (3.13)

$$r_d(t) = \dot{x}(t) + \frac{\dot{n_s}(t)}{I_s/\sqrt{2}}. \tag{3.12}$$

The ***weak noise assumption,*** which was mentioned and used in (3.12), implies that $N_0 B < I_s^2 / 2$, and consists of the simplification below. This simplification has been used in (3.12) to simplify the inverse tangent term in (3.10)

$$\tan^{-1}\left(\frac{n_s(t)}{I_s/\sqrt{2}+n_c(t)}\right) \approx \frac{n_s(t)}{I_s/\sqrt{2}+n_c(t)} \approx \frac{n_s(t)}{I_s/\sqrt{2}} \quad . \tag{3.13}$$

The above approximation is valid except for certain improbable time intervals during which $|n_s(t)|$ and/or $|n_c(t)|$ assume values much larger than usual. Excluding such intervals from consideration, the noise spectral power density, after passing the discriminator, can be calculated as

$$\begin{aligned}
\overline{n_{new}^2} &= \int_0^B S_{\dot{n}_s(t)}(f)\,df \\
&= \frac{1}{\left(I_s/\sqrt{2}\right)^2}\int_0^B N_0 \left|j2\pi f\right|^2 df \\
&= \frac{(2\pi B)^2}{3\left(I_s^2/2\right)} N_0 B \\
&= \frac{1}{3}(2\pi B)^2 \frac{N_0 B}{I_s^2/2} \\
&= \frac{1}{3}(2\pi B)^2 \frac{1}{CNR}
\end{aligned} \tag{3.14}$$

where $S_{\dot{n}_c(t)}(f)$ is the spectral density of the discriminated quadrature in-phase component of the noise, and $H(f) = j2\pi f$ the discriminator transfer function.

The SNR of an optical FMCD link using (3.9) and (3.14) can now be expressed as

$$SNR_{FMCD} = \frac{\overline{i_s^2}}{n_{new}^2}$$

$$= \frac{4\pi^2 \Delta f^2 \cdot \overline{m^2(t)}}{\frac{1}{3}(2\pi B)^2 \frac{1}{CNR}}$$

$$= 3 \cdot \left(\frac{\Delta f}{B} \right)^2 \overline{m^2(t)} \cdot CNR$$

$$\boxed{SNR_{FMCD} = 3 \cdot \beta^2 \cdot \overline{m^2(t)} \cdot CNR} \qquad (3.15)$$

where CNR is defined as in the shot noise limited reception of (3.8), and $\beta = \frac{\Delta f}{B}$ is the bandwidth expansion as defined before.

This is a typical SNR formula for FM, as derived in [7], [9], and shows that the SNR increases when either the CNR increases or the optical bandwidth is expanded. Also, the dependence of the SNR on the bandwidth expansion is of second order. Therefore, expanding the optical bandwidth is a wanted way of increasing the SNR of FM. However, this expression becomes invalid when the weak noise assumption fails to hold and then the approximation of (3.13) cannot be made. In this case, the phase noise cannot be calculated as in the above derivation and (3.15) fails to hold. This consists what is called the event of anomaly and it will be the topic of the following section. We also account for the possibility of anomaly in subsequent sections.

3.3.3 Probability of Cycle Skipping for Conventional FM

The analysis that we carried out above is only valid under the weak noise assumption; that is, when $N_0 B << I_s^2 / 2$. This assumption eventually breaks down as Δf increases, which can be understood by realizing that by increasing Δf, the FM system introduces more noise into the spectrum so that as degradation in SNR performance occurs, and a threshold phenomenon is consequently observed, which is directly related to the probability of cycle skipping that is analyzed in this section. This was observed in the early days of FM. Rice developed a useful model for the discriminator near its threshold by deriving the probability of anomaly [9]. His results on threshold behaviour compare favourably with experimental results [12].

The mechanism leading to anomalies with conventional FM receivers is inherent in the behaviour of the signal phase at the limiter-discriminator input. In the absence of modulation, we have used the approximation

$$\tan^{-1}\left(\frac{n_s(t)}{I_s/\sqrt{2}+n_c(t)}\right) \approx \frac{n_s(t)}{I_s/\sqrt{2}+n_c(t)} \approx \frac{n_s(t)}{I_s/\sqrt{2}} \tag{3.16}$$

But this approximation is valid only during intervals over which both $|n_s(t)|$ and $|n_c(t)|$ are small in relation to I_s, and even with weak noise, these conditions will occasionally be violated.

The unmodulated carrier can be represented as a rotating phasor, as shown in Fig. 3-3a. The frequency is just the rate of rotation, as shown in Fig. 3-3b. The noise vector adds onto the signal vector, as shown in Fig. 3-3c. Since the signal vector is rotating at a constant rate, we can simply plot the relative rotation of the total vector with respect to the signal vector. This is shown in Fig. 4d. When the noise vector is small (i.e., the weak noise assumption is invoked), as indicated in Fig. 3-3e, it causes a small perturbation in the instantaneous frequency, as shown in Fig. 3-3f. If the noise vector is large, the received vector circles the origin, as shown in Fig. 3-3g. This causes a 2π phase error (i.e., a cycle skip). If the encirclement is rapid, we can treat it as an approximate step in phase which leads to a narrow pulse in instantaneous frequency, as shown in Fig. 3-3h. The waveform in Fig 3-3h is the output of the low-pass filter.

Following Rice's arguments, we can estimate the probability of cycle skipping (or anomaly), denoted by $P[A]$; that is, that at least one encirclement occurs during the interval [0, 1/2B]. This analysis is extensively carried in [9, p. 663-664]. The resulting probability of anomaly is:

$$P[A] = \frac{1}{\sqrt{3}}(\beta + 2)\frac{e^{-CNR/(\beta+2)}}{\sqrt{4\pi \cdot CNR/(\beta + 2)}} \cdot \tag{3.17}$$

Commenting on (3.17), we observe that by increasing β the probability of anomaly becomes greater due to the exponential influence mainly, and therefore increasing the optical bandwidth induces more cycle skips. This is something expected since more noise accumulates inside the optical bandwidth. On the other hand, by decreasing the CNR we again enter the cycle skipping phase because of the low CNR which renders the weak noise assumption mentioned in (3.13) invalid. These two remarks represent two different views of the same threshold that leads to the cycle skipping condition.

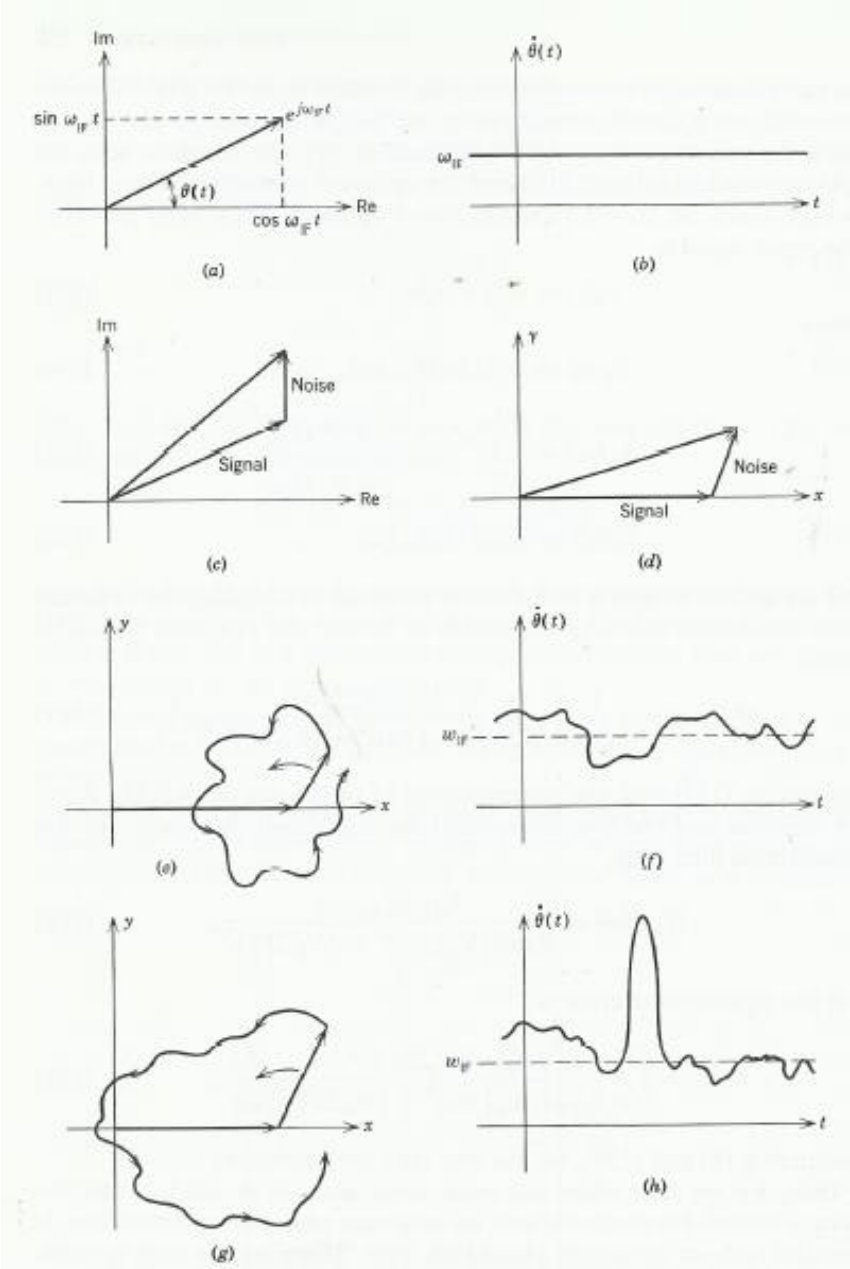

Figure 3-3: Phasor diagrams, [11]

(a) Signal phasor.

(b) Instantaneous frequency.

(c) Signal and noise phasors.

(d) Rotating coordinate system (carrier eliminated).

(e) Small noise (no origin encirclements).

(f) Instantaneous frequency.

(g) Origin encirclement, large noise.

(h) Instantaneous frequency

3.3.4 Complete SNR of FMCD

A one-parameter characterization of the performance of FM may be obtained by combining the mean square error in the absence of anomalous errors with the minimum mean square error (MMSE) contributed by the anomalies themselves. When an anomaly occurs, $\hat{m}$, the estimation of our signal *m*, is equally likely to be anywhere in the interval [-1, 1], regardless of the value of m. Furthermore, the anomaly event is independent of m, and thus $\hat{m}$ is independent of *m*.

$$E\left[\left(m-\hat{m}\right)^2 \mid Anomaly\right] = E\left[m^2 \mid A\right] + E\left[\hat{m}^2 \mid A\right] = \overline{m^2} + \frac{1}{3} \tag{3.18}$$

By dividing the mean square signal power $\overline{m^2(t)}$ by SNR_{FMCD} (3.15) in the absence of anomalies, we obtain the mean square noise power for signal *m(t)*. When dividing the mean square noise power by the signal's bandwidth *B* we obtain in (3.19) an expression for the minimum mean square error

$$E\left[\left(m-\hat{m}\right)^2 \mid weak-noise, no\_anomaly\right] == \frac{\overline{m^2(t)}}{SNR_{FMCD}\cdot B} = \frac{1}{3}\frac{1}{\beta^2}\frac{1}{CNR}\frac{1}{B} \tag{3.19}$$

We now obtain the following expression for the total mean square error based on (3.18) and (3.19)

$$\begin{aligned}\overline{\varepsilon_T^2} &\approx E[\left(m-\hat{m}\right)^2 \mid A'] \cdot (1-P[A]) + E[\left(m-\hat{m}\right)^2 \mid A] \cdot P[A] \\ &\approx \left[\frac{1}{3}\frac{1}{\beta^2}\frac{1}{CNR}\frac{1}{B}\right]\cdot\left(1-P[A]\right) + \left[\overline{m^2}+\frac{1}{3}\right]\cdot P[A]\end{aligned} \tag{3.20}$$

where A' is the complement of the event of anomaly.
The full formula for the SNR is now found to be:

$$SNR = \frac{\overline{m^2}}{\overline{\varepsilon_T^2}\cdot B} = \frac{\overline{m^2}}{\left[\frac{1}{3}\frac{1}{\beta^2}\frac{1}{CNR}\right]\cdot\left(1-P[A]\right) + \left[\overline{m^2}+\frac{1}{3}\right]\cdot P[A]\cdot B}. \tag{3.21}$$

By substituting in some boundary values for the probability of anomaly, we have:

For $P[A]=0$, (3.21) implies $SNR = 3\beta^2 \cdot \overline{m^2} \cdot CNR$ same as in (3.15).

For $P[A]=1$, (3.21) implies $SNR = \dfrac{\overline{m^2}}{\overline{m^2}+\dfrac{1}{3}}$, which is independent of the CNR because we have cycle skipping and we are guessing our signal. The weak noise assumption is no longer valid and the CNR cannot yield any change to the performance inside the phase of cycle skipping. Even for low CNR and more intense cycle skipping, we can only still guess the signal and thus even the lowest CNR cannot make performance worse.

3.3.5 FM Threshold Phenomenon

In order to be able to get some numerical results and provide a graphical representation of the FM threshold, we have to assume specific second order characteristics for the signal *m(t)*. Subsequently, in Section 3.4.6, we show that the threshold actually has a weak dependence on these characteristics.

For *m(t)*, which is normalized in [-1,1], we assume that it is also uniformly distributed in this range, which implies the second order characteristic $\overline{m^2(t)} = \frac{1}{3}$. The resulting mean square error of (3.18) is $E\left[\left(m - \hat{m}\right)^2 \mid Anomaly\right] = 2/3$. Then (3.21) becomes:

$$SNR = \frac{\overline{m^2}}{\overline{\varepsilon_T^2}} = \frac{1/3}{\left[\frac{1}{3}\frac{1}{\beta^2}\frac{1}{CNR}\right]\cdot\left(1 - P[A]\right) + \frac{2}{3}\cdot P[A]\cdot B} \tag{3.22}$$

where, for conventional FM receivers, the probability of error is defined in (3.17), but for completeness we present it below as well

$$P[A] = \frac{1}{\sqrt{3}}(\beta + 2)\frac{e^{-CNR/(\beta+2)}}{\sqrt{4\pi\cdot CNR/(\beta+2)}}.$$

The SNR in (3.22) is a function only of two parameters, namely the CNR and the modulation index β.

In Figure 3-4, the SNR is plotted as a function of these two parameters and we observe the FM threshold phenomenon. The three-dimensional graph allows us to see that for higher CNR we can achieve higher SNR by increasing the FM modulation index and thus further expanding the optical bandwidth. In Figure 3-5, we observe the FM threshold, which is defined as the value of CNR above which the probability of anomaly is practically 0. Below the FM threshold point, the noise signal may instantaneously have amplitude greater than that of the wanted signal and therefore applications may wish to operate within a margin above the FM threshold point (a few dB). For a certain values of the CNR, the SNR increases as the bandwidth expansion increases up to a maximum value (Figure 3-6), after which the noise accumulated in the expanded bandwidth decreases the SNR, as discussed.

Figures 3-5 and 3-6 actually represent cross-sections of Figure 3-4. Combining both of the constraints mentioned in the preceding paragraph - a required CNR above the threshold as presented in Figure 3-5 and a bandwidth expansion corresponding to the peak of Figure 3-6 - we conclude that we wish to operate on the right side slope of the three dimensional curve of Figure 3-4 and close to the peak SNR.

For a given CNR, if we wish to maximize the SNR performance we are required to choose the maximum bandwidth expansion, as can be seen in Figure 3-6. This $\beta_{\max}$ can be more formally defined as:

$$\beta_{\max} \stackrel{\wedge}{=} \left\{ \beta : \frac{\partial SNR\left(CNR, \beta, \overline{m^2(t)}\right)}{\partial \beta} = 0 \right\} \tag{3.23}$$

It is very difficult to get an analytical expression on $\beta_{\max}$ mainly because of the exponential nature of the probability of anomaly which affects the exponential dependence of $\beta_{\max}$ on CNR, as can be seen in Figure 3-7. Linear approximations within small regions of the CNR are possible but not a complete expression.

In Figure 3-7, the maximum value of the bandwidth expansion β is plotted as a function of the CNR and the corresponding calculated values are presented in Table 3-2. The β_{max} presented in this graph takes values close to unity for low CNR, and as the CNR increases we are able to utilize a higher β_{max}. Thus, we can expand the optical bandwidth more with a higher CNR. This has actually been the motivation behind FM: expanding β_{max} as much as possible to better utilize the available enormous bandwidth capacity of optical fibers, and consequently achieving higher SNR. Moreover, we can observe the exponential nature by which β_{max} increases as a function of the CNR.

Finally, Tables 3-2, 3-3 provide numerical values of β_{max} for a range of CNRs and fixed signal bandwidth. Table 3-2 corresponds to a signal of 1Hz and Table 3-3 to a signal of 50MHz. It is clear that the values of β_{max} for the 50MHz signal are lower and this is reasonable because a wider bandwidth means lower CNR according to (3.8). Thus, the lower the CNR, the less we can spread our signal as we have noticed in the previous graphs. It is not peculiar that the values of β are less than 1 in Table 3-3 since we can see in literature that indexes below 1 are realizable [p. 649, 9].

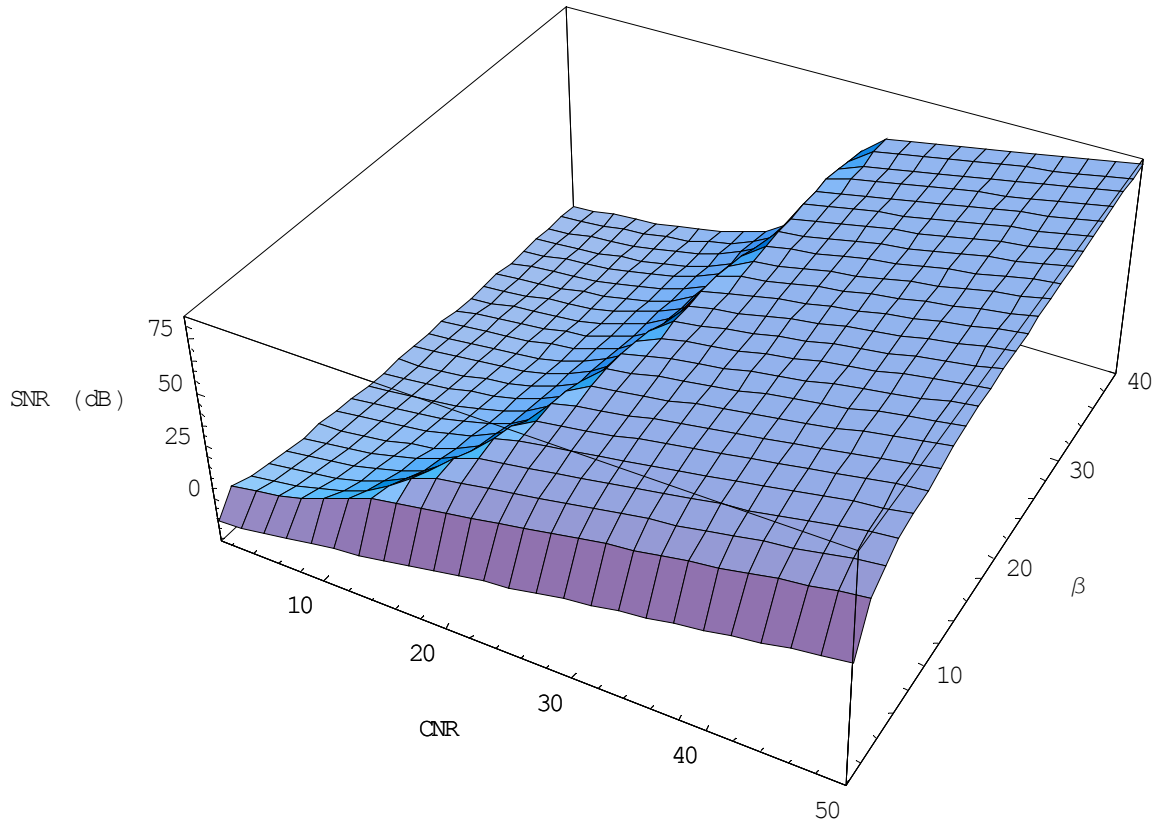

Figure 3-4: SNR of FM as a function of the CNR and the modulation index β for a conventional FM receiver

(*m(t)*uniformly distributed in [-1,1] and signal of 1Hz bandwidth)

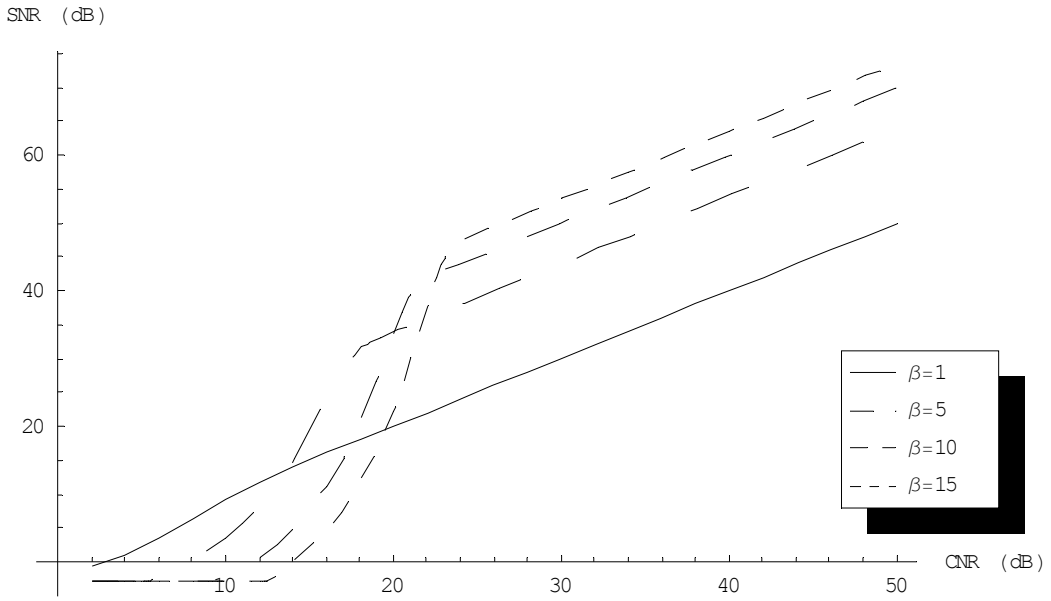

Figure 3-5: SNR as a function of CNR for different values of the modulation index β

(*m(t)* uniformly distributed in [-1,1] and signal of 1Hz bandwidth)

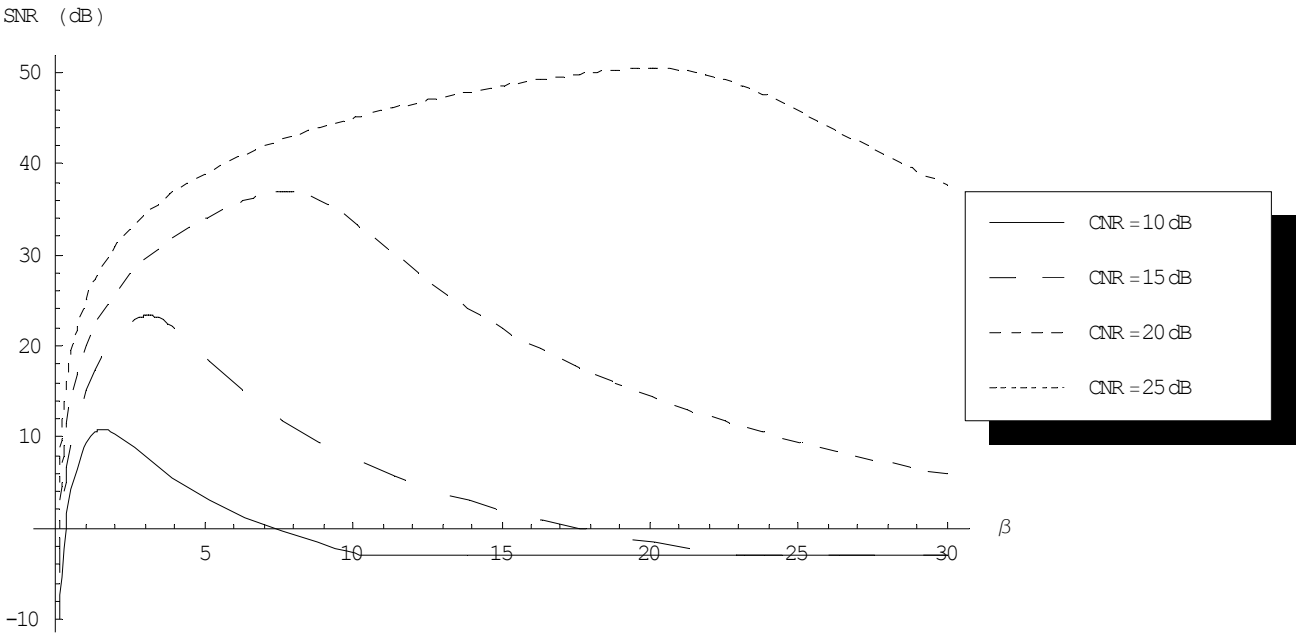

Figure 3-6: SNR as a function of β for different CNR values

(*m(t)* uniformly distributed in [-1,1] and signal of 1Hz bandwidth)

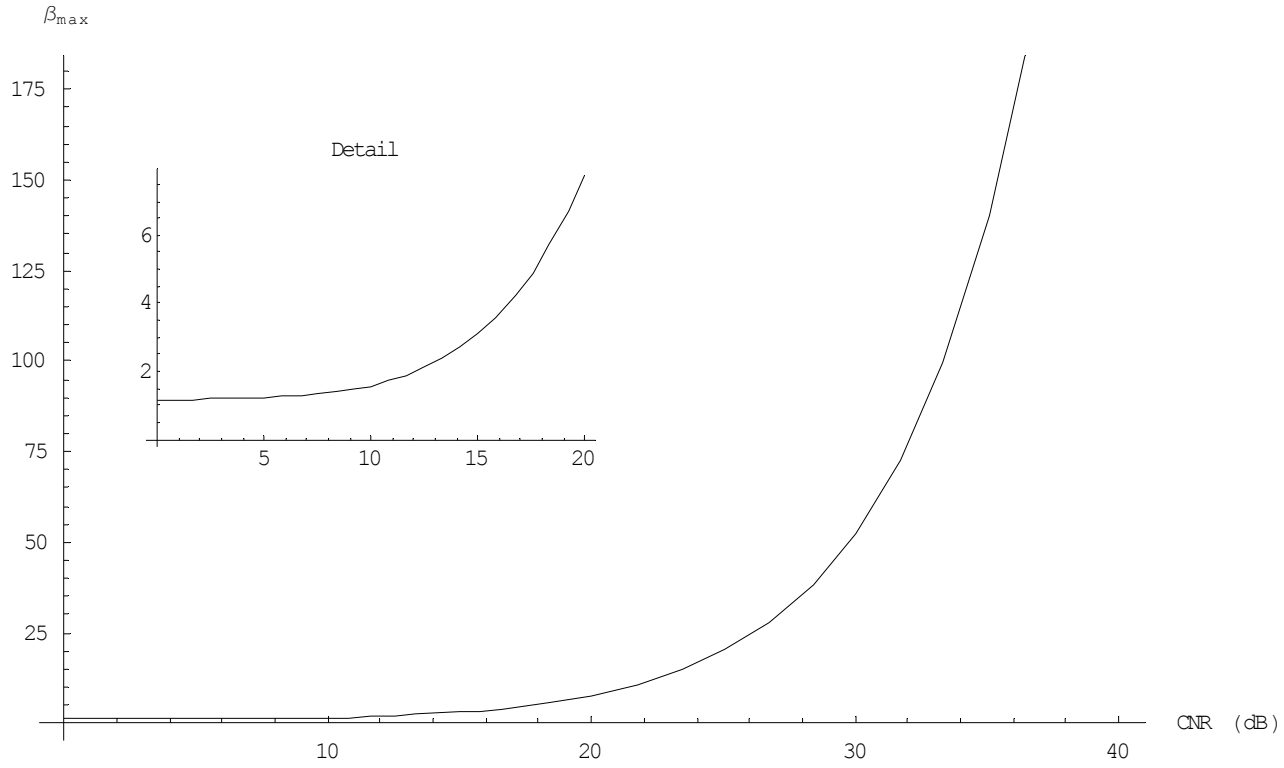

Figure 3-7: Maximum value of modulation index β_{max} as a function of CNR for conventional FM receiver with *m(t)*uniformly distributed in [-1,1]

(*m(t)* uniformly distributed in [-1,1] and signal of 1Hz bandwidth)

CNR (dB)	β_{max}
1	1.15846
2	1.17539
3	1.19021
4	1.20625
5	1.22703
6	1.25659
7	1.29974
8	1.36235
9	1.45151
10	1.57571
20	7.76616
30	52.0882
40	370.578
50	2825.88
60	22715.5
70	189497.

Table 3-2: β_{max} for different CNR values for a uniformly distributed signal in [-1, 1] of 1 Hz bandwidth

CNR (dB)	β_{max}
1	0.0037602
2	0.0037368
3	0.0038836
4	0.00399668
5	0.00417338
6	0.00444782
7	0.00487673
8	0.00555424
9	0.00665121
10	0.00849866
20	2.09859
30	26.9704
40	228.737
50	1917.15
60	16411.7
70	143280.

Table 3-3: β_{max} for different CNR values for a uniformly distributed signal of 50 MHz bandwidth

3.3.6 Dependence of Rician Approach on $<m^2(t)>$

In Section 3.3.5, we investigated the case in which *m(t)* is uniformly distributed. The second order statistics of *m(t)* seem to play a role in the Rician approach, especially in the value of β_{max}, judging from (3.21). The SNR has been plotted in Figure 3-8 for different values of the second order characteristics of *m(t)*. The conclusion of this section, judging also from the figures that present the FM threshold (Figures 3-9, 3-10), is that the threshold does not depend strongly on the second order characteristics. Thus, the whole analysis that we have carried so far for uniformly distributed signal *m(t)* remains valid for different distributions regardless of the second order characteristics. Regardless of the second order characteristics, our signal always has to be normalized to [-1,1] since the noise is also taken as normalized. As can be seen in Fig. 3-8, the FM threshold remains the same for variations of $m^2(t)$ from 0 to 4. Thus, even if we have slightly different second order characteristics, the β_{max} which we will calculate will be close to the real one, and very close to the peak performance of the FM. This weak dependence can intuitively be understood from (3.21), where the SNR depends linearly on $\overline{m^2(t)}$, whereas it depends exponentially on the CNR and β through the probability of anomaly term.

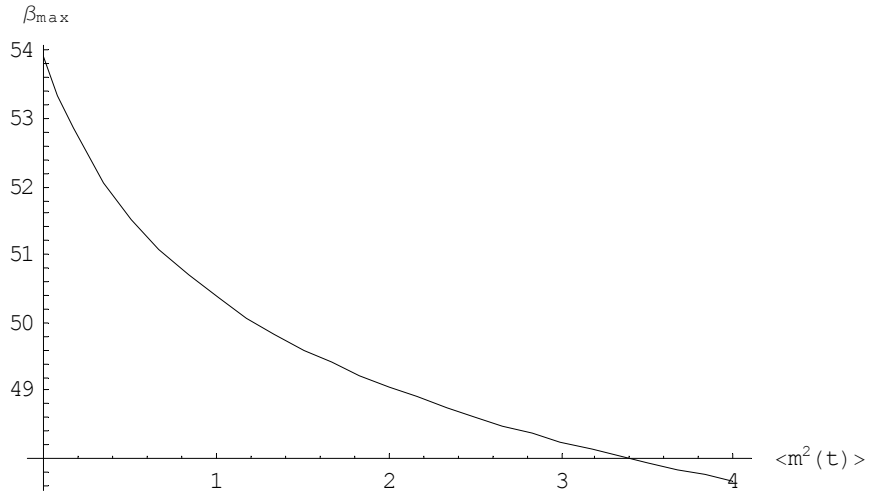

Figure 3-8: β_{max} for different second order characteristics of the unmodulated signal
(1Hz bandwidth, CNR=30 dB)

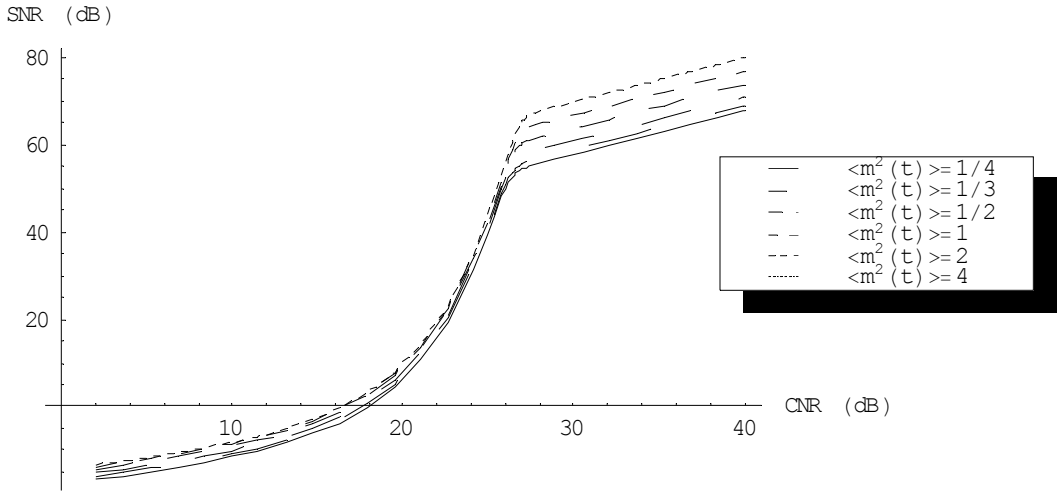

Figure 3-9: SNR for different second order characteristics of the unmodulated signal

(1Hz bandwidth, β=28 maximum value for 30dB CNR according to Table 3-2)

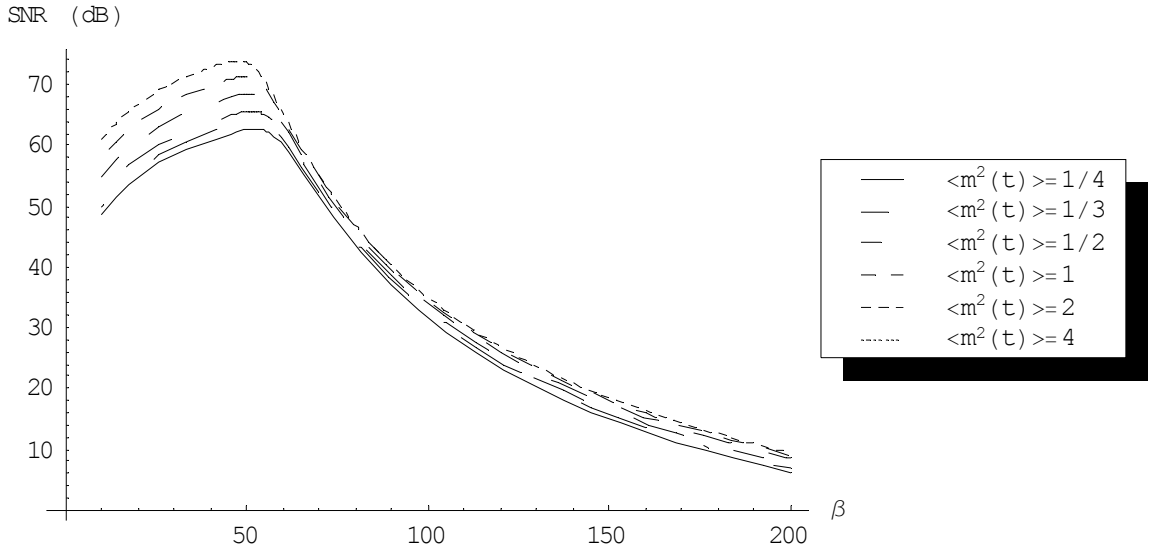

Figure 3-10: SNR for different second order characteristics of the unmodulated signal

(1Hz bandwidth, CNR=30 dB)

3.3.7 Optimum Angle Modulation Systems

The conventional FM receiver is not an optimum angle modulation system. An optimum modulation system's design can be approached by optimum linear filtering theory, in conjunction with either Wiener techniques or Kalman-Bucy techniques which take into account the type of power spectral density of the signal [11], [12]. However, above the threshold, the conventional discriminator with an optimum post-discriminator filter performs exactly like the optimum angle-modulation system. The only difference between the two systems is the location of the threshold [11].

In this thesis, we followed the classic Rician approach with an analytic expression for the discovery of the threshold by using the probability of anomaly for FM that Rice found [9]. There is substantial work in the bibliography which extends Rice's approach considering the message as a random process. For example, Chang studied the threshold for a Gaussian message with one-pole spectrum, and Rachel studied it for a second-order Butterworth spectrum [12]. The conclusion of the analysis [11], [12] is that the optimum system improves the threshold performance by 3 dB for the first-order Butterworth spectrum and by 6dB for the second-order Butterworth spectrum. These results have been verified by both theoretical analysis and simulation results [11].

In practice, in order to achieve optimality, engineers have tried to devise techniques to delay the onset of the FM threshold effect. These devices are generally known as FM threshold extension demodulators. Techniques such as FM feedback, phase locked loops and frequency locked loops have been used to achieve this effect.

As an example, though not a rigorous one because of the use of a lower bound, we demonstrate this effect in Figure 3-11 for feedback receivers versus the conventional FM receiver that we have studied. The classic Rician approach with an analytical expression for the probability of anomaly has also been deployed for this plot of the FM feedback receiver (FMFB), by using the notion that a lower bound for the probability of cycle skipping for feedback receivers would be the probability of anomaly for Frequency Position Modulation [9, pp.666]. In [9] it is not mentioned how tight this bound might be. Keeping this under considersation, it seems from Figure 3-11 possible to achieve better SNR under the same combination CNR when using a feedback receiver instead of a conventional one. We also observe from Figure 3-11 that above the threshold the conventional FM

receiver performs exactly like the FMFB system. The only difference in the two systems is the location of the threshold.

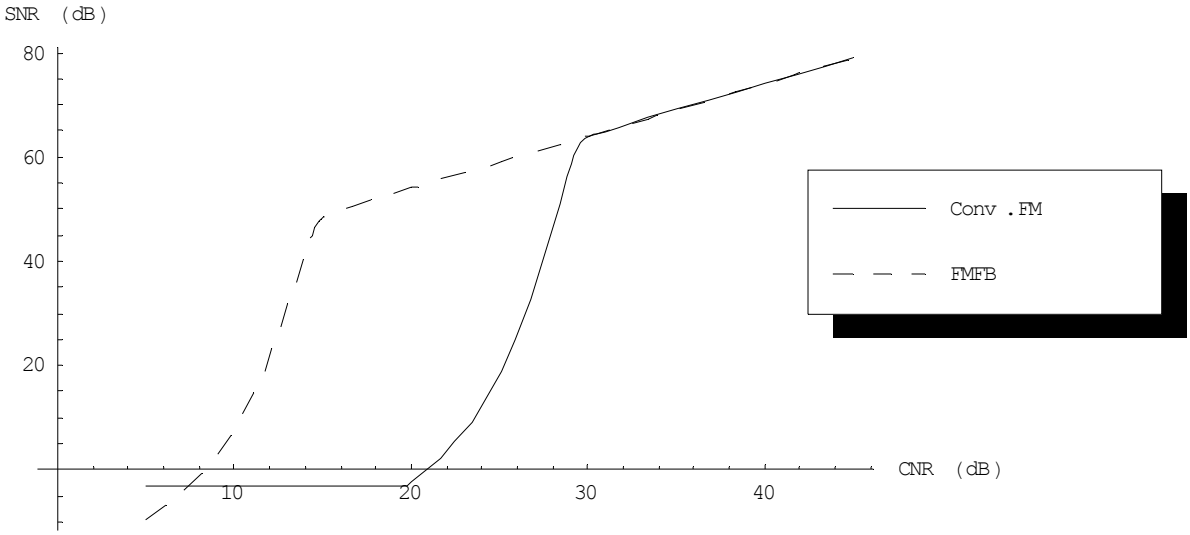

Figure 3-11: Threshold Extension using a Feedback Receiver (FMFB)

3.3.8 Approximation of SNR $_{\max,\ FMCD}$

The maximum SNR occurs at the peak of the graph presented in Fig. 3-4. The precise value of the SNR at this point is:

$$SNR_{\max} = \frac{\overline{m^2}}{\overline{\varepsilon_T^2}} = \frac{\overline{m^2}}{\left[\frac{1}{3}\frac{1}{\beta_{\max}^2}\frac{1}{CNR}\right]\cdot\left(1-P[A]\right)+\left[\overline{m^2}+\frac{1}{3}\right]\cdot P[A]\cdot B}. \tag{3.24}$$

In this section we wish to calculate the accuracy of approximating the above SNR_{max} of (3.24) with the SNR of (3.15) for $\beta = \beta_{\max}$, i.e.

$$SNR_{\max} = 3\cdot\beta_{\max}^2 \cdot\cdot CNR\cdot\overline{m^2(t)}. \tag{3.25}$$

As discussed in the previous section, (3.15) is valid for the area above the FM threshold, where negligible cycle skipping occurs, which means that $P[A]\approx 0$. We wish to know how accurate it is to use the simple expression in (3.25) in lieu of the more precise expression in (3.24). Figure 3-12 provides insight into this, as we plot the difference between (3.24) and (3.25). For every CNR, we use the $\beta_{\max}$ that corresponds to that CNR. The result is that our approximation is valid for high CNR, and is at most 6 dB different for the case of low CNR.

As for the second order characteristics of the signal, we can verify once again from Figure 3-12 that they play a negligible role in the analysis, yielding at most a difference of 1-2 dB.

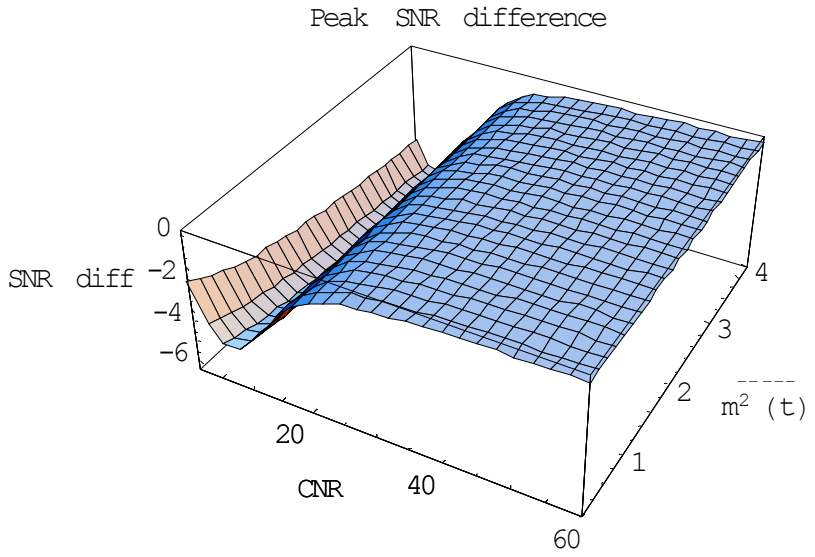

Figure 3-12: Peak SNR difference between true peak SNR and the approximation.

3.4 FMCD with O-D

In this subsection, an optical FM discriminator is employed in our system, whereas before an electrical (conventional) FM discriminator was used to perform discrimination after detection. The motive for this research has been the question of how much of the FM procedure we could transfer in the optical domain and create a more enhanced optical toolbox. The question which we will answer is whether moving the optical-electrical interface - by using an O-D instead of an electrical one - can yield a better SNR performance. It is not expected that using more optical components – in this case an O-D - will improve the SNR since maintaining the FMCD modulation until detection can provide significant suppression to the noise in the detection process. It is expected that FMCD O-D will be equivalent to IMDD. Evaluating the above argument is the goal of this section.

3.4.1 Configuration

The optical discriminator comprises a fiber optic Mach-Zehnder interferometer. The configuration, shown in Figure 3-13, has initially been studied in [16]. Unfortunately, the intuitive performance expectation from an optical discriminator is worse than that of the conventional discriminator because of the fact that the signal illuminates the photodiode after having being demodulated. The noise has, in this case, the same effect as in the IMDD case. Thus, we expect the results to be close to those of IMDD.

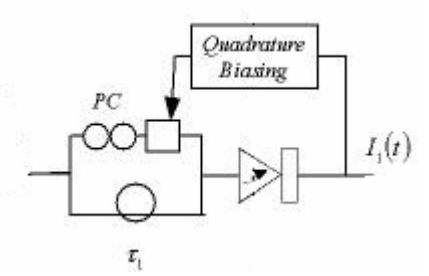

Figure 3-13: Optical Discriminator

The O-D shown above consists of a polarization controller (PC) and a phase shifter which are used to optimize discriminator performance by keeping the polarization steady and the interval of differentiation small enough for the O-D to perform accurate differentiation.

3.4.2 Analysis of O-D

We first note that the incident FM field on the typical Mach-Zehnder optical interferometer shown in Figure 3-13 is $E_{1a}(t)$, as in (3.1)

$$E_{1a}(t) = |E| \cdot \exp\left\{ j\left[\omega_s t + 2\pi \cdot \Delta f \int_{-\infty}^{t} [m(u)]du + \phi_1(t) \right] \right\}. \tag{3.26}$$

The photocurrent from the output square-law detector is given by:

$$I_1(t) = R\left| \frac{E_{1a}(t)}{\sqrt{2}} + \frac{E_{1a}(t-\tau_1)}{\sqrt{2}} \right|^2 \tag{3.27}$$

where we have assumed the presence of 3 dB directional couplers, matched output polarization states, and a differential time delay τ_1 for the recombining beams. We assume a quite laser inducing no laser phase noise

Substituting (3.26) into (3.27), the photocurrent can be expressed as:

$$\begin{aligned} I_1(t) &= R|E|^2 + R|E|^2 \cos\left[\omega_s \tau_1 + 2\pi\Delta f \left(\int_{-\infty}^{t_1} (m(u))du - \int_{-\infty}^{t-\tau_1} (m(u))du \right) \right] \\ &= I_s + I_s \cos\left[\omega_s \tau_1 + 2\pi\Delta f \left(\int_{-\infty}^{t_1} (m(u))du - \int_{-\infty}^{t-\tau_1} (m(u))du \right) \right] \end{aligned}. \tag{3.28}$$

where $I_s = R|E|^2$ so that and clearly P_u represents the carrier power as defined in Section 2.4 for IMDD and where we observe that the differential delay τ_1 also results in a phase shift $\omega_s \tau_1$ between the combining signal fields.

Fig. 3-14 shows how the photocurrent varies as a function of the differential delay shift. By adjusting the differential time delay (e.g., through the use of a phase shifter and locking circuit) or the average optical frequency, the interferometer can be held in quadrature (i.e., $\omega_s \tau_1 = 2\pi N \pm \frac{\pi}{2}$).

This condition is of importance since it allows the photocurrent to be made proportional to the phase difference $\Delta\phi(t) = 2\pi\Delta f\left(\int_{-\infty}^{t} m(u)du - \int_{-\infty}^{t-\tau_1} m(u)du\right) = 2\pi\Delta f \int_{t-\tau_1}^{t} m(u)du$ if $\Delta\phi(t)$ is kept small, allowing the O-D to operate as a discriminator by approximating

$$\cos\left(2\pi N \pm \frac{\pi}{2} + \Delta\phi(t)\right) \approx \sin(\Delta\phi(t)) \approx \Delta\phi(t).$$

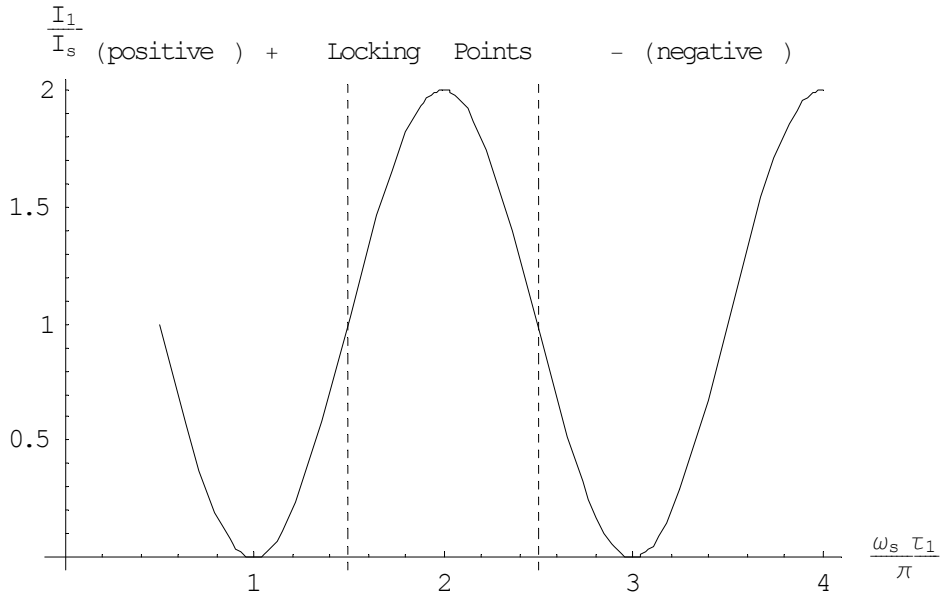

Figure 3-14: Variation of photocurrent at output of FM discriminator as a function of interferometer differential delay (τ) or input optical frequency (ωs)

Assuming quadrature biasing and a small phase difference $\Delta\phi(t)$, (3.28) can be rewritten

$$I_1(t) \cong I_s \pm 2I_s\pi \cdot \Delta f\left(\int_{-\infty}^{t} m(u)du - \int_{-\infty}^{t-\tau_1} m(u)du\right) \tag{3.29}$$

where the approximation $\sin(\Delta\phi(t)) \cong \Delta\phi(t)$ was made using the constraint $\Delta\phi(t) << 1$; this constraint can always be achieved by making the differential time delay τ_1 small enough. The plus or minus sign in front of the phase difference in (3.29) occurs since the quadrature condition can be satisfied by locking onto the positive or negative slopes, as shown in Fig. 3-15. Locking on a slope, either negative or positive, is not of particular interest as long as the value of the differential difference τ_1 is kept small and the above approximations are valid. In the following equations we show that the integral difference in (3.29) is proportional to the signal *m(t)*. Thus the Mach-Zehnder operates as a discriminator.

By neglecting the DC current term in (3.29) we can rewrite $I_1(t)$

$$
\begin{aligned}
I_1(t) &= \pm 2I_s\pi\cdot\Delta f\cdot\int_{-\infty}^{t_1}(m(u))du-\int_{-\infty}^{t-\tau_1}(m(u)))du \\
&= \pm 2I_s\pi\cdot\Delta f\cdot\left[\left(\int_{-\infty}^{t_1}m(u)du-\int_{-\infty}^{t-\tau_1}m(u)du\right)\right] \\
&\approx \pm 2I_s\pi\cdot\Delta f\left(\tau_1\frac{d\int_{-\infty}^{t}m(u)du}{dt}\right) \\
&\approx \pm 2I_s\pi\cdot\Delta f[(\tau_1\cdot m(t))] \\
&\approx \pm 2I_s\pi\cdot\Delta f[(\tau_1\cdot m(t))]
\end{aligned}
$$

where $dt = \tau_1$. (3.30)

Taking also into account the additive noise that comes from the detection process (shot noise limited), the photocurrent in (3.30) can be written

$$
\begin{aligned}
I_D^{'}(t) &= I_1(t)+n_1(t) \\
&= \pm 2I_s\pi\cdot\Delta f\tau_1\cdot m(t)+n_1(t)
\end{aligned}
\qquad (3.31)
$$

The noise spectral density is:

$$
S_{n_i}(f)=\begin{cases}N_0, & f<B\\ 0 & f>B\end{cases}\quad i=1,2 \qquad (3.32)
$$

where B is the signal's *m(t)* bandwidth. Thus, the noise power is $\overline{n_1^2(t)}=N_0B=2qI_sB$.

The signal-to-interference-and-noise ratio can be calculated as:

$$\left(\frac{S}{N}\right)_{optical} = \frac{\overline{I_1^2}}{\overline{n_1^2(t)}} = \frac{4I_s^2 \cdot \pi^2 \Delta f^2 \cdot \overline{m^2(t)} \cdot \tau_1^2}{N_0 B}$$
$$= 8\pi^2 \Delta f^2 \cdot \tau_1^2 \cdot \overline{m^2(t)} \cdot CNR_{O-D} \quad .$$
$$= 2\pi^2 \Delta f^2 \cdot \tau_1^2 \cdot \overline{m^2(t)} \cdot CNR \qquad (3.33)$$

where $CNR_{O-D} = \frac{I_s^2}{2N_0 B} = \frac{\eta |E|^2}{4hvB} = \frac{1}{4} CNR$ and $CNR = \frac{\eta |E|^2}{hvB}$ as defined in (3.8). This is in order to be able to make a fair comparison based on equal power fields at the end of the chapter.

We observe that the performance of the O-D in (3.33) is similar to that of IMDD (2.6) where $2\pi^2 \Delta f^2 \cdot \tau_1^2 = \frac{\gamma^2}{2} \Rightarrow \gamma = 2\pi \Delta f \cdot \tau_1$. This is expected since we have a linear channel and we can move the O-D from the receiver to the transmitter without changing the channel. The resulting system is a DD system and its performance is identical to IMDD.

Examining (3.33), if we try to increase, this will yield a smaller τ_1 because we want $\Delta\phi(t,\tau) = 2\pi\Delta f \left(\int_{-\infty}^{t_1} (m(u))du - \int_{-\infty}^{t-\tau_1} (m(u))du \right) << 1$ and this restriction is the one that derives the maximum frequency deviation threshold in this case. An interesting observation is the FM threshold phenomenon that appears in this case as well. If we increase the bandwidth expansion Δf , the *SNR* in (4.42) first increases until we reach the point that for one of the antennas, for example BS1, $\Delta\phi(t) = 2\pi\Delta f \int_{t-\tau_1}^{t} m(u - d_1 - t_1) + r(u - d_1 - t_3)du$ has increased more than the error tolerance of the approximation $\sin(\Delta\phi(t,\tau)) \approx \Delta\phi(t,\tau)$ and thus yields errors in the discrimination process. Then, in order to keep the approximations valid, we have to decrease the value of τ (τ takes discrete values for the quadrature condition to hold, i.e. $\omega_s \tau = 2\pi N \pm \frac{\pi}{2}$). Increasing the expanded bandwidth Δf further, we reach a point where τ has reached its smallest possible value, which is $\tau_{\min} = \frac{\pi}{2\omega_s}$, and further increasing the bandwidth Δf will make $\Delta\phi(t,\tau)$ larger and induce errors degrading the performance, much like the cycle skipping in the conventional FM

case. To summarize, an increase of Δf will ultimately decrease the SNR of FMCD O-D presenting a threshold phenomenon.

Before evaluating the limits of (3.33) we will assume a sinusoidal signal *m(t)* in Section 3.4.4. However, we first make a comparison with conventional FMCD in the following section.

3.4.3 Comparison with the Conventional FMCD

We derive the ratio of the SNRs for the best case scenario, which means maximum bandwidth expansion for the conventional FM case and **optimized choice of bandwidth expansion – time delay difference** for the optical discriminator case. By dividing (3.33) by (3.15) we obtain

$$\frac{\left(\frac{S}{N}\right)_{optical,\max}}{\left(\frac{S}{N}\right)_{conv,\max}} = \frac{2\pi^2 \Delta f_{opt}^2 \cdot \tau_{opt}^2}{3 \cdot \beta_{\max}^2} \tag{3.34}$$

where $\left(\Delta f_{opt}, \tau_{opt}\right) \in \left\{\left(\Delta f, \tau\right) : \Delta f \cdot \tau = \max\right\}$.

The ratio in (3.34) is further explored in the next section assuming a sinusoidal received signal *m(t)*. One special case is if we assume the ***same bandwidth expansion*** for both cases (not optimized case but realistic since we are using a bandwidth limited receiver) and a sinusoidal primary signal *m(t)*. Then Δf will cancel out, and this yields

$$\frac{\left(\frac{S}{N}\right)_{optical}}{\left(\frac{S}{N}\right)_{conv}} = \frac{2}{3}\pi^2 \cdot \left(\tau_1 \cdot B\right)^2 . \tag{3.35}$$

Assuming sinusoidal signal *m(t)* in (3.29), $\left(T = \frac{1}{B}\right)$, and by comparing the interval of integration τ_1 with its period *T,* we have $\omega_s \tau_1 = 2\pi N \pm \frac{\pi}{2} \Rightarrow \tau_1 B = \frac{\tau_1}{T} = \left(2\pi N \pm \frac{\pi}{2}\right)\frac{B}{\omega_s} << 1$. The very strong inequality holds because the optical carrier frequency ω_s is much larger than the frequency *B* of *m(t),* and this result also implies that the discriminator operates without errors because its integrating period is much smaller than the period of the signal. Finally, having proved that $\tau \cdot B = \frac{\tau}{T} << 1$, the SNR ratio will be:

$$\frac{\left(\frac{S}{N}\right)_{optical}}{\left(\frac{S}{N}\right)_{conv}} << 1 \tag{3.36}$$

verifying our intuition that the performance of the optical FM discrimination is far worse than that of the conventional discriminator.

3.4.4 Specific Case of Sinusoidal Signal

In (3.36) we proved that the FMCD O-D is much worse than conventional FM, but we desire to specify more precisely the performance of FMCD O-D. In order to find the optimum choice of τ_1, Δf in (3.33) we assume a normalized sinusoidal signal $m(t) = \cos(\omega_B t)$, where $\omega_B = 2\pi B$.

For the O-D to perform discrimination, we require $\Delta\phi(t,\tau) << 1$ so that $\sin(\Delta\phi(t,\tau)) \approx \Delta\phi(t,\tau)$ holds.We calculate $\Delta\phi(t,\tau)$ for the assumed sinusoidal signal:

$$\begin{aligned}
\Delta\phi(t,\tau) &= 2\pi\Delta f\left[\left(\int_{-\infty}^{t_1} m(u)du - \int_{-\infty}^{t-\tau_1} m(u)du\right)\right] \\
&= 2\pi\Delta f \int_{t-\tau_1}^{t} m(u)du \\
&= 2\pi\Delta f \int_{t-\tau_1}^{t} \cos(\omega_B t)du \\
&= \frac{2\pi\Delta f}{\omega_B}\cdot\left[\sin(\omega_B t)\right]_{t-\tau_1}^{t} \\
&= \frac{2\pi\Delta f}{\omega_B}\cdot\left[(\sin(\omega_B t) - \sin(\omega_B(t-\tau_1)))\right] \\
&= \frac{4\pi\Delta f}{\omega_B}\cdot\sin\left(\frac{\omega_B\tau_1}{2}\right)\cos\left(\omega_B\left(t-\frac{\tau_1}{2}\right)\right)
\end{aligned} \tag{3.37}$$

where ω_s is the optical carrier's frequency which is always much larger than that of the modulated signal ω_B, i.e. $\omega_s >>> \omega_B$. We could have approximated $\sin\left(\frac{\omega_B\tau_1}{2}\right) \cong \frac{\omega_B\tau_1}{2}$ above, but for precision we take the absolute value of the phase

$$\left|\Delta\phi(t,\tau)\right| \le \frac{4\pi\Delta f}{\omega_B}\cdot\left|\sin\left(\frac{\omega_B\tau_1}{2}\right)\right|\cdot\left|\cos\left(\omega_B\left(t-\frac{\tau_1}{2}\right)\right)\right|$$
$$\le \frac{4\pi\Delta f}{\omega_B}\cdot\frac{\omega_B\tau_1}{2}\cdot 1$$

Thus, $$\left|\Delta\phi(t,\tau)\right| \le 2\pi\left(\Delta f\cdot\tau_1\right) . \qquad (3.38)$$

We now explore the error tolerance for the discriminator's performance $\left(\Delta\phi(t,\tau) << 1\right)$. In other words, we wish to find the maximum value that $\Delta\phi(t,\tau)$ can have so that $Sin\left(\Delta\phi(t,\tau)\right) \cong \Delta\phi(t,\tau)$ within an x % error margin; that is, $\left|\frac{Sin\left(\Delta\phi(t,\tau)\right)-\Delta\phi(t,\tau)}{Sin\left(\Delta\phi(t,\tau)\right)}\right| \le x\%$, where x=1,2.

The figure below indicates the maximum value that $\Delta\phi(t,\tau)$ can take.

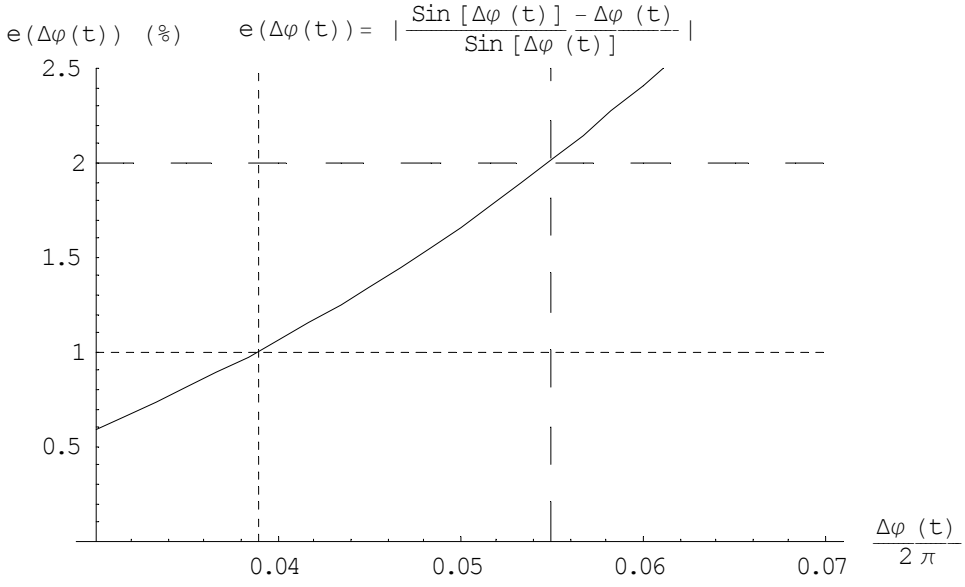

Figure 3-15: Optical Discriminator error tolerance

From Fig. 3-15 we can infer that

$$\Delta\phi_{\max,1\%}(t,\tau_1) = 3.9\% \cdot 2\pi \tag{3.39}$$

and

$$\Delta\phi_{\max,2\%}(t,\tau_1) = 5.5\% \cdot 2\pi \tag{3.40}$$

for N=0, 1, 2,...

Combining (3.38) with (3.39), (3.40) we derive the optimal values Δf_{opt}, τ_{opt} which maximize the $\left(\frac{S}{N}\right)_{optical}$:

$$\Delta f_{opt,1\%} \cdot \tau_{1opt,1\%} = 3.9\% \tag{3.41}$$

$$\Delta f_{opt,2\%} \cdot \tau_{1opt,2\%} = 5.5\% \tag{3.42}$$

As a side note, we observe that Δf in FMCD has its own limits in the optical fiber. We cannot expand a signal in FMCD more than the optical carrier's frequency $\frac{\omega_s}{2\pi}$ and we see below that with the calculated tolerance in (3.41), (3.42), these limits are not violated.

$$\omega_s \tau = 2\pi M \pm \frac{\pi}{2} \Rightarrow \tau = \frac{M \pm \frac{1}{4}}{f_s} \qquad \text{for M=0, 1, 2,…} \tag{3.43}$$

$$\Delta f_{\max,opt,2\%} = \frac{5.5\%}{\tau_{1\min,opt}} = \frac{5.5\% \cdot f_s}{M_{\min} \pm \frac{1}{4}} = 22\% \cdot f_s \tag{3.44}$$

As we see from (3.44), Δf occupies, in the worst case of a 2% error tolerance, 22% of the carrier's bandwidth. For operation wavelength of 1550 nm this would equal to 42 THz and clearly this frequency deviation cannot be achieved with current frequency tunable lasers. In [7] an estimation of 50 GHz peak deviation for the future is made and a peak deviation of 1.3 GHz is achieved. Therefore, we need to increase the time delay τ_{1opt} so that the expanded bandwidth can be decreased and made possible. Requiring $\Delta f_{\max,opt,2\%} = 50GHz$ according to (3.44) will give $\tau_{1\min,opt} = 1.1ps$ and for $\Delta f_{\max,opt,2\%} = 1.3GHz$ the result will be $\tau_{1\min,opt} = 42ps$.

Using now the results (3.41), (3.42) in (3.33)

$$\left(\frac{S}{N}\right)_{optical,\max,1\%} = 2\pi^2 \cdot (3.9\%)^2 \cdot \overline{m^2(t)} \cdot CNR. \tag{3.45}$$

$$\left(\frac{S}{N}\right)_{optical,\max,2\%} = 2\pi^2 \cdot (5.5\%)^2 \cdot \overline{m^2(t)} \cdot CNR. \tag{3.46}$$

By comparing equations (3.45) and (3.46) with equation (2.7), we conclude that the performance of FMCD O-D is exactly the same with IMDD for the corresponding modulation indexes, i.e. $\gamma = 2\pi \cdot 3.9\%$ for (3.45) and $\gamma = 2\pi \cdot 5.5\%$ for (3.46).

We can also verify the above conclusion by substituting into (3.34) the results from (3.45), (3.46) and by taking into account that $\beta_{\max} \geq 1$

$$\frac{\left(\frac{S}{N}\right)_{optical,\max,1\%}}{\left(\frac{S}{N}\right)_{conv,\max}} = \frac{2\pi^2 \cdot (3.9\%)^2}{3 \cdot \beta_{\max}^2} << 1 \tag{3.47}$$

$$\frac{\left(\frac{S}{N}\right)_{optical,\max,2\%}}{\left(\frac{S}{N}\right)_{conv,\max}} = \frac{2\pi^2 \cdot (5.5\%)^2}{3 \cdot \beta_{\max}^2} << 1. \tag{3.48}$$

3.5 Comparison among Modulation Schemes

In this section, we provide an overview of the modulation schemes investigated in this chapter - conventional FMCD, IMDD, and FMCD O-D - and we plot their performance (Figure 3-16). The SNR of FMCD (3.15) (using the approximation discussed in Section 3.3.8), IMDD (2.5), and FMCD O-D (3.45), (3.46) are presented in Table 3-4 below:

Each scheme's performance is expressed in terms of the $CNR = \frac{\eta P_u}{h\nu B} = \frac{\eta |E|^2}{h\nu B}$, $m(t) = \cos(\omega_B t)$.

FMCD with Conventional Electrical Discriminator	$\left(\frac{S}{N}\right)_{conv,\max} = 3 \cdot \beta_{\max}^2 \cdot \overline{m^2(t)} \cdot CNR$.
FMCD with Optical Discriminator (Mach-Zehnder)	$\left(\frac{S}{N}\right)_{optical,\max,1\%} = 2\pi^2 \cdot (3.9\%)^2 \overline{m^2(t)} \cdot CNR$. $\left(\frac{S}{N}\right)_{optical,\max,2\%} = 2\pi^2 \cdot (5.5\%)^2 \overline{m^2(t)} \cdot CNR$.
IMDD	$\left(\frac{S}{N}\right)_{IMDD} = \frac{\gamma^2}{2} \overline{m^2(t)} \cdot CNR$.

Table 3-4: Performance of modulation schemes

Figure 3-16 shows the superiority of FMCD using an electrical discriminator. The vertical lines indicate the CNR when the modulation index of conventional FMCD has modulation index greater than 1. The grey graph corresponds to a signal of bandwidth 1Hz. The continuous black line corresponds to a broader in bandwidth signal of 50MHz and requires a higher CNR for β_{max}>1. Following FMCD in performance, but more than 20dB lower, is the performance of IMDD with intensity modulation depth 1 and 0.5. Lower performance than IMDD with modulation index 0.5 presents FMCD O-D with 2% error tolerance and last follow FMCD O-D with 1% error tolerance and IMDD with modulation depth 0.1, which has the lowest SNR of all.

Let us now consider an example to further enhance our argument. Let us suppose a sinusoidal signal $\left(\overline{m^2(t)} = 1/2\right)$ and carrier power $P_u = 7.12nW$, which, according to Table 3-1 in shot-noise-limited reception, implies CNR=30dB (for signal of B=50MHz and detector efficiency η=0.9). Then the maximum modulation index is found by our analysis for $\overline{m^2(t)} = 1/3$ to be β=26 (Table 3-4). This, according to (3.15), results in SNR=60 dB. By making the approximations discussed in Sections 3.3.6, 3.3.8 we are over the exact threshold value as it would be given by (3.21) by 0.1 dB. The expansion bandwidth is now $\Delta f = \beta \cdot B$ = 26·50MHz = 1.3 GHz which is possible under the peak frequency deviations that frequency tunable lasers can achieve. In [7] a maximum frequency deviation up to 1.3 GHz is reported and the paper claims that a 50 GHz bandwidth should be achievable.

The SNR of using IMDD according to (2.5) would in this case be 24 dB for γ=1, 18 dB for γ=0.5, and 4 dB for γ=0.1.

The SNR for FMCD-OD would be 15 dB for 2% tolerance and 12 dB with 1% tolerance. Its performance is dominated by the restrictions imposed for the error tolerance of the discriminator (3.41), (3.42).

This yields a gain of 36 dB for FMCD over IMDD with γ=1, 42 dB over IMDD with γ=0.5, 45 dB for FMCD O-D 2% tolerance, 48 dB over FMCD O-D 1% error tolerance, and 56 dB over IMDD with γ=0.1.

The superiority of conventional FMCD over IMDD and FMCD O-D can be intuitively understood because FM offers noise compression due to the fact that our signal lies inside the phase and the noise that comes into the phase is properly scaled by the amplitude of the carrier and therefore

suppressed. This is why the weak noise analysis can be carried out and this is the gain that the FM offers. On the other hand, IMDD or FMCD O-D have the signal intensity modulated or not modulated at all so that the noise adds directly to the signal amplitude upon detection. This is the element that makes IMDD and FMCD O-D inferior to the conventional FMCD.

The latter calculations provide a sense of the FM gain over the other modulations and justify our choice of FM for superior SNR performance, although as it has been discussed previously that it is not as easily implemented as the widely-used IMDD. The FM gain can be significant - 30 dB in our calculations above - and make reasonable the cost in complexity that has to be paid for a coherent system like conventional FMCD.

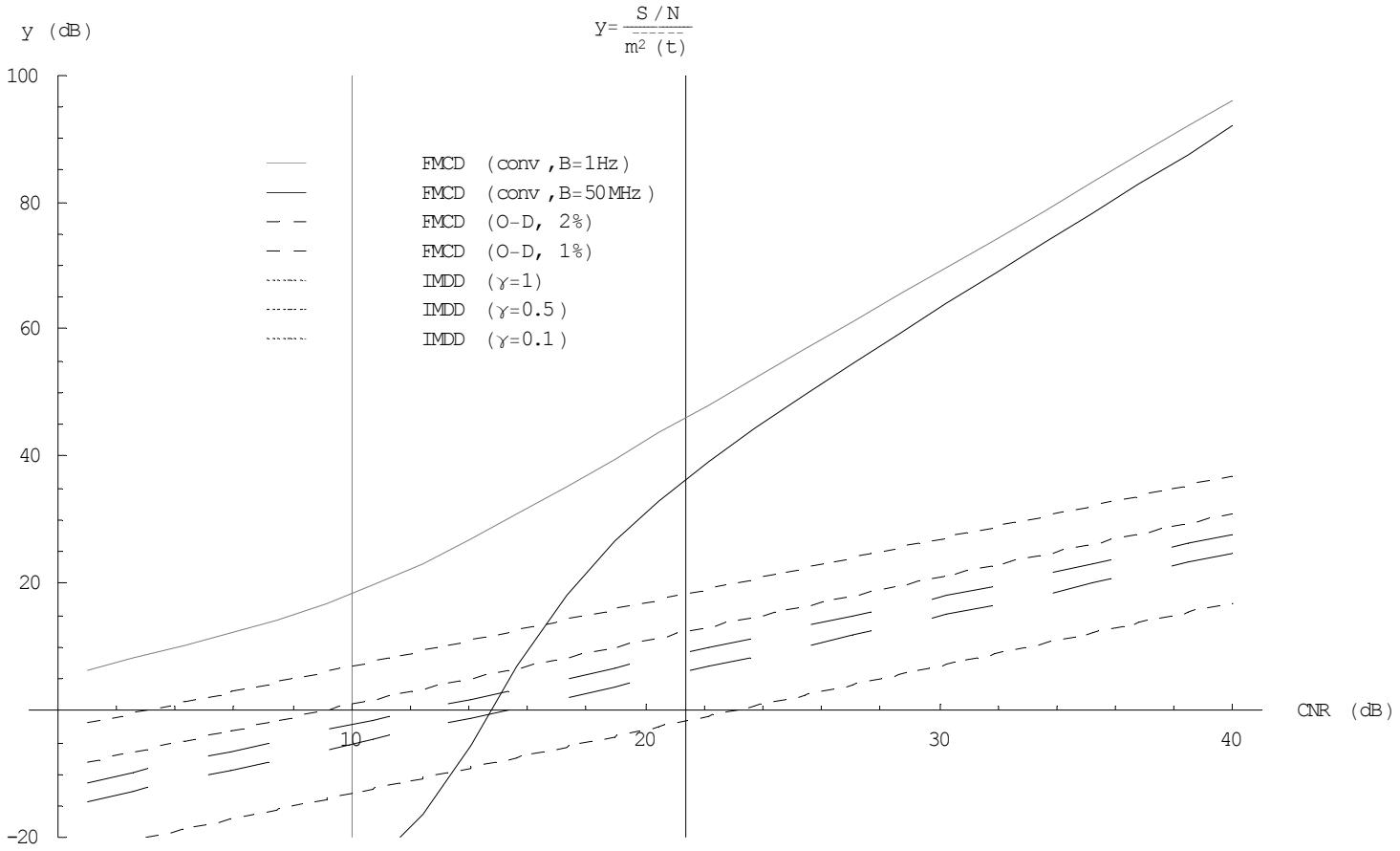

Figure 3-16: Performance comparison among types of modulation

3.6 Discussion

The significant results of this chapter are mainly embodied in Figures 3-4 – 3-7. The FM threshold has been a concept that has been discussed much in the past, although the Rician analysis for it, complete with an analytic expression, had not been carried out. The difficulty in providing an FM threshold in the literature has been the stochastic nature of the phase induced noise, which we addressed by taking using the Rician analysis [9]. Rachel [12] has verified the close proximity of the Rician analysis to simulated results and we therefore feel comfortable using it. Figure 3-5 is a typical picture of what defines the FM threshold [9], [11], [13], whereas Figure 3-6 truly answers the question of the β_{max} for every CNR.

The results found for FMCD have a great implication in the transmission of analog microwave signals. Combining CNR with the maximum bandwidth expansion FMCD links can achieve a considerable SNR gain (Section 3.5). This has been our motivation all along and answers directly the question of why it is worth bearing the complexity of a CD over preferring a simplistic DD system. It is also important to remember that this superior performance of conventional FMCD can be further enhanced by using feedback receivers (Section 3.3.7).

Moreover, by investigating the SNR performance of an FMCD O-D system in Section 3.4, we answer the question of whether optical discrimination can be beneficial. As it turns out in our calculations, its behavior is identical to that of IMDD and far inferior to that of conventional FMCD because of the fact that the signal reaches the phot-detector demodulated (in FMCD O-D) and intensity modulated (in IMDD) respectively and the noise directly adds to the signal without being suppressed.

The chapter ended with a comparison of all the modulation schemes, including a plot of the results, showing once more the superiority in performance of conventional FMCD and the relative position of FMCD with respect to IMDD for different modulation depths.

The conclusion of Chapter 3 can be described succinctly as the performance superiority of conventional FMCD, and this is the reason we focus on this modulation scheme in Chapter 4.

Chapter 4

4 Optical/Electrical Processing of Remote Antenna Signals

4.1 Introduction

In this chapter we apply FMCD over the fiber links of a simple remote antenna scheme and perform electrical/optical processing by using fiber delay lines and detection. The simplest remoting application which we primarily study is one consisting of two antennas and two users. We assume that all fiber FM links - from every antenna to the base station - are operating at their maximum SNR by employing the proper β_{max} which was derived in Chapter 3 for conventional FM receivers.

Starting with Section 4.2, we explain how we can align a signal received by two antennas when using FMCD. The result is important in the sense that it provides intuition behind the necessary condition for nulling subsequently discussed. Section 4.3 is an adaptation of the equations derived for the conventional FM receiver of Section 3.3 for the remoting application. The main difference is that there is no LO and the field received from the first antenna acts as a LO to the second. Other than that, the resulting SNR of Section 4.3.2 resembles that of conventional FM. In this remote setup, every optical field - capturing the whole spectrum the antenna receives - contains a replica of the signal and the spectrum of the interferer. We wish to maximize the SNR by properly adjusting the fiber delay lines over the FM links. Owing to the difference in position of the interfering user relative to the two antennas, two shifted interfering signal replicas are present during detection. By adjusting this term - through adjustment of the fiber delay lines - we can achieve suppression or nulling of the interfering signal and thus increase or even maximize the SNR. In Section 4.3.4 we derive the necessary condition for nulling. Although suppressing the noise is known to be better, we will restrict our attention to nulling for the rest of the thesis. We propose also in Section 4.3.7 an equivalent scheme with separate heterodyne detection for every

fiber link. This scheme is proved to be equivalent in function with the conventional FMCD using one detector but performs better up to 5 dB for high CNR.

Using the condition for nulling, which is independent of the modulation scheme due to the alignment argument in Section 4.1, we present in Section 4.4 nulling achieved in the same antenna remote scheme with IMDD over the fiber links.

In Section 4.5, the third type of modulation that we met in Chapter 3, FMCD O-D, is used in the remoting application. The performance results again are similar to those of Section 3.5 with a slight difference. In the O-D, the interferer adds to the phase, which the O-D has to differentiate and this changes its performance compared to having just a single signal as in Section 3.4.

The chapter continues in Section 4.6 with a comparison, similar to that of Section 3.5, among the performance of the different modulation schemes, but this time in the context of the remote antenna setup. The performance of FMCD O-D is now different due to the existence of interference and the conventional FMCD with heterodyne detection proves the best combination of topology and modulation.

Section 4.7 is an investigation of remote antenna setups operating under FMCD which can scale for N users and N antennas. Section 4.7.2 describes the adaptive beamforming technique based on the least-mean-square (LMS) algorithm and shows how the weights can be translated in an FMCD remote antenna. Through Sections 4.7.3-4.7.6 we study three candidate cases for generalization and conclude that the technique for elimination known as Davis beamforming does not work for FMCD since an FM signal cannot be eliminated at stages. Also, scaling the - in the previous section 4.2 - used Scheme 1 might be possible but has increased complexity and requires many filters operating at center frequencies separated at least by the amount of the optically utilized bandwidth of the fiber link. Finally, we show that by generalizing the newly proposed Scheme 2 of Section 4.3.7 and by using an LMS algorithm we can achieve adaptive beamforming for narrowband signals using FMCD and we suggest the use of fully tunable optical filters for the case of broadband signals.
Finally, a conclusions section summarizes the significant results of Chapter 4.

4.2 Remote Antenna Setup and Aligning FM Signals

A typical remote antenna scheme is shown in Fig. 4-1.

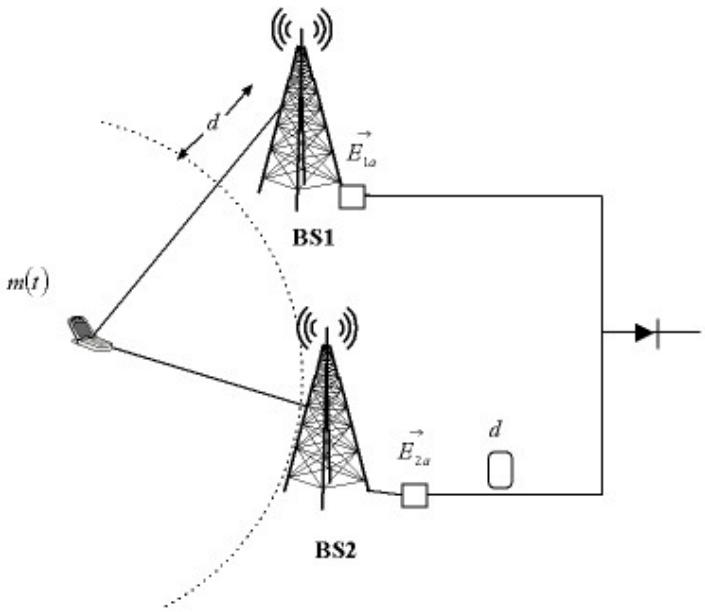

Figure 4-1: Remote Antenna – Aligning FM signals

A single user transmits a signal and two remote antennas receive it. Each antenna modulates the signal directly in the optical domain by using FMCD. We claim that if we use a fiber delay line on the one fiber link compensating for the path delay difference from the user to each antenna, then it is possible to align the signals. This is the very principle that we will use to derive in the next sections a necessary condition for nulling. In fact, this same principle applies to every modulation scheme that we use in this section.

Assuming that we receive a signal $m(t)$ on BS 2, then the signal received on BS 1 is delayed $m(t-d)$, where d is

$$d = \frac{x}{c}$$

where c is the speed of light, x the distance difference between *m(t)* - BS 1 and *m(t)*- BS 2.

The signal is optically modulated in frequency and the resulting electrical field is

$$E_1(t) = |E| \exp\left(j(\omega_s t + 2\pi \cdot \Delta f_{\max} \int_{-\infty}^{t} m(u-d)du) + \phi_1(t) \right)$$
$$= |E| \exp\left(j(\omega_s t + 2\pi \cdot \Delta f_{\max} \int_{-\infty}^{t-d} m(u)du) + \phi_1(t) \right) \quad (4.1)$$

$$E_2(t) = |E| \exp\left(j(\omega_s (t-d) + 2\pi \cdot \Delta f_{\max} \int_{-\infty}^{t-d} m(u)du) + \phi_2(t) \right) \quad (4.2)$$

where ω_s is the optical frequency, and $\Delta f_{\max}$ the maximum optical bandwidth as discussed in Section 3.3.5. The $\phi_1(t)$, $\phi_2(t)$ are random initial phases which for the time being we will assume equal to zero. This assumption is valid if we use a phase noise cancellation technique as reported in [31].

The two fields in (4.1) and (4.2) differ just by a constant phase difference $\omega_s d$. If we wish to perfectly align the signals, we can perturb the value of the fiber delay line value *d* by a small ε such that $\omega_s(d+\varepsilon) = 2n\pi$, and given that the signal *m(t)* does not change that much in that time frame, the two fields become identical. Under this assumption, we can say that the signals are aligned.

The purpose of this first section is merely to show that, when in the next sections we will try to null out a signal that is received by two antennas spatially distributed, it is reasonable to expect that the value of the fiber delay line that nulls the signal is the one that aligns the two signals. This intuition of alignment will prove useful in Sections 4.4 and 4.5 where we study IMDD and FMCD O-D and the same principle for nulling applies.

4.3 Conventional FMCD in a Simple Remote Antenna Scheme

4.3.1 Configuration

Assuming the scheme of Figure 4-2 with two users and two fiber delay lines, the distance between the base stations is arbitrary but the distances between the base stations and the users are considered known. (x_i for i = 1, 2, 3, 4) so that we are able to adjust our fiber delay lines properly compensating for time delays from the users to the base stations.

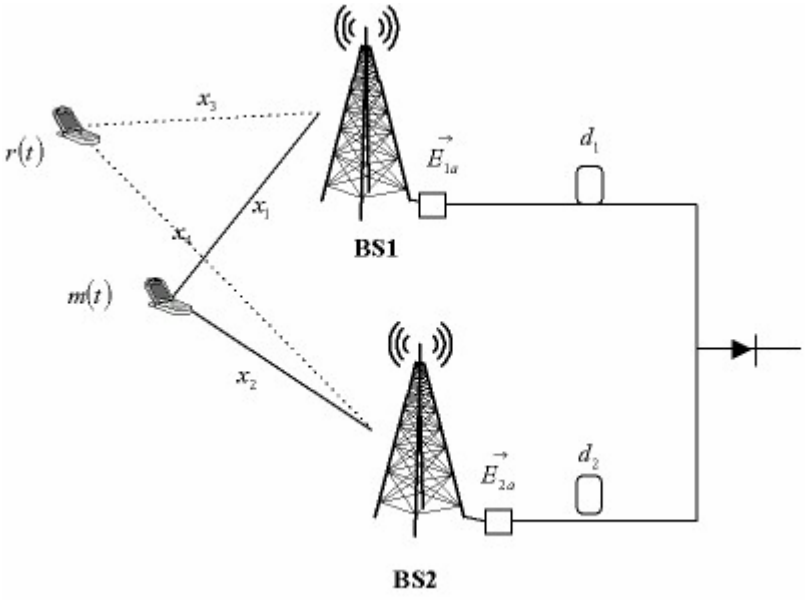

Figure 4-2: Remote Antenna Setup

In our analysis, we assume that the path losses from each user to the antennas are negligible. Therefore each base station receives only time shifted versions of the primary signal and the interferer's signal. Thus, for example, BS1 receives $m(t-t_1)+r(t-t_3)$ and BS2 receives $m(t-t_2)+r(t-t_4)$, where $t_i = \frac{x_i}{c}$ for i=1,2,3,4. and c is the speed of light.

At each base station, all of the received signals are instantaneously optically modulated on an optical carrier and the resulting electrical field for BS1 after the FM modulator is for BS1:

$$E_{1a}(t) = |E| \cdot \exp\left\{ j\left[\omega_{s,1} t + 2\pi \cdot \Delta f_{\max} \int_{-\infty}^{t} \left[m(u - t_1) + r(u - t_3) \right] du + \phi_1(t) \right] \right\} \tag{4.3}$$

and for BS2:

$$E_{2a}(t) = |E| \cdot \exp\left\{ j\left[\omega_{s,2} t + 2\pi \cdot \Delta f_{\max} \int_{-\infty}^{t} \left[m(u - t_2) + r(u - t_4) \right] du + \phi_2(t) \right] \right\}. \tag{4.4}$$

The two fields operate on different wavelengths with frequencies $\omega_{s,1} \neq \omega_{s,2}$ so that there is an IF term which will allow the electrical discriminator to lock onto its signal input. Again, $\phi_1(t)$, $\phi_2(t)$ are assumed to be zero according to the reported phase noise cancellation technique [31].

After the signal is optically modulated, it propagates through a fiber optic network to a central location where it undergoes optical processing before detection. In this setup, the optical processing unit consists of two fiber-delay lines (one at each end of the fiber line) with values d_1, d_2, as well as a combiner and detector.

After passing through the fiber delay lines, the signal fields are $E_{1a}(t-d_1)$, $E_{2a}(t-d_2)$.

The square law detector's output is equal to the incoming signals' power times the responsitivity of the photodetector. Therefore:

$$\begin{aligned} I(t) &= R\left| E_{1a}(t - d_1) + E_{2a}(t - d_2) \right|^2 \\ &= R\left(E_{1a}(t - d_1) + E_{2a}(t - d_2) \right)\left(E_{1a}(t - d_1) + E_{2a}(t - d_2) \right)^* \\ &= R\left| E_{1a}(t - d_1) \right|^2 + \left| E_{2a}(t - d_2) \right|^2 + 2R \cdot \mathrm{Re}\left[E_{1a}(t - d_1) E_{2a}{}^*(t - d_2) \right] \\ &= 2R|E|^2 \\ &\quad + 2R|E|^2 \cos\left[\begin{array}{l} (\omega_{s,1} - \omega_{s,2})t + \omega_{s,2} d_2 - \omega_{s,1} d_1 + \\ 2\pi\Delta f_{\max}\left(\int_{-\infty}^{t-d_1} m(u - t_1)du - \int_{-\infty}^{t-d_2} m(u - t_2)du \right) \\ + 2\pi\Delta f_{\max}\left(\int_{-\infty}^{t-d_1} r(u - t_3)du - \int_{-\infty}^{t-d_2} r(u - t_4)du \right) \end{array} \right] \end{aligned} \tag{4.5}$$

We follow again the weak noise analysis, as explained in Section 3.3.2 and we consider the noise *n(t)* being additive at the detection stage, accumulating all the noise from the components of the antennas, the modulator, and the fiber optic network. The electric current is thus:

$$\begin{aligned} I(t) &\approx 2R|E|^2 \\ &+ 2R|E|^2 \cos\left[(\omega_{s,1}-\omega_{s,2})t + \omega_{s,2}d_2 - \omega_{s,1}d_1 + 2\pi\Delta f_{\max}\left(\int_{-\infty}^{t-d_1} m(u-t_1)du - \int_{-\infty}^{t-d_2} m(u-t_2)du + \int_{-\infty}^{t-d_1} r(u-t_3)du - \int_{-\infty}^{t-d_2} r(u-t_4)du\right)\right] \\ &+ n(t) \end{aligned} \tag{4.6}$$

where *n(t)* is additive white Gaussian noise.

4.3.2 SNR of FMCD in this Scheme

In this section, we adjust the analysis of Section 3.3.2 to the characteristics of our remote antenna setup. We proceed through the steps of Section 3.3.2 recalling that the major difference in this setup is that we have detection with the one field acting as a LO to the other. The fields are at different wavelengths so that there is an IF term which will help the electrical discriminator to lock onto the phase of its signal input.

The fact that we have two fields instead of a field and a LO now yields a different CNR. The new CNR, by observing the amplitude of the carrier in (4.6), is:

$$CNR = \frac{\left(2R|E|^2\right)^2/2}{N_0 B} = \frac{2R^2|E|^4}{2q(I_0+I_{dk})B} = \frac{2R^2|E|^4}{2q\left(R\cdot 2|E|^2\right)B} = \frac{R|E|^2}{2qB} = \frac{\frac{\eta q}{h\nu}|E|^2}{2qB} = \frac{\eta|E|^2/2}{h\nu B} \tag{4.7}$$

where the noise density contains only shot noise components, as defined in Section 2.3

The weak noise assumption (3.13) remains valid with the only difference that the carrier power $\frac{I_s^2}{2}$ is, by observing (4.6) in this case, equal to $2R^2|E|^4$.

The noise power is calculated as in (3.14) and is:

$$\overline{n_{new}^2} = \frac{1}{3}(2\pi B)^2 \frac{1}{CNR} \tag{4.8}$$

where the CNR is the one provided by (4.7).

The signal power is calculated as the mean square value of the time derivative of the argument of (4.6)

$$\overline{i_s^2} = 4\pi^2 \Delta f_{\max}^2 \overline{\left[m(t-d_1-t_1) - m(t-d_2-t_2) + r(t-d_1-t_3) - r(t-d_2-t_4)\right]^2} \tag{4.9}$$

By assuming a zero-mean, wide-sense stationary (WSS) signal *m(t)* and interference *r(t)*, the mean current (4.9) can be rewritten as:

$$\begin{aligned}\overline{i_s^2} = \quad &= 4\pi^2 \Delta f_{\max}^2 \left(\begin{array}{l} \overline{\left[m(t-d_1-t_1) - m(t-d_2-t_2)\right]^2} + \overline{\left[r(t-d_1-t_3) - r(t-d_2-t_4)\right]^2} + \\ + 2\overline{\left[m(t-d_1-t_1) - m(t-d_2-t_2)\right]\left[r(t-d_1-t_3) - r(t-d_2-t_4)\right]} \end{array} \right) \\ &= 4\pi^2 \Delta f_{\max}^2 \left(\begin{array}{l} 2R_{mm}(0) - 2R_{mm}(d_2-d_1+t_2-t_1) + 2R_{rr}(0) - 2R_{rr}(d_2-d_1+t_4-t_3) \\ + 2R_{mr}(t_3-t_1) - 2R_{mr}(d_2-d_1+t_4-t_1) + \\ + 2R_{mr}(t_4-t_2) - 2R_{mr}(d_2-d_1+t_2-t_3) \end{array} \right)\end{aligned} \tag{4.10}$$

where $R_{mm}(\tau) = E[m(t)m(t+\tau)]$, $R_{rr}(\tau) = E[r(t)r(t+\tau)]$, $R_{mr}(\tau) = E[m(t)r(t+\tau)]$ are the auto-correlations and cross-correlations between the signal and the interferer.

By taking into consideration that in (4.10) the signal is represented by the quantity

$$2R_{mm}(0) - 2R_{mm}(d_2-d_1+t_2-t_1)$$

the interference part by

$$2R_{rr}(0) - 2R_{rr}(d_2-d_1+t_4-t_3)$$

and by considering the cross correlation terms equal to zero

$$2R_{mr}(t_3 - t_1) - 2R_{mr}(d_2 - d_1 + t_4 - t_1) + 2R_{mr}(t_4 - t_2) - 2R_{mr}(d_2 - d_1 + t_2 - t_3) = 0$$

the resulting SNR by taking into consideration (4.10) is:

$$SINR = \frac{\overline{i_s^2}(signal\_part)}{n_{new}^2 + \overline{i_s^2}(\text{int}\, erf.\_part)}$$

$$= \frac{4\pi^2 \Delta f_{\max}^2 \left(2R_{mm}(0) - 2R_{mm}\left(d_2 - d_1 + t_2 - t_1\right)\right)}{\frac{1}{3}(2\pi B)^2 \frac{1}{CNR} + 4\pi^2 \Delta f_{\max}^2 \left(2R_{rr}(0) - 2R_{rr}\left(d_2 - d_1 + t_4 - t_3\right)\right)} \qquad (4.11)$$

In this thesis we will restrict our attention to the case of nulling. Although it is known that suppression can be better than nulling if the interferer and user are closer than one beam-width [20], we will consider only the case of nulling because it is mathematically easier to define the values of the fiber delay lines. The purpose of the thesis is to evaluate the performance of different FMCD, IMDD schemes over the same technique of signal suppression. Thus, for reasons of fair comparison among the schemes and also of simplicity, we will consider only nulling.

In order to null the interferer we first observe from (4.6) the current after detection is:

$$I(t) \approx 2|E|^2 + 2|E|^2 \cos\left[\omega_s (d_2 - d_1) + 2\pi\Delta f_{\max}\left(\int_{-\infty}^{t-d_1} m(u - t_1)du - \int_{-\infty}^{t-d_2} m(u - t_2)du + \int_{-\infty}^{t-d_1} r(u - t_3)du - \int_{-\infty}^{t-d_2} r(u - t_4)du\right)\right] + n(t)$$

Note that requiring the interference to be nulled out is equivalent to the condition:

$$\int_{-\infty}^{t-d_1} r(u - t_3)du - \int_{-\infty}^{t-d_2} r(u - t_4)du = 0\,.$$

This expression, after a change of variable, can be rewritten as:

$$\int_{-\infty}^{t-d_1} r(u - t_3)du - \int_{-\infty}^{t-d_2+t_3-t_4} r(u - t_3)du = 0$$

Requiring both integrals to be equal at any time t is the same as requiring the sides of the bounds of the integrals to be equal. Thus, we have

$$\boxed{d_2 - d_1 = t_3 - t_4\,.} \qquad (4.12)$$

The SNR can be found from (4.11). The following hold in (4.11) for Case 2:

1) The interfering part $2R_{rr}(0) - 2R_{rr}\left(d_2 - d_1 + t_4 - t_3\right)$, because of (4.13), is equal to zero.

2) The cross-correlation between the signal and interference will be assumed zero and therefore expression $2R_{mr}(t_3 - t_1) - 2R_{mr}(d_2 - d_1 + t_4 - t_1) + R_{mr}(t_4 - t_2) - 2R_{mr}(d_2 - d_1 + t_2 - t_3)$ will be equal to zero.

Thus, the resulting SNR from (4.11) is:

$$SNR_2 = \frac{4\pi^2 \Delta f_{\max}^2 \left(2R_{mm}(0) - 2R_{mm}\left(t_3 - t_4 + t_2 - t_1\right)\right)}{\frac{1}{3}(2\pi B)^2 \frac{1}{CNR}}$$

$$= 3\beta_{\max}^2 \cdot \left(2R_{mm}(0) - 2R_{mm}\left(t_3 - t_4 + t_2 - t_1\right)\right) \cdot CNR \qquad (4.13)$$

Special Case: Single Signal

The remote antenna setup of Figure 4-2 can provide significant gain in the case of one signal. The setup with one signal is shown in Figure 4-3.

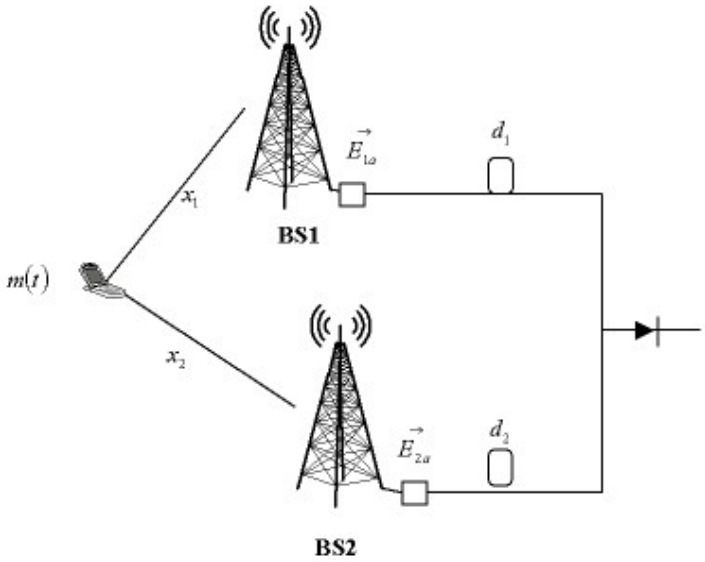

Figure 4-3: Remote antenna scheme with single user

In this case there is no interference. We therefore try to adjust the delay lines so that we maximize the resulting SNR through constructive interference between the two transmitted replicas of the signal.

In the calculations of (4.11) we consider *r(t)* = 0 and the SNR is consequently:

$$SNR_1 = \frac{4\pi^2 \Delta f_{\max}^2 \left(2R_{mm}(0) - 2R_{mm}\left(d_2 - d_1 + t_2 - t_1\right)\right)}{\frac{1}{3}(2\pi B)^2 \frac{1}{CNR}}$$

$$SNR_1 = 3 \cdot \beta_{\max}^2 \cdot \left(2R_{mm}(0) - 2R_{mm}\left(d_2 - d_1 + t_2 - t_1\right)\right) \cdot CNR\,. \tag{4.14}$$

where we can adjust the term $d_2 - d_1$ so that we maximize the SNR.

4.3.3 Alternative FMCD Setup

In this section we would like to investigate the performance of two different schemes yielding the same result.

Two of the possible optical processing schemes for FM signals are shown in Figure 4-4.

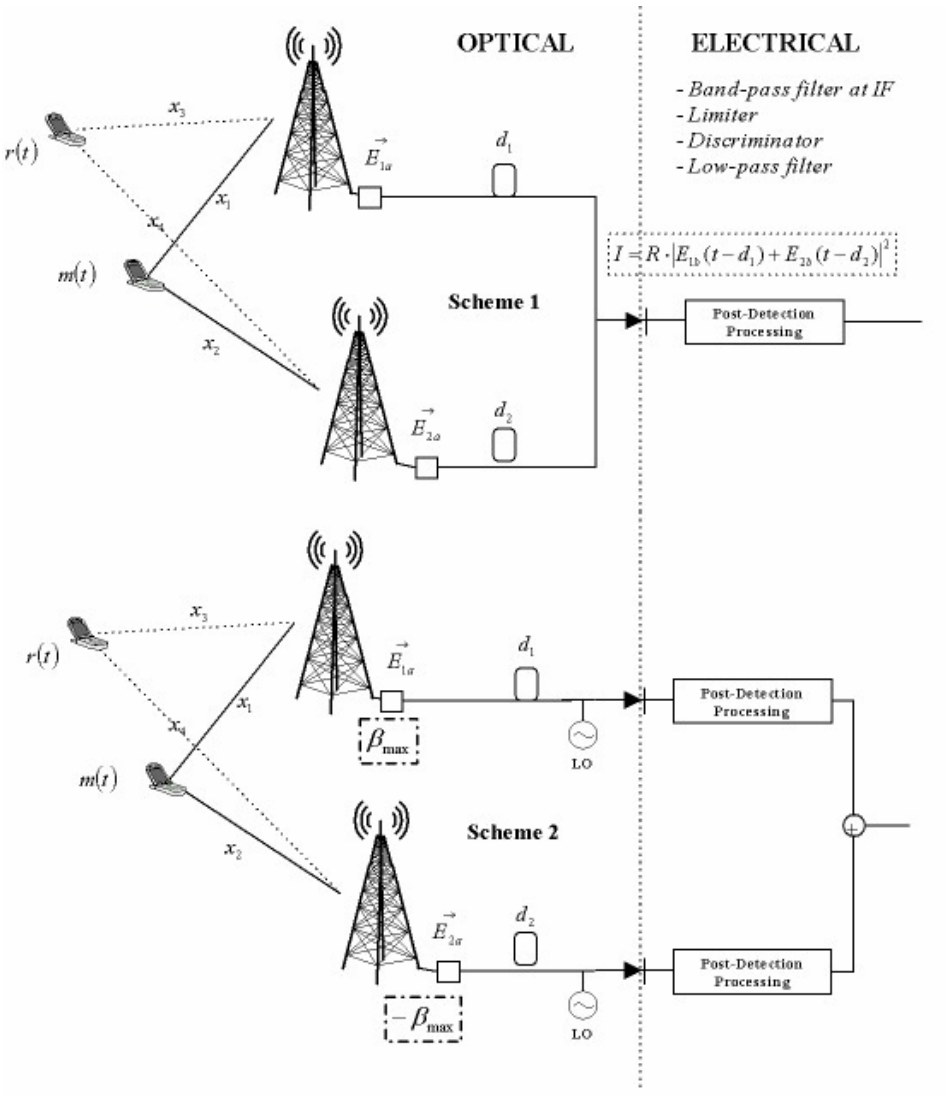

Figure 4-4: Two-Antenna Schemes

Scheme 1 is the one used in Section 4.3.2, where, by adjusting properly the delay lines and combining the fields and detecting, we managed to null the interfering signal at the point of detection.

Scheme 2 represents an independent detection process scheme. We use the same values for the fiber delay lines that align the interfering signal, we detect each field separately, and we perform post detection processing (electrical discrimination). We then sum the resulting currents from the detection processes and, since the received spectrum of each antenna has been modulated with opposite modulation index, we achieve nulling. We should note at this point that β_{max} does not take the same value in both schemes since it depends on the CNR, as we discussed in Chapter 3.

By comparing the CNR of Scheme 1, given by (4.7),

$$CNR_1 = \frac{\eta |E|^2}{2hvB} \tag{4.15}$$

to the CNR of Scheme 2 - for single signal detection - as given by (3.8) for $P_u = |E|^2$,

$$CNR_2 = \frac{\eta P_u}{hvB} = \frac{\eta |E|^2}{hvB} \tag{4.16}$$

we observe that the CNR in (4.15) is half the CNR of (4.16) and therefore the maximum modulation indexes - given that the optical fields all have the same power $|E|^2$ - are different.

Scheme 2 has not been analyzed yet in this thesis, but it consists of single detection processes which have been analyzed. The signal received after discrimination is from the first antenna $m(t-d_1-t_1)+r(t-d_1-t_3)$ and from the second, $-m(t-d_2-t_2)-r(t-d_2-t_4)$. By adding the two resulting electrical signals, the interferer is nulled since the fiber delay lines have been adjusted to $d_2-d_1=t_3-t_4$. The resulting signal is $m(t-d_1-t_1)-m(t-d_2-t_2)$, which is the same as in Scheme 1. The noise power will be twice the noise power of single detection since the

noises are added and are independent processes (different detectors). Thus the total noise will be twice that of (3.14), i.e.

$$\overline{n^2}_{total,2} = 2 \cdot \frac{1}{3}(2\pi B)^2 \frac{1}{CNR_2}. \tag{4.17}$$

We can see, comparing (4.17) where CNR_2 appears with (4.8) for Scheme 1, and by taking into account that $CNR_2=2CNR_1$, that the noise power in both cases is the same.

We also discussed above that the resulting signal $m(t-d_1-t_1)-m(t-d_2-t_2)$ is also the same in both cases. Thus, the signal power is also equal.

The SNR_1 for FMCD in the Scheme 1 is given in (4.13) for CNR=CNR_1,

$$SNR_1 = 3\beta_{\max,1}^2(2R_{mm}(0)-2R_{mm}(t_3-t_4+t_2-t_1))CNR_1 \tag{4.18}$$

and for Scheme 2 the SNR_2 is:

$$\begin{aligned} SNR_2 &= \frac{4\pi^2 \Delta f_{\max,2}{}^2 (2R_{mm}(0)-2R_{mm}(t_3-t_4+t_2-t_1))}{\overline{n^2}_{total,2}} = \\ &= 6\beta_{\max,2}^2(2R_{mm}(0)-2R_{mm}(t_3-t_4+t_2-t_1))CNR_2 \\ &= 3\beta_{\max,2}^2(2R_{mm}(0)-2R_{mm}(t_3-t_4+t_2-t_1))CNR_1 \\ &> 3\beta_{\max,1}^2(2R_{mm}(0)-2R_{mm}(t_3-t_4+t_2-t_1))CNR_1 = SNR_1 \end{aligned} \tag{4.19}$$

Since the maximum modulation index in Figure 2 is greater than that of Scheme 1 ($CNR_2 > CNR_1$ implies $\beta_{\max,2} > \beta_{\max,1}$ as discussed in Chapter 3) the SNR of the second scheme (4.19) is greater than that of Scheme 1. This result is expected since we are using local oscillators in the second case which allows us to have more available power and thus better CNR.

The gain of Scheme 2 over Scheme 1 is:

$$G = \frac{SNR_2}{SNR_1} = \frac{\beta_{\max,2}^2}{\beta_{\max,1}^2} = \left(\frac{\beta_{\max}(2CNR_1)}{\beta_{\max}(CNR_1)} \right)^2 \tag{4.20}$$

The plot of (4.20) is in Figure 4-5. We can see that the gain varies from 1.9 dB for CNR = 10dB to 5.6 dB for CNR=80 dB.

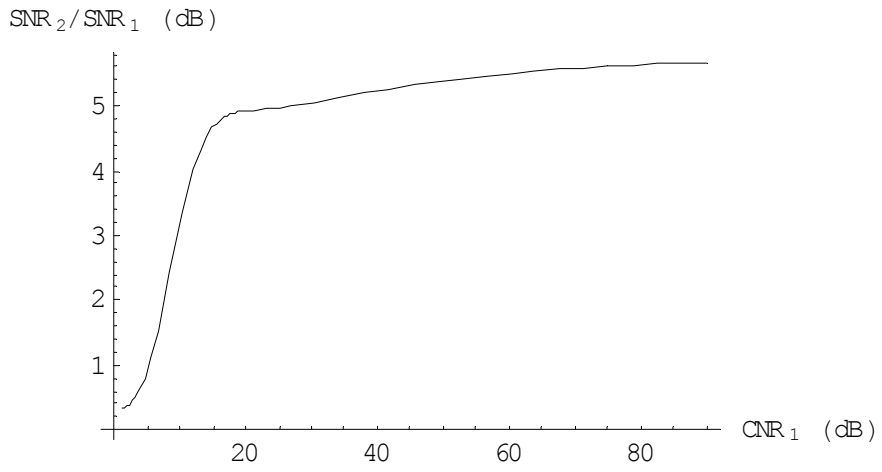

Figure 4-5: Gain of Scheme 2 over Scheme 1

(for equal optical field power)

The purpose of this section was to compare how both schemes can perform if we adjust the delay lines with the necessary condition for nulling (4.12). The fact that their performance is different allows us further to support our argument that Scheme 2 is better, not only because it can null the interference and has better performance, but also because it can scale, as we will see in the next sections.

4.4 Nulling Interference with IMDD

1. IMDD Configuration

For the same simple antenna scheme consisting of two antennas and two users, we wish now to employ IMDD over the fiber links. Signals that are intensity modulated, according to Section 2.4, have an expression for the optical power similar to (2.1):

$$P_o = P_u\left[1 + \gamma \cdot m(t)\right] \tag{4.21}$$

The antenna setup is the same as in the previous setups. The only optical components required for IMDD are fiber delay lines, a combiner, and a detector. The setup is shown in Fig. 4-6.

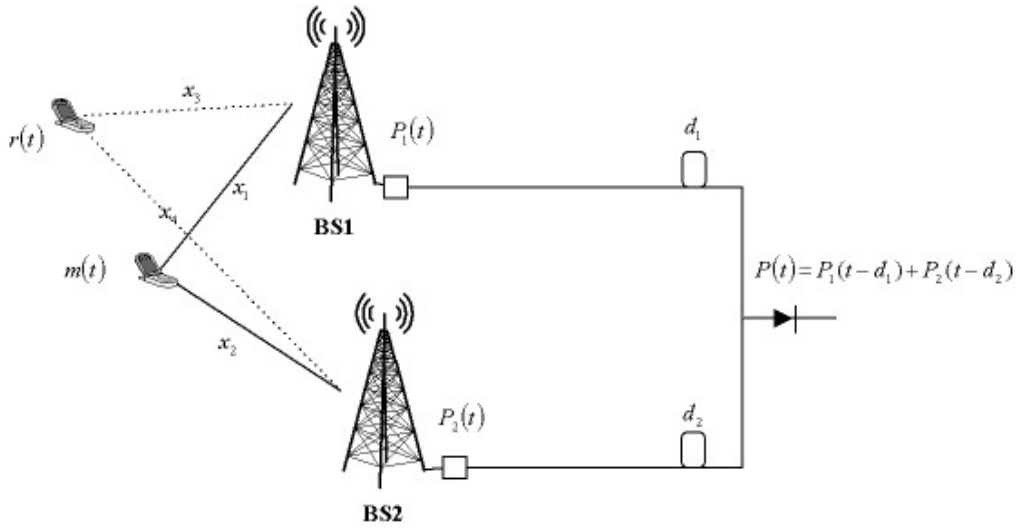

Figure 4-6: Remote Antenna Setup for IMDD

Each BS receives a delayed version of the signal *m(t)* and the interference *r(t)*. At each BS, the received signals are intensity modulated onto the optical carrier. So for BS1:

$$P_1(t) = P_u\left[1 + \gamma \cdot \{m(t - t_1) + r(t - t_3\}\right]. \tag{4.22}$$

For BS2 in order to be able to null the interfering signal, we modulate the inverted version of the received spectrum

$$P_2(t) = P_u\left[1 - \gamma \cdot \{m(t - t_2) + r(t - t_4\}\right]. \tag{4.23}$$

Delaying the signals implies delaying the power as well, so after combining the signals the output of the combiner contains the sum of the power at its input. Thus, we have

$$\begin{aligned} P_1(t-d_1)+P_2(t-d_2) &= P_u\left[1+\gamma\cdot\{m(t-d_1-t_1)+r(t-d_1-t_3\}\right] \\ &+ P_u\left[1-\gamma\cdot\{m(t-d_2-t_2)+r(t-d_2-t_4\}\right] \\ &= P_u\left[1+\gamma\cdot\{(m(t-d_1-t_1)-m(t-d_2-t_2))+(r(t-d_1-t_3)-r(t-d_2-t_4\}\right] \end{aligned} \quad . \tag{4.24}$$

If we adjust the delay lines such that $d_2-d_1=t_3-t_4$ we can completely null the interference and the resulting power will be:

$$P_1(t-d_1)+P_2(t-d_2)=P_u\left[1+\gamma\cdot\{(m(t-d_1-t_1)-m(t-d_2-t_2))\}\right] \tag{4.25}$$

The mean square value of the photocurrent at the output of the detector is similar to (2.2):

$$\begin{aligned} \overline{I_s^2} &= (RP_u\gamma)^2\cdot\overline{(m(t-d_1-t_1)-m(t-d_2-t_2))^2} \\ &= (RP_u\gamma)^2\cdot(2R_{mm}(0)-2R_{mm}(t_3-t_4+t_2-t_1)) \end{aligned} \quad . \tag{4.26}$$

where R is the responsivity of the p-i-n photodiode.

We assume that we have shot noise limited reception**,** which means according to Section 2.4 that $N_0=2q(RP_u)$.

The resulting SNR is:

$$SNR_{DD}=\frac{RP_u\cdot\gamma^2\cdot(2R_{mm}(0)-2R_{mm}(t_3-t_4+t_2-t_1))}{2qB}$$

$$=\frac{\gamma^2\overline{(2R_{mm}(0)-2R_{mm}(t_3-t_4+t_2-t_1))}}{2}\left(\frac{\eta P_u}{h\nu B}\right)$$

$$=\frac{\gamma^2}{2}(2R_{mm}(0)-2R_{mm}(t_3-t_4+t_2-t_1))CNR'$$

$$=\gamma^2(2R_{mm}(0)-2R_{mm}(t_3-t_4+t_2-t_1))CNR \tag{4.27}$$

where

which implies that the SNR of (4.27) is similar to the case of one signal in (2.5), with the only difference that $\overline{m^2(t)}$ has been substituted with $2R_{mm}(0)-2R_{mm}(t_3-t_4+t_2-t_1)$, which is sum of

the power of two versions of the same signal. This can either be constructive or positive interference.

4.5 Nulling Interference with FMCD O-D

4.5.1 Initial Observation on FMCD O-D

In this section, we will use FMCD O-D for the simple remote antenna setup of two antennas and two users. There is an important difference between this modulation and the previously mentioned ones which distinguishes its performance in the remote antenna context from that of Section 3.5. The difference is that the O-D has some limitations in the value of its phase in order to operate as a discriminator. Thus, when a second signal exists, such as the one coming from the interferer, the limitations for the error tolerance of the discriminator yield different results. Of course, the performance does not change significantly: it still remains comparable to IMDD and but it can change the relative performance among FMCD O-D and the different modulation depths of IMDD.

4.5.2 Configuration

The typical setup of Fig. 4-2 for a single user and a single interferer is also used in this section with the proper modifications to include optical discriminators. The optical toolbox in this case is now more enhanced, containing not only the fiber delay lines but also the Mach Zehnder interferometer which operates as an optical discriminator. The configuration with FMCD O-D is presented in Fig. 4-7. Each optical discriminator, as discussed in Section 3.4, consists of a polarization controller and a phase shifter which are used to optimize discriminator performance [16]. We differentiate the signals received in the optical domain, we detect them separately, and then subtract their currents. A complete analysis follows.

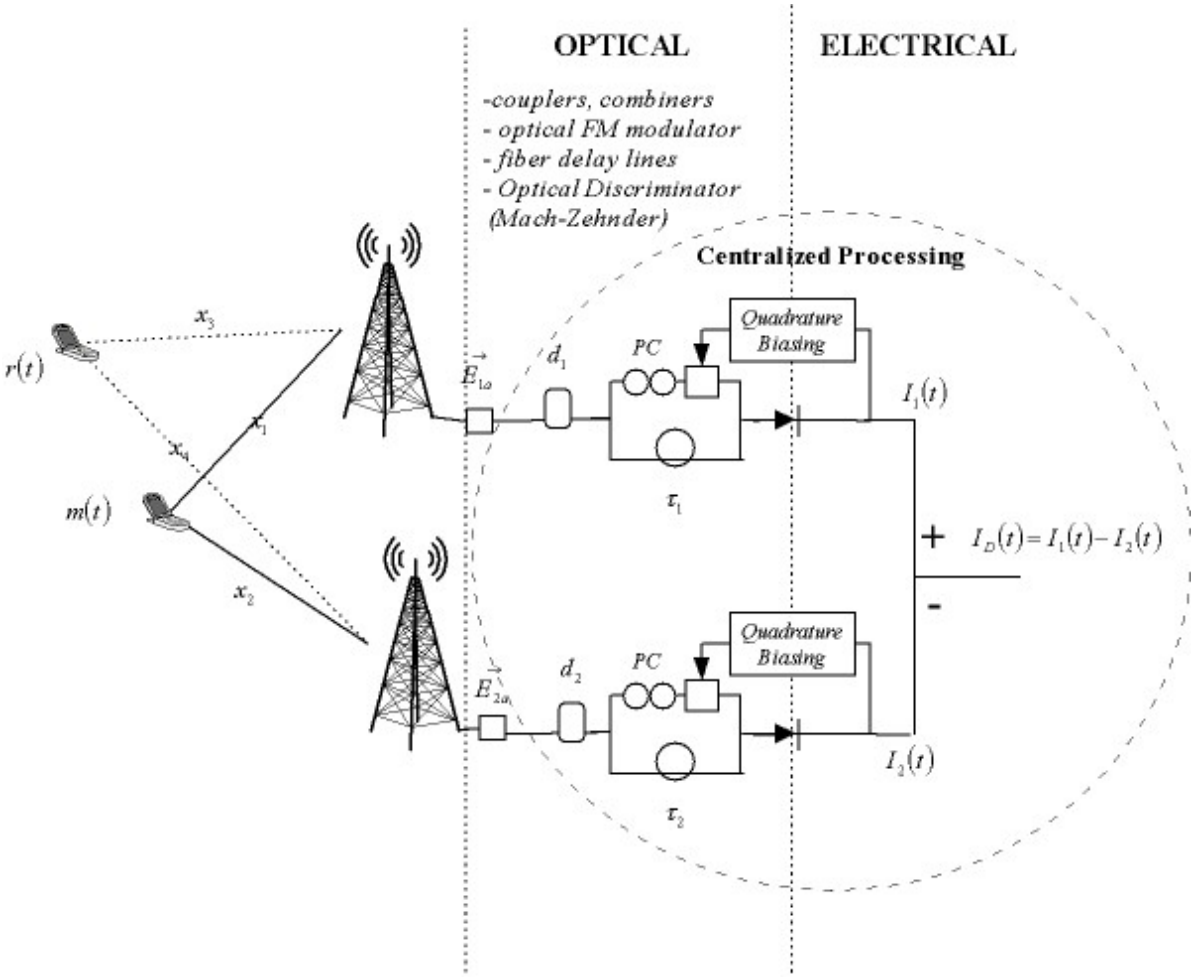

Figure 4-7: Single User - Single Interferer Scheme with Optical Discriminators

The optically FM modulated signal fields are:

for BS#1
$$E_{1a}(t)=|E|\cdot\exp\left\{j\left[\omega_s t+2\pi\cdot\Delta f\int_{-\infty}^{t}\left[m(u-t_1)+r(u-t_3)\right]du+\phi_1(t)\right]\right\} \tag{4.28}$$

for BS#2
$$E_{2a}(t)=|E|\cdot\exp\left\{j\left[\omega_s t+2\pi\cdot\Delta f\int_{-\infty}^{t}\left[m(u-t_2)+r(u-t_4)\right]du+\phi_2(t)\right]\right\}. \tag{4.29}$$

The simplifying assumption of zero initial phases $\phi_1(t)=\phi_2(t)=0$ is also made. Each one of the signals is frequency modulated using a value of bandwidth expansion which is certainly not the specific maximum that had been calculated before. This is because the values that had been calculated were based on the conventional electrical FM discriminator with the usual weak noise suppression, while in this case an optical discriminator is used and there is no prior knowledge in literature of a threshold phenomenon. In the next sections we will optimize the parameters of FMCD O-D and we will prove that a threshold phenomenon occurs in this case as well but due to different reasons. The only limitations is the available optical fiber bandwidth and the error free operation of the discriminator.

The modulated fields pass through the two delay lines yielding $E_{1a}(t-d_1)$, $E_{2a}(t-d_2)$. By following the analysis in 3.4.2 and by substituting $m(t)$ in (3.30) of that section with $m(t-d_1-t_1)+r(t-d_1-t_3)$ for the first antenna and $m(t-d_2-t_2)+r(t-d_2-t_4)$ for the second antenna, we have the following currents:

$$I_1(t)\cong\pm 2I_s\pi\cdot\Delta f\cdot\tau_1\left(m(t-d_1-t_1)+r(t-d_1-t_3)\right) \tag{4.30}$$

$$I_2(t)\cong\pm 2I_s\pi\cdot\Delta f\cdot\tau_2\left(m(t-d_2-t_2)+r(t-d_2-t_4)\right). \tag{4.31}$$

Passing now to the electrical domain, we subtract the photocurrents from the two detectors, yielding an output $I_D(t)$ equal to:

$$I_D(t)=I_1(t)-I_2(t). \tag{4.32}$$

Taking also into account the noise that comes from each detection process (shot noise limited), the photocurrent can be written as:

$$\begin{aligned} I_D^{'}(t) &= I_D(t) + n(t) \\ &= I_1(t) - I_2(t) + n_1(t) - n_2(t) \\ &= \pm 2 I_s \pi \cdot \Delta f \left(\tau_1 \cdot m(t - d_1 - t_1) - \tau_2 \cdot m(t - d_2 - t_2) \right) + \\ &\quad + \left(\tau_1 \cdot r(t - d_1 - t_3) - \tau_2 \cdot r(t - d_2 - t_4) \right) \cdot + n_1(t) - n_2(t) \end{aligned} \tag{4.33}$$

We have two sets of delay parameters in this case that can lead to aligning our signal. The first one is the set of delays at the discriminators $\{\tau_1, \tau_2\}$ and the second one is the set of fiber delay lines $\{d_1, d_2\}$. We fix the value of the second set to that of nulling as in (4.12), i.e. $d_2 - d_1 = t_3 - t_4$ and we explore further the required condition now that we have the interfering signals aligned.

Then (4.36) becomes:

$$\begin{aligned} I_D^{'}(t) &= \pm 2 I_s \pi \cdot \Delta f \left(\tau_1 \cdot m(t - d_1 - t_1) - \tau_2 \cdot m(t - d_2 - t_2) \right) + \\ &\quad + \left(\tau_1 - \tau_2 \right) \cdot r(t - d_2 - t_4) \cdot + n_1(t) - n_2(t) \end{aligned} \tag{4.34}$$

We observe that the interfering signal *r(t)* cannot be nulled unless the delays τ_1 and τ_2 are made equal which we will investigate in the next section.

Proceeding with this setup, the noise spectral density is:

$$S_{n_i}(f) = \begin{cases} N_0, & f < B \\ 0 & f > B \end{cases} \quad i = 1,2 \tag{4.35}$$

where *B* is the signal's m(t) bandwidth.

Thus, the noise power is $\overline{n_1^2(t)} = \overline{n_2^2(t)} = N_0 B = 2 q I_s B$ assuming shot noise limited reception and the cross-correlation is 0 because the two detecting processes are independent.

$$\overline{n^2(t)} = \overline{n_1^2(t)} + \overline{n_2^2(t)} = 2 N_0 B \tag{4.36}$$

The signal-to-interference-and-noise ratio can be calculated as:

$$\frac{S}{N+I} = \frac{\overline{I_D^2}}{\overline{n^2(t)}} = \frac{I_s^2 \cdot 4\pi^2 \Delta f^2 \cdot \left(\left(\tau_1^2 + \tau_2^2 \right) R_{mm}(0) - 2\tau_1 \tau_2 R_{mm}\left((t_3 - t_4 + t_2 - t_1) \right) \right)}{2 N_0 B + \left(\tau_1 - \tau_2 \right)^2 R_{rr}(0)} \tag{4.37}$$

In (4.36) we observe that, due to $\tau_1 \neq \tau_2$, the interfering signal is not completely nulled and an interfering term $(\tau_1 - \tau_2)^2 R_{rr}(0)$ remains. In Section (4.3.6) we concluded that nulling is close to the optimal solution of suppression for most of the interfering angles. In order to do a fair comparison with the previously mentioned antenna scheme we will null interference in this case as well. Therefore we will explore a new setup where both of the O-D delays are made equal and perfect nulling is achieved.

4.5.3 Equal Delay Time Differences

By ensuring that $\tau_1 = \tau_2 = \tau$, we are able to completely null out the interferer and also make comparisons with the conventional FM discriminator.

This is possible under the scheme of Figure 4-8, where $\tau = \min\{\tau_1, \tau_2\}$, i.e. the quadrature biasing device chooses the smallest phase difference that keeps both O-Ds in quadrature and also both phase differences greatly smaller than 1 so that both O-Ds perform differentiation properly.

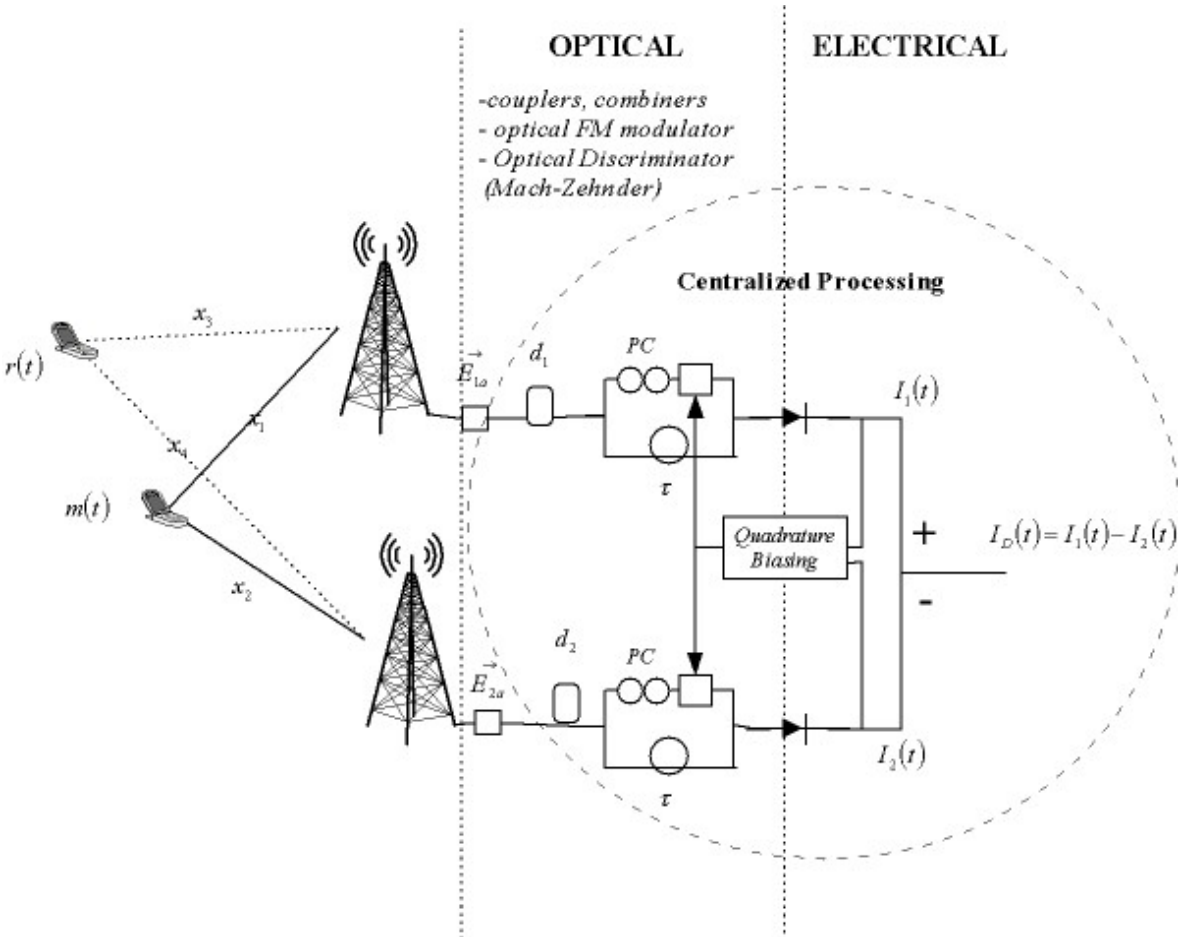

Figure 4-8: Optical Discriminators with equal time delays

By making these adjustments, the interferer in (4.36) can be completely nulled and the SNR is:

$$\left(\frac{S}{N}\right)_{optical} = \frac{\overline{I_D^2}}{\overline{n^2(t)}} = \frac{I_s^2 \cdot 4\pi^2 \Delta f^2 \cdot \tau^2 \left(2R_{mm}(0) - 2R_{mm}\left(\left(d_2 - d_1 + t_2 - t_1\right)\right)\right)}{2N_0 B} \tag{4.38}$$

$$\begin{aligned}\left(\frac{S}{N}\right)_{optical} &= 4\pi^2 \Delta f^2 \cdot \tau^2 \left(2R_{mm}(0) - 2R_{mm}\left(\left(t_3 - t_4 + t_2 - t_1\right)\right)\right) \cdot CNR_{O-D} \\ \left(\frac{S}{N}\right)_{optical} &= 2\pi^2 \Delta f^2 \cdot \tau^2 \left(2R_{mm}(0) - 2R_{mm}\left(\left(t_3 - t_4 + t_2 - t_1\right)\right)\right) \cdot CNR\end{aligned} \tag{4.39}$$

where $CNR_{O-D} = \frac{I_s^2}{2N_0 B} = \frac{\eta |E|^2}{4h\nu B} = \frac{1}{2} CNR_{FMCD} = \frac{1}{2} CNR$. In this section we have taken as CNR reference the CNR derived in Section 4.3.2 for FMCD with one detector. Due to the fact that we have double the noise than that of using one detector and that the power is split into half with respect to the FMCD with one detector scheme we obtain the same SNR formula as before.

We proceed now to compare all of the modulation schemes proposed in Chapter 3 and 4.

4.6 Comparing Nulling in Remote Antennas using FMCD, IMDD, FMCD O-D

Table 4-1 summarizes the SNR expressions of all the mentioned modulations for the case of the simple remote antenna application and for complete nulling of the interfering signal when both the user's and interferer's signals are sinusoids, i.e $R_{mm}(t)=\frac{1}{2}\cos(\omega_B t)$. The latter assumption has been made for the comparison between modulation schemes to be fair since the results of FMCD O-D have been found for the case of sinusoidal signal. Moreover, for the comparison to be fair with respect to power, we assume equal optical field power in every setup and use the same expression for the CNR.

Figure 4-9 shows the superiority of FMCD using an electrical (microwave) discriminator. The thick grey and black lines represent the conventional FMCD with separate heterodyne detection for 1Hz and 50 MHz of signals' bandwidth respectively. It can be seen as in Section 4.3.7 the superiority that this scheme achieves over the conventional FMCD with one detector. This is because of the higher CNR that it can achieve through the presence of a LO. The graph is very similar to Figure 3-16 since the SNR is plotted normalized over the signal's power $\overline{m^2(t)}$ in Figure 3-16, and over the received power $2R_{mm}(0)-2R_{mm}(t_3-t_4+t_2-t_1)$ in Figure 4-9.

However, there are two major differences:

The first difference is that IMDD with modulation depth equal to one is very close to FMCD with one detector for low CNR. This is because the dB gain of FMCD in chapter 3 over IMDD is lost due to half the CNR that the FMCD with one detector has with respect to the heterodyne scheme. As we can see, FMCD with independent heterodyne detection still preserves its gain over IMDD.

The second difference which can be observed between the two Figures is the relative position of the performance of FMCD O-D with respect to the IMDD. This is due to two reasons. First, there is worse performance due to the larger phase – the FM phase contains in the remote antenna setup not only the signal but the interferer as well – that the O-D has to differentiate. Since the analysis of Section 3.4.4 had set limits on the phase of the FM in order for the O-D to operate accurately, the parameters have to change for the same tolerance probability to be kept equal. Secondly, the noise added at the output of the O-Ds' detectors is two times the noise that we had before whereas

in IMDD we are still using one detector and the noise remains the same. The combination of these two reasons deteriorates the performance of the O-D and as it can be seen it becomes equivalent to the lowest modulation depths of IMDD.

Each scheme's performance is expressed in terms of the $CNR = \frac{\eta P_u}{2h\nu B} = \frac{\eta |E|^2}{2h\nu B}$ and $R_{mm}(\tau) = \cos(\omega_B \tau)$.

FMCD with Conventional Discriminator and one detector	$\left(\frac{S}{N}\right)_{conv,\max} = 3 \cdot \beta_{\max}^2 \cdot (2R_{mm}(0) - 2R_{mm}((t_3 - t_4 + t_2 - t_1))) \cdot CNR$
FMCD with Conventional Discriminator and heterodyne detection	$\left(\frac{S}{N}\right)_{conv-het.,\max} = 3 \cdot \beta_{\max}^{*\ 2} \cdot (2R_{mm}(0) - 2R_{mm}((t_3 - t_4 + t_2 - t_1))) \cdot CNR$ where $\beta_{\max}^{*}(CNR) = \beta_{\max}(2 \cdot CNR)$
IMDD	$\left(\frac{S}{N}\right)_{IMDD} = \gamma^2 (2R_{mm}(0) - 2R_{mm}((t_3 - t_4 + t_2 - t_1))) \cdot CNR$
FMCD with Optical Discriminator	$\left(\frac{S}{N}\right)_{optical,\max,1\%} = 2\pi^2 \cdot (1.95\%)^2 (2R_{mm}(0) - 2R_{mm}((t_3 - t_4 + t_2 - t_1))) \cdot CNR$ $\left(\frac{S}{N}\right)_{optical,\max,2\%} = 2\pi^2 \cdot (2.75\%)^2 (2R_{mm}(0) - 2R_{mm}((t_3 - t_4 + t_2 - t_1))) \cdot CNR$

Table 4-1: SNR for different kinds of FMCD and IMDD

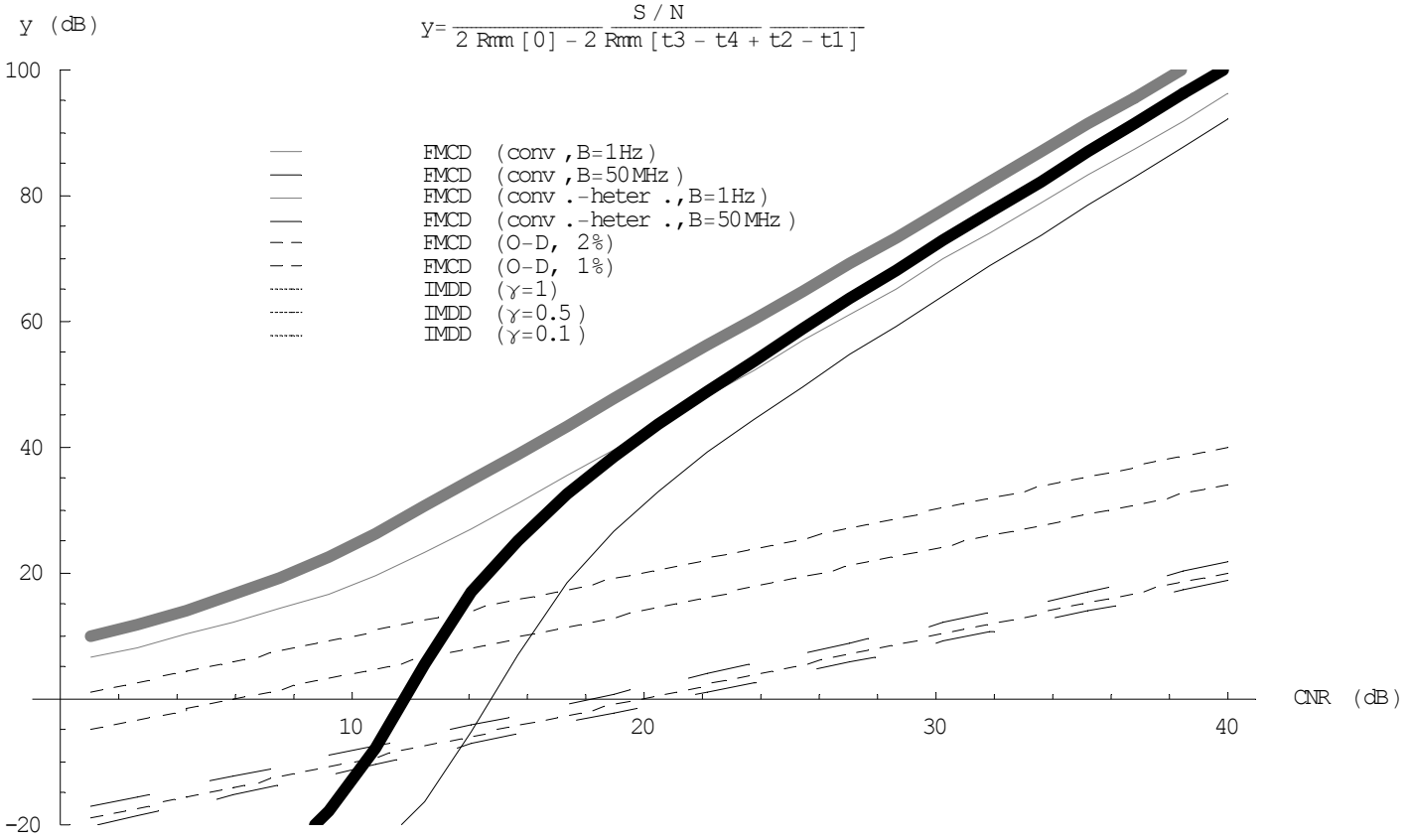

Figure 4-9: Performance Comparison of different modulations and schemes

(a) grey thin line: conventional FMCD with one detector and B=1MHz

(b) black thin line: conventional FMCD with one detector and B=50MHz

(c) grey thick line: conventional FMCD with two separate heterodyne detectors and B=1Hz

(d) black thick line: conventional FMCD with two separate heterodyne detectors and B=50 MHz

(e) upper first close-dashed line: IMDD with $\gamma = 1$

(f) upper second close-dashed line: IMDD with $\gamma = 0.5$

(g) upper third wider-dashed line: FMCD O-D with error tolerance 2%

(h) upper fourth close-dashed line: IMDD with $\gamma = 0.1$

(i) bottom wider-dashed line: FMCD O-D with error tolerance 1%

4.7 Generalizing FMCD for N Antennas and N Users

4.7.1 Introductory Note

In the previous sections, we showed the superior performance of conventional FMCD over the other modulation schemes considered. In our present setting in which we generalize the simple antenna scheme of the previous section (Figure 4-2) to permit N users and N antennas, we therefore restrict our consideration of modulation schemes to FMCD. As we shall see shortly, the setup of Figure 4-2 as it is cannot be scale proposed simply to accommodate N users and N antennas. In particular, we cannot null more than one user by simply adjusting the delay lines, but must employ delaying (rotating the antenna beam pattern) in conjunction with applying weights (changing the beam pattern) to place nulls at the positions of the interferers. Therefore, proper weights, in addition to delays, have to be applied to the signals. Indeed, this is the concept behind a technique in remote antennas known as adaptive beamforming [18], [19], [20], [28]. Adaptive beamforming has been investigated in the literature thoroughly, and many algorithms have been found assuming no modulation, since the weights and delays apply directly to the signals that the antennas receive. In our case, since our fields are FM modulated, containing the received signals inside the phase, we propose a method to optically apply weights and delays to the signals by properly adjusting parameters of the optical field such as its delay and modulation index (Section 4.7.3).

4.7.2 Adaptive Beamforming in FMCD

Adaptive beamforming is a technique widely used in antenna arrays to enhance the signal sensitivity and reduce interfering directional noise sources [18] - [20], [28], [29]. Whereas in the case of two users, only delays are needed so that the antenna beam can be rotated to place a null at the position of the interferer, when more signals need to be nulled the antenna pattern needs to be rotated and altered too. This is why adaptive beamforming includes an adaptive processor which determines the complex weights that are applied to the spectrum that every antenna element – or base station in our remoting application – receives so as to minimize the mean square error with respect to a pilot signal. Variable weights are adjusted in adaptive beamforming by a simple adaptive technique based on the least-mean-squares algorithm (LMS) [18], [20]. During the adaptive process, an injected pilot signal simulates a received signal from a desired look direction. This allows the array to be "trained" so that its antenna pattern has a main lobe in the previously specified look direction. At the same time, the array processing system can reject any incident noises whose directions of propagation are different from the desired look direction, by forming appropriate nulls in the antenna pattern. The array adapts itself to form a main lobe, with its direction and bandwidth determined by the pilot signal, and to reject signals and noises occurring outside the main lobe as well as possible in the minimum mean-square-error sense.

What was discussed above is a well-known technique developed 40 years ago and there is the very well-established LMS algorithm which is available for these weights to be determined. Our goal in this section is to determine how we can apply these weights for the received signals, not on the electrical domain but in the optical domain while our signals are frequency modulated.

The weights that need to be applied are complex numbers. Thus, we need to apply a real weight w_i and a time delay d_i for every antenna in our remoting application. We use a fiber delay line with value d for the fiber link connected to the antenna. If we assume that the optical field is

$$E_a(t) = |E| \exp\left\{ j\left[\omega_s t + 2\pi \cdot \Delta f_{\max} \int_0^t m(u)du \right] \right\} \tag{4.40}$$

,

delaying it by d will yield

$$E_a(t-d) = |E| \exp\left\{ j\left[\omega_s (t-d) + 2\pi \cdot \Delta f_{\max} \int_0^{t-d} m(u)du \right] \right\}$$

$$= |E| \exp\left\{ j\left[\omega_s (t-d) + 2\pi \cdot \Delta f_{\max} \int_0^{t} m(u-d)du \right] \right\}. \quad (4.41)$$

After heterodyne detection and discrimination, the resulting signal $m(t-d)$ will appear and thus we have managed to apply some phase to the received spectrum of this antenna.

In order to apply a weight of real value *w* to the signal, we propose in this section to change the maximum modulation index from $\beta_{\max}$ to $w \cdot \beta_{\max}$, where $|w| \le 1$ so that we do not operate over the maximum modulation index (this would degrade the performance since $\beta_{\max}$ has been found for yielding the maximum SNR; note that our signals m(t) are always normalized in [-1,1]).

Thus, for the field of (4.39), changing the modulation index gives

$$E_a(t) = |E| \exp\left\{ j\left[\omega_s t + 2\pi \cdot w \cdot \Delta f_{\max} \int_0^{t} m(u)du \right] \right\}$$

$$= |E| \exp\left\{ j\left[\omega_s t + 2\pi \cdot \Delta f_{\max} \int_0^{t} w \cdot m(u)du \right] \right\} \quad (4.42)$$

By combining both delaying and change of the modulation index the resulting optical field is:

$$E_a(t-d) = |E| \exp\left\{ j\left[\omega_s (t-d) + 2\pi \cdot \Delta f_{\max} \int_0^{t} w \cdot m(u-d)du \right] \right\}. \quad (4.43)$$

After detection and discrimination the term $w \cdot m(t-d)$ appears and we have managed to apply a complex weight onto the signal. We will see later on, that by using FMCD in the generalized Schemes 1 and 2 and by applying the weights in the manner we discussed above for FM, we shall be able to perform adaptive beamforming for a remoting application with conventional FMCD.

4.7.3 Case Study 1: Davies Beamforming for FMCD

In this section we show that nulling an interfering signal without detecting – just by delaying at stages – which is possible under IMDD and for unmodulated signals - is not possible under FMCD.

This technique of aligning signals at different stages and subtracting them has been used for uniform linear antenna arrays by Davies [29] and has been extended to wideband signals [24]. The setup of [24] for three antennas and three users is shown in Fig. 4-10. We assume this to be a linear antenna so that if the first antenna receives signal $m_i(t)$, the second receives $m_i(t+\tau_i)$, and the third receives $m_i(t+2\tau_i)$ for all the user signals i=1,2,3. It is easy to observe that when using IMDD the signals are aligned, at the first stage user 2 is nulled, and at stage two user 3 is nulled. For FM, the technique is not so straightforward and we derive the equations for the case of three antennas and three users as shown in Fig. 4-10.

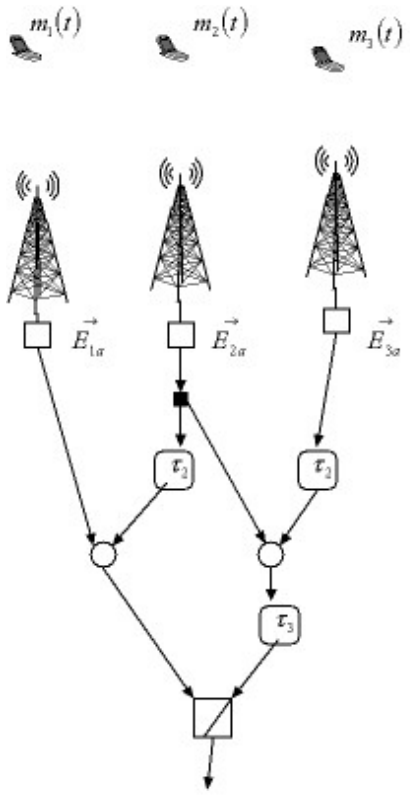

Figure 4-10: Davies Beamforming with three antennas and three users

Each antenna modulates its spectrum using FM and the corresponding optical field for antenna *i* is:

$$E_{ia}(t)=|E|\cdot\exp\left\{j\left[\omega_{s_i}t+2\pi\cdot\Delta f\int_{-\infty}^{t}\left[m_1(u+(i-1)\cdot t_1)+m_2\left(u+(i-1)\cdot t_2\right)+m_3\left(u+(i-1)\cdot t_3\right)\right]du\right]\right\} \quad (4.44)$$

for i=1,2,3.assuming also in this case different optical carrier frequencies among the BSs' lasers.

The black square boxes in Fig 4-10 represent splitters, whereas the white circles represent Mach Zehnder interferometers for subtraction as in [24]. However, we could have used combiners instead of Mach Zehnder interferometers since in the case of FM the Davies nulling procedure - delaying and subtracting - is expected to come from the multiplication with the conjugate delayed field during the detection process and thus the negative sign is not needed to come from the Mach Zehnder but does not make a difference since the scheme under FMCD fails to null. Thus, we proceed by assuming Mach Zehnder interferometers.

At the square law detector, the output the electrical current will be:

$$\begin{aligned}
I(t) &= R\cdot V_{in}V_{in}^{*}= \\
&= R\left(E_{1a}(t)-E_{2a}(t-\tau_2)+E_{2a}(t-\tau_3)-E_{3a}(t-\tau_3)\right)\left(E_{1a}(t)-E_{2a}(t-\tau_2)+E_{2a}(t-\tau_3)-E_{3a}(t-\tau_3)\right)^{*} \\
&= 4R|E|^2+2R\cdot\mathrm{Re}\begin{bmatrix}E_{1a}(t)E_{2a}^{*}(t-\tau_2)-E_{1a}(t)E_{2a}^{*}(t-\tau_3)-E_{1a}(t)E_{3a}^{*}(t-\tau_3)\\-E_{2a}(t-\tau_2)E_{2a}^{*}(t-\tau_3)+E_{2a}(t-\tau_2)E_{3a}^{*}(t-\tau_2-\tau_3)-E_{2a}(t-\tau_3)E_{3a}^{*}(t-\tau_2-\tau_3)\end{bmatrix}
\end{aligned} \quad (4.45)$$

By taking into account that the real parts produce sinusoids with the difference of the signals inside their argument, we have, for the first term of the real part in (4.45)

$$\begin{aligned}
&\mathrm{Re}[E_{1a}(t)E_{2a}^{*}(t-\tau_2)]= \\
&=|E|^2\cos\left(\left(\omega_{s1}-\omega_{s2}\right)t-\omega_2\tau_2+2\pi\cdot\Delta f\int_{-\infty}^{t}\begin{bmatrix}m_1(u)+m_2(u)+m_3(u)\\-m_1(u+\tau_1+\tau_2)-m_2(u)-m_3(u+\tau_3-\tau_2)\end{bmatrix}du\right)
\end{aligned} \quad (4.46)$$

In the same way, we can evaluate the rest of the terms of (4.45). We observe that the first term $E_{1a}(t)E_{2a}^{*}(t-\tau_2)$ yields a sinusoid of frequency $\omega_{s1}-\omega_{s2}$ and the second term $E_{1a}(t)E_{2a}^{*}(t-\tau_3)$ also yields a term of the same frequency. Therefore, even if we use electrical filters again – with the known restrictions - after the detector these sinusoids at the same frequency add together and, as a

result, we have a sinusoid with varying envelope. This means that the FM discriminator will not be able to extract efficiently the phase of the sinusoid, and therefore no possible null can be realized other than the cancellation of the terms inside the phase. For example, inside the phase of (4.46) the second user signal is cancelled but there will be replicas of it in the rest of the combinations of this field because the second signal's field is not eliminated at stage 1.

The main difference with using Davies beamforming for IMDD schemes is that the FM field cannot be decomposed in terms of the different user signals as in IMDD and therefore the nulling process cannot happen at stages. Davies beamforming nulls out one user per stage and in this way performs beamforming. Nulling completely by aligning the signals at every stage is equivalent to placing a null at a user, eliminating him from this stage and then rotating the beam to place a null to the second user and so on. However, the key point is that the user at each stage is eliminated, whereas in FM the user is present until detection. This is because nulling in FM can only happen upon detection where the phases of the optical fields are joined in a sinusoid.

In this section, we investigated a scheme for nulling in remoting applications of N antennas and we concluded that the nature of FM allows for nulling to happen only after the detection process when the phases of our signals are joined.

4.7.4 Case Study 2: Scaling Scheme 1

Scaling Scheme 1 means combining the fields of all the fibers into a single fiber and detect using a single square law detector.

The optical field of antenna i = 1,2, … , N receiving all the signals $m_j(t)$ from the j=1,2,…,N user is:

$$E_{ia}(t) = |E| \exp\left\{ j\left[\omega_{s,i} t + 2\pi \cdot w_i \Delta f_{\max} \int_0^t \sum_{j=1}^{N} m_j(u - t_{ji}) du \right] \right\} \tag{4.47}$$

where w_i is the weight applied on the signals antenna i receives and t_{ji} is the delay of signal $m_j(t)$ in reaching antenna i. As we discussed before, in order to be able to perform nulling of more than one user we need to include, in addition to delay lines, weights for every fiber link.

Thus the resulting electrical current is:

$$I(t) = R\left|\sum_{i=1}^{N} E_{ia}\left(t - d_i\right)\right|^2 \tag{4.48}$$

where d_i is the fiber delay line for the fiber connected to antenna *i*.

Eq. (4.48) can now be written as

$$I(t) = NR\left|E\right|^2 + R\sum_{\substack{\forall\{i,j\} \\ i\neq j}} E_{ia}(t-d_i)E_{ja}^{*}(t-d_j)\,. \tag{4.49}$$

Combining (4.50) and (4.52) we have:

$$I(t) = NR\left|E\right|^2 + 2R\left|E\right|^2 \sum_{\substack{\forall\{i,k\};i,k=1,..,N \\ i\neq k}} \cos\left(\begin{array}{l}(\omega_{s,i}-\omega_{s,k})t + \omega_{s,i}d_i - \omega_{s,j}d_k \\ + 2\pi\cdot\Delta f_{\max}\int_0^t \sum_{j=1}^{N}\left((w_i m_j(u-t_{ji}-d_i) - w_k m_j(u-t_{jk}-d_k))\right)du)\end{array}\right) \tag{4.50}$$

As (4.50) stands, it is evident that combining the sinusoids will give products of sinusoids which cannot be combined into a single sinusoid. A single sinusoid is needed so that the discriminator can extract the phase from the argument of the sinusoid. But we can overcome this difficulty by using an array of $\frac{N(N-1)}{2}$ electrical filters at different intermediate frequencies. All these filters have to be separated from each other more than the maximum frequency deviation that we have used. Moreover, they have to be close in wavelength so that the intermediate frequencies belong to the microwave region and realizable separating filters can be constructed. This presents an increased difficulty. Given that we could manage to realize all these filters, we would separate the frequency terms in (4.50) and then discriminate the output of every filter separately. If we then added the currents from every discriminator output, the result would be:

$$2\pi \cdot \Delta f_{\max} \sum_{\substack{\forall\{i,k\}: i,k=1,..,N \\ i \neq k}} \sum_{j=1}^{N} \left(w_i m_j (u - t_{ji} - d_i) - w_k m_j (u - t_{jk} - d_k) \right). \tag{4.51}$$

The beating combinations that have occurred in the detection process lead to the complicated expression of (4.51). To get a sense of what (4.51) implies, the weighted spectrum that BS 1 receives, $w_1 \sum_{j=1}^{N} m_j (t - t_{j1} - d_1)$), appears N-1 times with positive sign, whereas the spectrum of BS 2, $w_2 \sum_{j=1}^{N} m_j (t - t_{j2} - d_2)$, appears N-2 times with positive sign and 1 time with negative sign, thus N-3 replicas of the spectrum of BS 2 whereas N-1 replicas of BS 1.

Thus the spectrum of antenna i will have a multiplying factor in (4.51) of *N-(1+(i-1)*2) = N-2i+1* for *i=1 ,..., N*. Thus, we can change the weights that are defined by the LMS algorithm into new weights $w_i^{'}$

$$w_i^{'} = \frac{1}{N - 2i + 1} w_i \qquad \text{for i=1,…,N}$$

where w_i are the weights which would be defined by the LMS algorithm for the same remote antenna if it didn't have fiber optic links connected to the BSs and the output of every BS was weighted, delayed and added.

Scheme 1 has been proved able to scale but the complexity is increased, requires every fiber link to operate at a different and close frequencies so that the resulting products can be separated with microwave filters. The passband bandwidth of such a filter would also have to equal to the expanded received spectrum of each BS. Thus, a spacing of greater than $\Delta f_{\max}$ is required among the center filter frequencies. Therefore, by observing the resulting electrical signals after detection from (4.50) we conclude that the bottleneck in this structure is to create filters at the frequencies $\omega_{s,i} - \omega_{s,k}$ which would be able to filter out all the terms of equation (4.50). On the other hand, if we could heterodyne as in Scheme 2 it would be possible to realize a microwave discriminator.

Also, if we consider avoiding these post-detection filters and think in terms of optical filters so as to separate the fields before detecting and then detect separately, we can see that this is exactly the

same solution as separately heterodyning before combining the fields. This is the generalization of Scheme 2 which is studied in the next Section.

4.7.5 Case Study 3: Scaling Scheme 2

In Davies beamforming, we concluded that when using FM signals for every user, we cannot eliminate a user's signal at every stage under FM modulation and thus progressive rotation of the beam and elimination of one user at a time is not possible using FM. In Case 2, we also concluded that even by deploying a very complex setup with filters separating the frequency terms and then adding the currents, there is the difficulty of realizable filters at high frequencies and with passband bandwidth of the size of the optically utilized bandwidth.

In this section, we proceed with Scheme 2 of Figure 4-3. We saw in Section 4.3.7 that this scheme can achieve even 5.6 dB better SNR performance than Scheme 1, but in this section we will provide the setup for N antennas and N users and we shall apply weights for the FM modulation as discussed in 4.7.2.

The setup is shown in Fig. 4-11, where each antenna $i = 1, \ldots, N$ receives its spectrum, modulates it in FM using the properly defined (by the LMS algorithm) weighted modulation index $w_i \cdot \beta_{\max}$. The signal is then delayed through the fiber delay line and is finally heterodyned at the photodetector. The resulting electrical current passes through the conventional FM post-detection processing (band-pass filter, limiter, discriminator, low-pass filter) and adds to the rest of the currents. The resulting total current, according to the notation of Figure 4-11, is:

$$\sum_{i=1}^{N} w_i \sum_{j=1}^{N} \left(m(t-\tau_{ji}) + \sum_{k=1}^{N-1} r_k (t-\tau_{ji}) \right). \tag{4.52}$$

(4.52) is exactly the same result as if our signals were never modulated and they were just received by a remote antenna and weighted-delayed properly to perform beamforming. The novel aspect of our proposal in this section consists of using FMCD with its known advantages, simultaneously being able to perform adaptive beamforming based on the well known and effective LMS algorithm, and finally applying the LMS defined weights entirely in the optical domain.

We should note at this point that our demand for the absolute value of the weights to be less than 1 in order for FMCD to perform out of the region of cycle skipping results in using a constrained LMS algorithm such as the one proposed by Frost [19] which requires the sum of all weights to be

1 (and thus all the weights are less than 1). Also, Griffiths proposed a constrained least mean-squares processor not requiring a-priori knowledge of the signal statistics [30].

The beamforming remote antenna of Fig. 4-11 works only for narrowband signals, since the weights-delays are applied to all frequencies without discrimination. In the case of broadband signals, we need to steer the beam at different frequencies properly. Thus, we need to apply different weights-delays to different frequencies. This can possibly be realized with fully tunable optical filters as in Fig. 4-12 which will allow complete control of the gain and phase at each frequency in the passband.

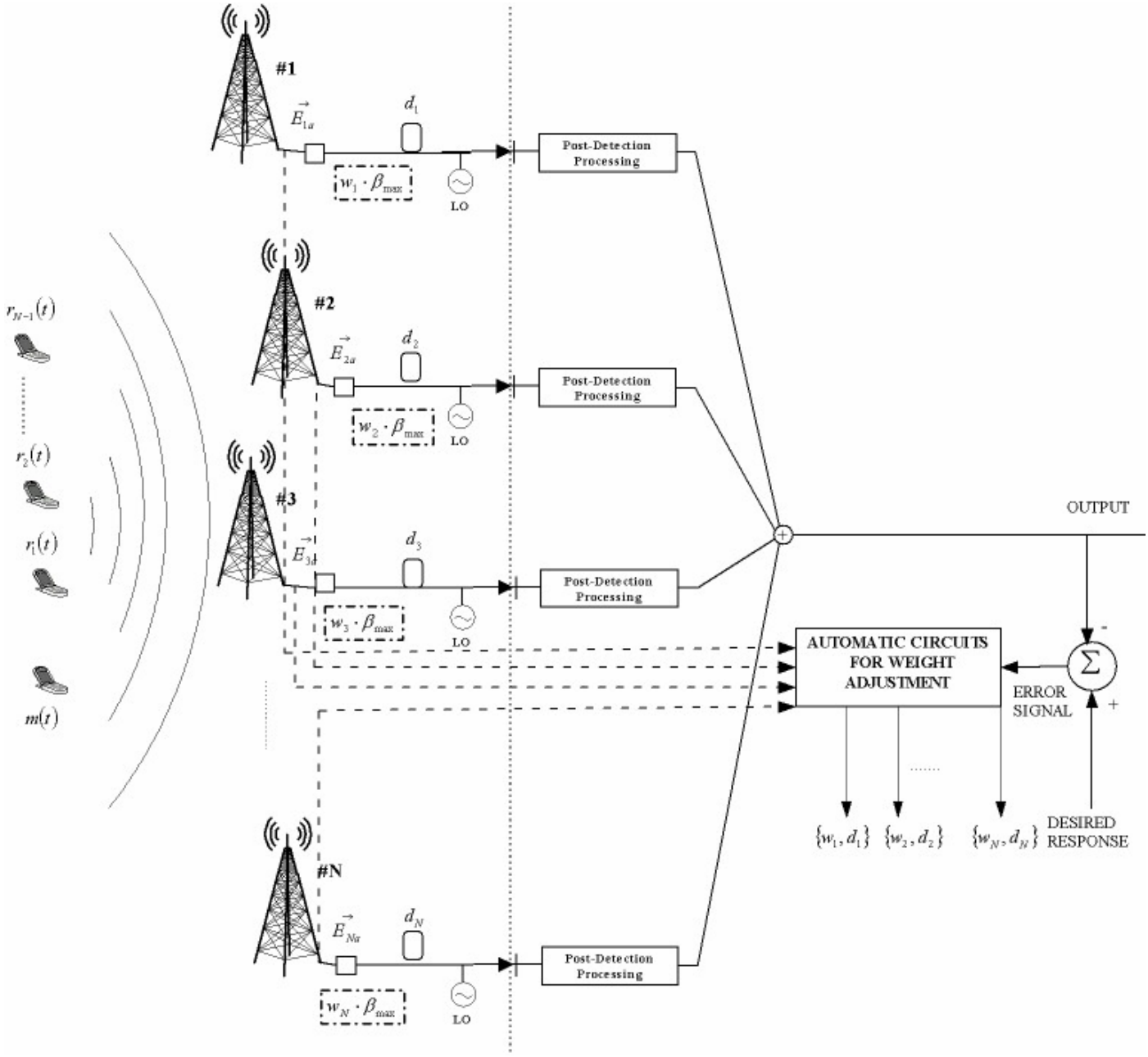

Figure 4-11: N Antennas, N users, Adaptive Beamforming for Narrowband Signals at high frequencies

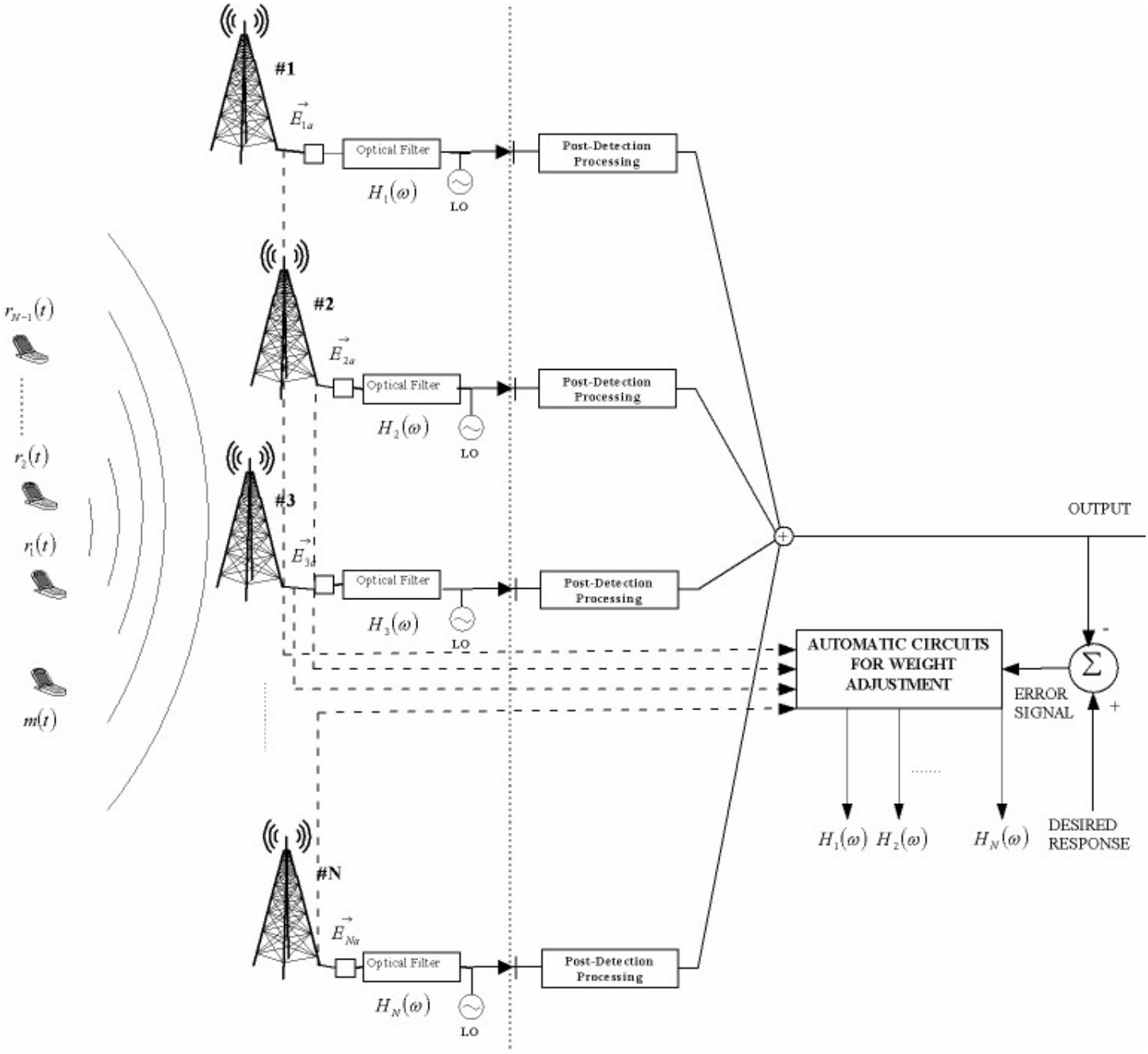

Figure 4-12: N Antennas, N users, Adaptive Beamforming for Broadband Signals at high frequencies

4.7.6 Conclusion of Generalization

Section 4.7 was an investigation of remote antenna setups operating under FMCD which scale for N users and N antennas. We described the adaptive beamforming technique based on the LMS algorithm and showed how the weights could be translated in an FMCD remote antenna. After this we study, three candidate cases for generalization were examined, and we concluded that: Davies beamforming does not work for FMCD since an FM signal cannot be eliminated at stages; scaling Scheme 1 is theoretically possible but requires too many wideband filters; finally, by generalizing Scheme 2 and using an LMS algorithm we see that we can achieve beamforming for narrowband signals, and we suggest the use of fully tunable optical filters for the case of broadband signals.

4.8 Conclusions

Chapter 4 has been an application of conventional FMCD, IMDD and FMCD O-D in a simple remote antenna application consisting of two antennas and two users. The target in the remote antenna scheme – under whatever modulation – has been to null out the interfering signal.. Moreover, we presented a new simple scheme with heterodyne detection performed by a LO which has the same operation as the one previously used, but performs 1.8 – 5.6 dB better depending on the CNR. The comparison result among all the modulation schemes in the remote antenna context - when nulling of the interferer is performed - has been nearly identical to the comparison among modulation schemes of chapter 3.Conventional FMCD with separate heterodyne detection and conventional FMCD with one detector have proved superior in performance which is justified by the noise suppression that they achieves during detection. IMDD and FMCD O-D proved similar in performance with FMCD O-D presenting worse performance than that of chapter 3 for a single signal. The reason is because the interferer adds to the phase that the O-D has to discriminate.

The scheme with heterodyne detection was also shown to be able to scale by adjusting the principles of adaptive beamforming to the characteristics of FMCD. On the other hand, the so far used scheme with one combiner and one detector requires the use of many filters at frequencies separated at least by the size of the optically modulated bandwidth. What is more, we showed that Davies beamforming cannot be applied to FMCD due to the inability of an FM signal to partially eliminate its containing modulated signals at stages.

Thus, the resulting remoting application has superior performance due to FMCD and can perform narrowband adaptive beamforming with the required weights applied in the optical domain. If we further consider tapped- fiber delay lines- we shall be in future work able to treat wideband signals effectively as well.

5 Observations and Conclusions

5.1 Introduction

In this chapter, we will compile the results of the foregoing four chapters. We first summarize the characteristics of the different proposed methods of modulation, namely IMDD, conventional FMCD, FMCD O-D. We next discuss the process of nulling in remote antenna schemes, both simple and generalized, which applies to all of the above modulations. Finally, we utilize these observations to discuss optimal combinations of modulation and suppressing techniques for a remoting application.

5.2 Proposed Modulation Methods

In this section we review the performance and characteristics of the three proposed modulation schemes: IMDD, conventional FMCD, and FMCD O-D. Starting with the most widely used modulation type, IMDD offers the advantage of being simple. Conventional FMCD is a coherent type of modulation, and is thus able to operate in shot noise limited reception by increasing the power of the LO. What is more, the noise added in the detection process is suppressed due to the angle modulation used, which is known in FM systems as weak noise suppression. This is the biggest advantage of FM and results in its superior performance. Throughout Chapter 3 we investigated the limits of FM modulation, known as the FM threshold. This threshold implies that we cannot expand the user's signal in the optical bandwidth as much as we wish because the accumulated noise results in phase errors during the discrimination process. Numerical results on the maximum expansion have been presented by using the powerful Rician analysis for the probability of cycle skipping. The Rician modeling has been found to be very close to simulated results in literature [7]. Therefore, by knowing the maximum bandwidth expansion, we can deduce the best achievable SNR by the conventional FM technique. FMCD O-D is also a coherent type of detection and can perform discrimination for a wide variety of signal frequencies due to its optical nature. However, the disadvantage of this scheme is that the signal is demodulated at the time of detection and the additive Gaussian noise is not suppressed as in the case of the conventional FMCD. Moreover, the presence of a second signal – even if it is nulled at the detector – degrades

its performance. We have seen that the performance of FMCD O-D for a single sinusoidal signal is analogous to IMDD and becomes worse in the antenna remote scheme. This is because the second signal adds to the phase that has to be demodulated and the tolerance limits for optimal discrimination can more easily be violated. By assuming specific percentages for error tolerance, we derived the SNR of this modulation scheme. A comparison among all of them verified our intuition that conventional FMCD is superior due to its weak noise suppression.

5.3 Remote Antenna Schemes and Techniques

A simple antenna scheme was investigated throughout this thesis, consisting of two antennas and two users. The purpose was to suppress the interferer in order to achieve the highest possible SNR for our user. By taking a numerical example using FMCD with one detector – but without loss of generality – we observed that suppressing is always the optimized choice, and that suppression often results in nulling. Due to the complexity of handling the formula for suppressing, and the numerical results showing that in the vast majority of interfering angles suppressing is equivalent to nulling, we restricted our attention to the case of nulling. The nulling procedure occurs by adjusting the values of two fiber delay lines. This action actually rotates the beam pattern of the remote antenna so that a null is placed in the looking direction of the interferer. This procedure becomes more complicated when more users are involved and we need to null more than one interferer. In this case, if the nulls of the beam pattern are not placed at an angle difference equal to that of the interfering signals, it will be needed not only to rotate the beam but also to change its shape. The latter can be achieved by applying proper weights on the received spectrum of each remote antenna. This technique has been known as adaptive beamforming and is very effective in remote antenna applications. The weights are determined by the least mean-square (LMS) algorithm. There are also many constrained versions of the LMS algorithm which we can also use. Another technique discussed was the Davies beamforming technique, according to which a tree of delay lines nulls one user at a time, in a way by rotating the beam – nulling – eliminating a user, and then again rotating to null the next user. All the aforementioned techniques –adaptive beamforming, Davies – have been demonstrated for unmodulated signals.

5.4 Combining Modulations with Remote Antenna Schemes

We now review the fundamental motivation of this thesis: to employ the best in SNR performance analog modulation scheme in a remote antenna application so that we can perform nulling and scale the structure to include N users and N antennas. The comparison in Chapter 4 of all the modulation schemes proved that by using the same condition for nulling – adjusting the delay difference to compensate for path time delay – the performance hierarchy of the modulation schemes does not change significantly. Conventional FMCD remains atop with separate heterodyne detection performing better up to 5 dB than the scheme with one detector. FMCD O-D changed its relative position within the limits of IMDD performance. Thus, the question on which modulation scheme to choose in terms of performance is answered: conventional FMCD. The next issue to address is whether FM in remote antennas can provide us with the ability that the easily implemented IMDD gives us: adaptive beamforming. We have proved that the Davies beamforming technique cannot apply to FMCD in remote antennas and we have shown that the initially proposed simple structure requires too many filters with wide passband. Thus, the new architecture of separate heterodyne detection which was proposed investigated in terms of performance and is now proved to scale. By proposing a technique for applying weights and delays - through changing the modulation index and with fiber delay lines - in the FM case, we managed to weight the users' signals. Given that the weights can be applied and that we want the weights to have absolute value less than 1 to avoid surpassing the FM threshold, we proposed using a constrained LMS algorithm as found in literature [19], [28]. [30]. Thus, using conventional FMCD at the point of its maximum SNR in remote antenna schemes, combined with separate heterodyne detection on each antenna's fiber link, forms the proposed architecture in this thesis. This offers the advantages of analog angle modulation in fibers with the capabilities of optically applied adaptive beamforming in remote antennas.

5.5 Avenues for further Research

Other architectures of remoting antenna schemes with K number of detectors and combining signals in pairs could be investigated so that the cost of the many receivers is reduced. These architectures would also have to scale and performance results would have to be studied. Finally, feedback receivers for FMCD could be used to further improve the performance.

References

[1] A. J. Seeds: “Optical Transmission of Microwaves”, *The Review of Radio Science* 1993-1996, pp 335-343, 1996.

[2] R. F. Kalman, J. C. Fan, L. G. Kazovsky: “Dynamic Range of Coherent Analog Fiber-Optic Links”, *Journal of Lightwave Technology*, Vol. 12(7), pp. 1263-1277, 1994.

[3] C. Cox, E. Ackerman, R. Helkey, and G. E. Betts, “Techniques and performance of intensity-modulation direct-detection analog optical links”, IEEE Trans. Microwave Theory Tech., vol. 45, pp. 1375-1383, Aug. 1997

[4] R. B. Taylor and S. R. Forrest, “Steering of an optically driven true-time delay phased-array antenna based on a broad-band coherent WDM architecture”, IEEE Photn. Techn. Lett., vol. 10, pp. 144-146, Jan. 1997

[5] C. H. Cox, G. E. Betts, and L. M. Johnson, “An analytic and experimental comparison of direct and external modulation in analog fiber-optic links”, IEEE Trans. Microwave Theory Tech., vol. 38, pp. 501-509, May 1990

[6] W. E. Stephens and T. R. Joseph, “System characteristics of direct modulated and externally modulated RF fiber optic link”, J. Lightwave Technol. , vol. 5, pp. 380-387, Mar. 1987

[7] B. Cai, A. J. Seeds: “Optical Frequency Modulation Links: Theory and Experiments”, *IEEE Transaction on Microwave Theory and Techniques* ,vol. 45(4), pp505-511, 1997

[8] V. D. Pol, “The fundamental principles of frequency modulation”, *Proc. Inst. Elec. Eng*., Vol. 93, pt. III, pp.153, 1946.

[9] Wozencraft and Jacobs, “Principles of Communication Enginnering”, JohnWiley & Sons, Inc., 1965.

[10] Ackerman, Cox, Riza, “Selected Papers on Analog Fiber-Optic Links”, SPIE Milestone

Series, Vol. MS149, 1998.

[11] Harry L. Van Trees, "Detection, Estimation and Modulation Theory, Part II", Willey-Interscience, 2003.

[12] Todd Leonard Rachel, "Optimum FM System Performance – An Investigation Employing Digital Simulation Techniques", MIT M.Sc. Thesis, 1966

[13] A. J. Viterbi, "Principles of Coherent Communication", McGraw-Hill, 1966.

[14] T. Kimura, "Coherent Optical Fiber Transmission", *Journal of Lightwave Technology*, Vol. LT-5(4), pp. 414-428, 1987.

[15] G. P. Agrawal, "Fiber-Optic Communication Systems", *John Wiley & Sons Inc*, 2002.

[16] W. V. Sorin, K. W. Chang, Geraldine A. Conrad and Paul R. Henday, "Frequency Domain Analysis of an Optical FM Discriminator", *Journal of Lightwave Technology*, Vol. 10(6), pp. 787-793, 1992.

[17] Arthur James Lowery, Phil C. R. Gurney, "Comparison of Optical Processing Techniques for Optical Microwave Signal Generation", *IEEE Transactions on Microwave Theory and Techniques*, Vol. 46 (2), 1998.

[18] B. Widrow, P. E. Mantey, L. J. Griffiths, B. B. Goode, "Adaptive Antenna Systems", *Proceedings of the IEEE*, Vol. 55(12), pp. 2143-2159, 1967.

[19] Otis Lamont Frost, "An Algorithm for Linearly Constrained Adaptive Array Processing", *Proceedings of the IEEE*, Vol. 60(8), 1972.

[20] Harry L. Van Trees, "Optimum Array Processing Part IV", *John Wiley & Sons Inc*, 2002.

[21] G. L. Abbas, V. W. S. Chan, and T. K. Lee, "Local-Oscillator Excess Noise Suppression for Heterodyne and Homodyne Detection", *Optics Letters*, Vol. 8, pp. 419-421, 1983.

[22] G. L. Abbas, V.W. S. Chan, and T. K. Lee, “A Dual-Detector optical Heterodyne Receiver for Local Oscillator noise Suppression”, *Journal of Lightwave Technology*, Vol. LT-3 (5), pp. 1110-1122, 1985.

[23] Robert A. Minasian, Erwin H. W. Chan, “Photonic Signal Processing of High-Speed Signals“ Invited Paper, *Optical Society of America,* 2005

[24] P. Saengudomlert, V. W. S. Chan, “Hybrid Optical and Electronic Signal Processing for Wideband RF Antenna Arrays”, LIDS Publication 2640, August 2004

[25] B. Glance, “Polarization independent optical receiver”, Journal of Lightwave Technology, LT-5, pp. 274-276, 1987

[26] M. Okai and T. Tsuchiva, “Tunable DFB lasers with ultra-narrow spectral linewidth”, Electronics Letters, 29, pp. 349-351

[27] N. G. Walker and G. R. Walker, “Polarization control for coherent communications”, Journal of Lightwave Technology, LT-8, pp. 438-458.

[28] L. J. Griffiths and C. W. Jim, “An Alternative Approach to Linearly Constrained Adaptive Beamforming”, IEEE Transaction on Antennas and Propagation, Vol. AP-30, No. 1, January 1982

[29] D. Davie, “Independent angular steering of each zero of the directional pattern for a linear array”, IEEE Transactions on Antennas and Propagation, vol. 15, no. 2, pp. 296-298, March 1967

[30] L. J. Griffiths, “Signal Extraction using real-time adaptation of a linear multichannel filter”, Stanford Electron, Lab. Stanford, Calif., Doc. SEL-60-017, Tech. Rep. TR 67881-1, Feb. 1968

[31] Tamura, K., S.B. Alexander, V.W.S. Chan, D.M. Boroson, "Phase-Noise-Canceled Differential Phase-Shift-Keying (PNC-DPSK) for Coherent Optical Communication Systems", Journal of Lightweight Technology, Vol. 8, No. 2, 3 February 1989, pp. 190-201.